UNIVERSITY OF CALIFORNIA
SANTA CRUZ

RARE FLUCTUATIONS OF ENTROPY IN QUANTUM SYSTEMS

A dissertation submitted in partial satisfaction of the
requirements for the degree of

DOCTOR OF PHILOSOPHY

in

PHYSICS

by

Dana Faiez

June 2020

The Dissertation of Dana Faiez
is approved:

Professor Anthony Aguirre, Chair

Professor Josh Deutsch

Professor David Haussler

Quentin Williams
Acting Vice Provost and Dean of Graduate Studies

Copyright © by

Dana Faiez

2020

Table of Contents

List of Figures

Abstract

Rare fluctuations of entropy in quantum systems

by

Dana Faiez

The notion of entropy has been at the core of thermodynamics and statistical physics since the 19th century, originally mentioned in the statement of the second law of thermodynamics as "entropy is non-decreasing in an isolated system." In the context of both classical and quantum mechanics, there are cases where the second law is violated. In other words, entropy of the system may fluctuate downward. The question of how low or high the entropy of a quantum system can get is of interest in the context of small systems that can maintain quantum coherence for short times, and in the context of our universe, assuming it is an isolated quantum system. We explore the rare and extreme fluctuations of two well-developed notions of entropy that are relevant and interesting in isolated thermodynamic quantum systems, namely the observational and entanglement entropy. We find several fundamental differences in the behavior of the two when fluctuating to their extremes. We also provide an analytical proof of a tight upper bound on entanglement entropy for systems constrained to conservation laws.

To Mahshid and Reza.

Acknowledgments

This thesis is motivated by previous works of Anthony Aguirre, Josh Deutsch, and Dominik Šafránek. Each of whom had tremendous influence on my thinking, understanding, and writing. Many thanks to my advisors, Anthony Aguirre and Josh Deutsch. Your way of thinking is inspiring and I'm grateful I had the opportunity to work with you both. Thank you for guiding me through this unknown journey while giving me enough freedom to follow my own curiosity.

Dominik, I wouldn't be exaggerating if I say I learned writing papers from you and won't ever forget the long hours of editing we did on every single word of our papers. I learned an incredible amount of what I am presenting in this thesis from you. So thank you!

This journey would have been incomplete without the presence of my friends in the physics department. You all became my family and I can't ask for a more fun and down to earth cohort. David and Brett, I have many memories with you two, from getting mad at you both for joking around while working on assignments to having long conversations about life and the universe! Michael, thank you for being a great friend to me at any hour of the day, any day the year through the past few years. I'm glad we got to share an office for a few years and a road trip to our favorite parks. Drew, your curiosity and honesty is inspiring. I learned a lot from you and it's been a fun journey working on a project together that we knew almost nothing about in the beginning. I hope our friendship endures.

To my family who I miss very much. Thank you for the support and love, even though we are continents apart. You are always on my mind and can't wait to see you all soon.

Last but not least, to Devin. Thank you for being there for me patiently through all the ups and downs, ensuring me that "this is all going to work out just fine!" This journey would have been incomplete and much more difficult without your presence.

The text of this thesis includes reprints of the following previously published material in Refs. [115, 114]. The co-authors listed in these publications supervised the research presented in this thesis.

Chapter 1

Introduction

"You should call it entropy, for two reasons. In the first place your uncertainty function has been used in statistical mechanics under that name, so it already has a name. In the second place, and more important, no one really knows what entropy really is, so in a debate you will always have the advantage."

- John von Neumann

1.1 Motivation

The second law of thermodynamics, one of the most fundamental laws of nature, can be stated in various forms. For instance, it can be a statement about the limits of heat transfer to mechanical work in a cyclic process, or the impossibility for heat to flow spontaneously from a cold to a hot reservoir. But the statement that will be the focal point of this thesis is one that concerns the concept of entropy, a concept coined by Rudolf Clausius in the mid 19th century. A formulation of the second law in terms of entropy takes a simple form of $\Delta S^{tot} \geq 0$ where S^{tot} refers to the entropy of an isolated system. In other words, "the entropy of an isolated system

never decreases over time."

A statistical interpretation of entropy came about with the introduction of statistical mechanics by Ludwig Boltzmann, Josiah Willard Gibbs, and James Clerk Maxwell in the late 19th century. Boltzmann introduced the well-known *H-theorem* [46], which led to a new definition of entropy that makes use of the statistical weight of the macrostate. For a given macrostate, Boltzmann entropy is given by,

$$S_B = k_B \ln \Omega, \tag{1.1}$$

where k_B is Boltzmann constant.[1] A concept Boltzmann took advantage of in developing statistical mechanics and this definition of entropy is the distinction between micro- and macrostates. The complete specification of a system's microscopic degrees of freedom is what constitutes the microstates M(t), whereas the macrostate $\Omega(t)$ is given by values of the "observables of interest" – those that characterize the system on the macroscopic level, such as volume, temperature, and pressure. Microstates would belong to the same macrostate if they look macroscopically the same. As a result, macrostates are composed of a set of microstates, i.e., $\Omega(t) = \Omega(M(t))$.

If the observable of interest is an energy macrostate (which consists of all microstates in an energy shell), Boltzmann entropy is equal to thermodynamic entropy of the microcanonical ensemble [92, 163, 277, 53], and is proportional to Clausius's entropy for systems in thermal equilibrium. Considering general (not necessarily energy) macrostates, Boltzmann entropy is typically time-dependent and able to describe systems out of equilibrium, unlike the original definition of entropy [136].

Let's look at an example for a better intuition about Boltzmann entropy. Consider flipping ten fair coins one at a time. The chance that all coins turn out to be heads – a seemingly ordered configuration and one with a small number of constituent microstates (only

[1] We will set both k_B and Planck constant $\hbar$ to unity from now on.

one in this case), is much less than finding equal number of heads and tails – a less ordered macrostate and one with high number of constituent microstates. This is only a statistical truth: larger macrostates are more likely to occur. Boltzmann entropy quantifies this likelihood based on the size of the macrostate.

A related concept that will be a crucial tool for the studies of this thesis, is the notion of *coarse-graining*; a set consisting of macrostates achieved by partitioning the microstates into macroscopically distinct configurations [194]. This concept has been utilized in the development of other notions of entropy primarily to describe dynamical systems, such as entropy of partition [180], Kolmogorov-Sinai entropy [117, 192, 180, 121], or topological entropy [117, 192, 180]. Take the volume coarse-graining for example in the case of gas particles inside an isolated box evolving according to the laws of physics. Depending on the initial condition as well as the size of the coarse-graining, the system's entropy either stays about the same if the gas particles were initially at equilibrium, or increases towards a maximum value as the system reaches a highly disordered state. An example of the latter case is when all particles are initially localized at one corner of the box and hence occupying a small volume.

A formulation of the second law in terms of entropy is commonly stated as "the entropy of the universe never decreases over time." In this statement, the universe contains all the matter and energy there is and therefore by definition is considered an isolated system. The second law implies then that this isolated system evolves towards the most random and disordered macrostate (with the constraint of constant total energy), the thermal equilibrium state, and that the earlier times in the history of the universe are associated with more orderly macrostates. The fact that we associate the *earlier times* with more orderly states and the *later times* with more disordered states seems to be why we can distinguish the *past* from the *future*.

Interestingly, this apparent thermodynamic arrow is in the presence of time-symmetric laws of nature; a CPT invariant quantum field theory coupled to a classical cosmological geom-

etry is an example of a contemporary theory governing the dynamics of the universe that does not distinguish the forward direction of time from its reversal [141, 148].[2] It is therefore only the increase in entropy described by the second law that is correlated to the irreversibility of natural processes and the asymmetry between future and past [191, 185, 152]. This thermodynamic arrow is often correlated to the cosmological arrow of time [60, 105, 159].

In order to account for this observed entropy increase in only one time direction, one would appeal to the hypothesis that an extremely low entropy initial state (presumably close to the Big Bang) is what grounded the asymmetric behavior of natural processes. This is known as the *Past Hypothesis* [9, 95]. This is of course an extremely fine tuned initial condition and one of the oldest problems of cosmology [44, 8, 57, 194]. As Boltzmann put in writing: "The second law of thermodynamics can be proved from the [time-reversible] mechanical theory, if one assumes that the present state of the universe. . . started to evolve from an improbable [i.e. special] state" [45]. Our thermodynamic arrow of time, from which the psychological arrow of time follows – our subjective sense of time [150, 149, 159, 225] – is an emergent feature of a special initial condition of the universe. A possible resolution to the open question of why the universe started from such an improbable low entropy state is a rare downward fluctuation of entropy from a thermal equilibrium state.[3]

The occurrence of such fluctuations was mentioned by Zermelo [51] in a criticism of Boltzmann for not considering the possibility of downward fluctuations of entropy in an isolated system. As a counter example, he brought up the Poincaré recurrence theorem which shows that an isolated classical system can return arbitrarily close to its initial state, given enough time [319].

In response to Zermelo [51], Boltzmann explains that fluctuations in entropy are pos-

[2] Although it has been shown experimentally that processes such as the $K^0\bar{K}^0$ transitions violate time-symmetry, it is widely believed that the concept of time reversal in the basic laws of nature is not connected to that of the arrow of time [280].

[3] See [94, 3, 238, 58] for examples of various objections to this resolutions.

sible but unlikely. For example, particles can spontaneously contract into a small space (e.g., corner of a room), and correspond to a macrostate with lower entropy. Boltzmann was the first person to estimate the recurrence time and estimated that the time needed for a cm^3 of gas to return to its original state is of the order of many trillion of digits [310]. This laid the groundwork for the study of fluctuations in entropy. Much later, the relations that constrain the probability distribution of entropy fluctuations, the fluctuation theorems, became one of the most significant discoveries in non-equilibrium statistical physics [111, 173, 68, 284, 211].

These fluctuations become especially relevant in small isolated systems with few degrees of freedom, as well as large systems that have access to extremely long timescales. Although exponentially rare, fluctuations can be of interest in the context of cosmology and understanding of the origin of our universe. Several scenarios such as the formation of black (and white) holes in de Sitter or thermal anti de Sitter [156], thermal transitions in cosmological inflation [96], creation of a Big-Bang universe from an eternal thermal bath [10], and formation of the so-called Boltzmann Brains have been discussed in [3]. These processes all have a particular trait in common, a localization of matter and energy in an orderly manner. One interesting and important question is about the choice of a suitable entropy that can characterize such localization. Another relevant question is whether this localization can occur for an isolated quantum system and if so, to what extent this localization can occur given time-scales of the order of the Poincaré time; after all, the universe is quantum mechanical (although the question of how one must apply quantum theory to the universe is an open and subtle question).[4] A suitable entropy is one that is well-defined out of equilibrium. This raises other questions: Do the out of equilibrium fluctuations of different entropies describe qualitatively the same state of a given system, and to what degree do their non-equilibrium behavior carry over from the

[4]For instance, there are no satisfactory and widely accepted quantum theory of gravity. Also, whether one can associate a wavefunction to the whole universe, without any observers on the"outside" is not well established [153, 226].

equilibrium case?

In this thesis, we address these questions by studying numerically the out-of-equilibrium behavior and the extreme fluctuations of two well-developed notions of entropy that are relevant and interesting in isolated thermodynamic quantum systems, the observational entropy and entanglement entropy.

The observational entropy [168, 269, 268] is a generalization of Boltzmann entropy to quantum systems. Originally introduced by von Neumann [316, 315] as a resolution to the fact that the [von Neumann] entropy does not increase in isolated systems, then briefly mentioned by Wehrl [320] as "coarse-grained entropy," observational entropy has experienced a recent significant resurgence. It was generalized to multiple coarse-grainings [168, 269], found to dynamically describe thermalization of isolated quantum [269, 199] and classical [268] systems, discussed in relationship with other types of entropies [137], found to increase under Markovian stochastic maps [128], and argued for as a natural candidate for entropy production [293] because its definition does not need an explicit temperature dependence.

Entanglement entropy [243, 140, 313, 314] on the other hand is a well-known entropy measure that quantifies the amount of non-local correlation (entanglement) between a subsystem and its complement. It has a wide range of use and is important in understanding thermalization in isolated systems [81, 334, 181], quantum correlations and phase transitions [242, 193, 312], the holographic principle and black hole entropy [106, 236], as well as quantum information theory [227, 308, 64].

We take these two entropies and explore the extreme values they can reach during the time evolution of a given isolated system. We also look for how high entropy can get beyond its typical value. The latter is particularly important due to the fact that states with high entanglement entropy correspond to highly entangled states and such entangled states are the backbone of quantum information protocols as they are considered a resource for tasks

such as quantum teleportation [33, 161], cryptography [104], and dense coding [36]. In these quantum information protocols, more entanglement usually leads to a better performance. As a result, setting precise upper bounds on how much entanglement in principle is available in performing these tasks is essential [336, 202, 175, 14, 290, 314, 313, 26, 24, 123, 167, 166]. This is indeed one of the accomplishments of this thesis: The derivation of a general tight upper bound on entanglement entropy for closed systems (i.e. a thermodynamic system that can exchange energy with its surroundings while keeping the number of particles fixed) along with a numerical confirmation of this bound on an isolated system of one-dimensional fermionic gas.

Besides the aforementioned practical applications, the study of entropy and its fluctuations in the context of quantum mechanics incites historical yet not fully resolved discussions around the concept of the arrow of time on the cosmological and local scale. For instance, how does an observational entropy with a suitable coarse-graining relate to the cosmological arrow of time and as a result the psychological arrow of time[150, 149, 159, 225]?[5]

Throughout the first half of this thesis, we take entanglement entropy as our case study as it is a commonly used entropy especially for studying thermalization. We discuss the conceptual differences between entanglement and observational entropy and raise further questions for the reader in the context of open systems: if both entropies increase towards the canonical entropy, do they reconcile in what they might indicate to the observer about the equilibration time of the subsystem? Also, does the use of observational entropy mean that whether a system is in thermal equilibrium depends upon the use of coarse-graining and is a subjective matter?

These questions, some of which are still considered unresolved, have been a subject of fascination for physicists since the birth of quantum mechanics. It concerns the interpretation

[5]The connection between the psychological arrow of time with that of thermodynamics has been indicated by many authors. See, for example, [100, 155, 262].

of quantum mechanics, the role of the observer in this theory, as well as the concept of time – whether this is an emergent phenomenon or a fundamental one, whether it is objective or depends on the observers knowledge of the system and is therefore subjective. This thesis touches on a few of these questions and provides numerical evidence that may improve one's intuition regarding observational and entanglement entropy of isolated quantum systems.

1.2 Preliminaries

In this section, we cover the essentials from quantum mechanics that build the foundation for the studies presented in this thesis. We introduce the extended Hubbard model that we utilize throughout this work, as well as a few definitions of entropy and their properties in the context of both classical and quantum systems.

1.2.1 States and systems

In standard Schrödinger quantum mechanics, for any physical quantum system which we denote here as A or B, there exists a corresponding complex vector space, known as the Hilbert space, $\mathcal{H}$, in which inner product is defined. In this thesis, we will only consider finite dimensional Hilbert space, with $\dim(\mathcal{H}) > 0$. Using Dirac bra-ket notation, a vector in this space is denoted as $|\psi\rangle \in \mathcal{H}$ with $\langle\psi| \in \mathcal{H}^*$ as its dual vector. We later use $|\psi\rangle_S$ to specify the quantum state associated with the physical system S. For two vectors $|\psi\rangle$, $|\phi\rangle \in \mathcal{H}$, $\langle\psi|\phi\rangle$ and $|\psi\rangle\langle\phi|$ indicate the inner and outer products respectively.

Extending these definitions to a composite system AB, the corresponding Hilbert space is the tensor product of the Hilbert spaces of the two subsystems, $\mathcal{H}_{AB} = \mathcal{H}_A \otimes \mathcal{H}_B$. The tensor product symbol $\otimes$ between the vectors may be neglected at times for simplicity. The dimension of $\mathcal{H}_{AB}$ is the product of $dim(\mathcal{H}_A)$ and $dim(\mathcal{H}_B)$. $\mathcal{H}_{AB}$ includes all vectors that can be written

as

$$|\psi\rangle = \sum_{i,j} c_{i,j}|a_i, b_j\rangle, \tag{1.2}$$

with complex coefficients $c_{i,j}$, and $|a_i\rangle$ and $|b_j\rangle$ the basis states of $\mathcal{H}_A$ and $\mathcal{H}_B$ respectively. We often will use the more compact notation $|a_i, b_j\rangle$ or $|a_i\rangle|b_j\rangle$ in place of $|a_i\rangle \otimes |b_j\rangle$.

The state vector $|\psi\rangle$ describes what is known as the "pure" state; an idealized description of a state and when all information about the state is encoded in $|\psi\rangle$ and known. Therefore, the state vector can not describe statistical mixtures; when there are ensembles of quantum states, one needs to make use of the notion of density matrices, also known as density operators. In general, the density matrix has the following properties:

- $\hat{\rho}^\dagger = \hat{\rho}$ (hermiticity),
- $\mathrm{tr}\hat{\rho} = 1$ (normalization),
- $\hat{\rho} \geq 0$ (positivity).

One can write a generic description of density matrix as a mixture of K pure states,

$$\hat{\rho} = \sum_{i=1}^{K} p_i |\psi_i\rangle\langle\psi_i|. \tag{1.3}$$

$\{|\psi_i\rangle\}$ is a set of pure states, not necessarily orthogonal. The number K is not necessarily the dimension of Hilbert space and the coefficients $\{p_i\}$ are non-zero and less than one and although $\sum_{i=1}^{K} p_i = 1$, one must be careful in interpreting them as the probability to find the system in the state $|\psi_i\rangle$. On the other hand, if one choses to describe density matrix as a mixture of orthogonal pure states, then $K = \dim(\mathcal{H})$ and the coefficients become the eigenvalues of $\hat{\rho}$, $\{\lambda_i\}$ such that $0 \leq \lambda_i \leq 1$ and $\sum_{i=1}^{K} \lambda_i = 1$.

A pure state is a special case of (1.3) where all coefficients p_i are zero except one, i.e., $\hat{\rho} = |\psi\rangle\langle\psi|$ and hence $\mathrm{tr}(\hat{\rho}^2) = 1$. Otherwise, it is considered a "mixed" state and $\mathrm{tr}(\hat{\rho}^2) < 1$. One would have what is known as the "maximally mixed" state when the probability associated with

each orthogonal state $|\psi_i\rangle$ is the same and equal to $1/K$. In this case the density matrix is of the following form

$$\hat{\rho} = \frac{1}{K}\sum_{i=1}^{K} |\psi_i\rangle\langle\psi_i| = \frac{I}{K}. \tag{1.4}$$

The time evolution of $\hat{\rho}$ for an isolated system is described by the von Neumann equation. Given a state $\hat{\rho}_0$ at some initial time $\tau = 0$, the state at later time $\tau > 0$ is given by

$$\hat{\rho}_\tau = U_\tau \hat{\rho}_0 U_\tau^\dagger, \tag{1.5}$$

where $U_\tau = e^{-i\tau\hat{H}}$ is the Hermitian, unitary time evolution operator. $\hat{H}$ is the Hamiltonian operator of the system and can be diagonalized using the spectral decomposition

$$\hat{H} = \sum_i E_i \hat{P}_{E_i}, \tag{1.6}$$

with $\{E_i\}$ as the eigenvalues of the Hamiltonian and $\hat{P}_{E_i}$ as the *projector* onto a subspace $\mathcal{H}_{E_i}$. The *projection operator* or *projector* $\hat{P}_{E_i}$ is a linear map $\hat{P} \in \mathcal{L}(\mathcal{H})$ with the following properties:

- $\hat{P} = \hat{P}^\dagger$ (hermiticity),
- $\hat{P}^2 = \hat{P}$ (idempotency),
- $\sum_{i,j} \hat{P}_i \hat{P}_j = \delta_{ij}$ (orthogonality).

In the case of a pure state, which we will take as our case study for the main portion of this thesis, $\hat{\rho}$ commutes with H, i.e. $[\hat{\rho}, H] = 0$ and does not evolve with time.

Making use of the spectral decomposition again and expanding $\hat{\rho}$ in energy basis, we define what is called the thermal state, also known as *Gibbs state*. At any given temperature, $T = 1/\beta$, the thermal (Gibbs) state is given by

$$\hat{\rho}_{th} = \frac{e^{-\beta\hat{H}}}{Z}, \tag{1.7}$$

where $Z = \mathrm{tr} e^{-\beta \hat{H}}$ is the partition function. More intuitively, this is the state that an open quantum system (a system that can exchange energy/particles with the environment) would evolve to upon reaching equilibrium with its surroundings. However, the unitary dynamics of isolated systems does not allow a pure state to reach thermal equilibrium (unless started from such state). However, according to strong Eigenstate Thermalization Hypothesis [82, 292], a pure state is likely to be in a state that resembles $\hat{\rho}_{th}$ given long enough time.

Another state that we make use of in the numerical portions of this thesis is the following *random pure thermal state* (RPTS) (also known as the thermal pure quantum or canonical thermal pure quantum) [294, 295, 228]),

$$|\psi\rangle = \frac{1}{\sqrt{Z}} \sum_E c_E e^{-\beta E/2} |E\rangle, \tag{1.8}$$

where $|E\rangle$'s are the eigenstates of the Hamiltonian. The coefficients $\{c_E\}$ are random complex or real numbers, $c_E \equiv (x_E + i y_E)/\sqrt{2}$, and $c_E \equiv (x_E + y_E)/\sqrt{2}$ respectively, which leads to what will refer to as the *complex* or the *real* RPTS, with x_E and y_E obeying the standard normal distribution $\mathcal{N}(0,1)$, and $Z = \sum_E |c_E|^2 e^{-\beta E}$ is the normalization constant. These states emulate a thermal state, while being pure.

We choose an extension of the Hubbard Hamiltonian, for the unitary evolution of this RPTS state. This model consists of a kinetic term allowing for tunneling (hopping) of particles between sites of the lattice and a potential term consisting of an on-site interaction. Despite its simplicity, the Hubbard model exhibits almost all interesting phenomena one observes in nature: magnetic ordering, a metal-insulator transition, superconductivity, a Tomonaga-Luttinger liquid in one space dimension, among others. We choose this Hamiltonian since it has been extensively studied in the literature [263, 275, 274, 81, 39, 7, 224].

We consider a system of n spin-less fermions in a one-dimensional lattice of size L with hard wall boundary conditions. The Hamiltonian describing fermions in L sites is given by,

$\hat{H} \equiv \hat{H}^{(1-L)}$,

$$\hat{H} = \sum_{i=1}^{L}[-t(f_i^\dagger f_{i+1} + h.c.) + V n_i^f n_{i+1}^f \\ -t'(f_i^\dagger f_{i+2} + h.c.) + V' n_i^f n_{i+2}^f]. \tag{1.9}$$

(Due to the hard-wall boundary conditions, terms with f_{L+1}, n_{L+1}^f, f_{L+2}, and n_{L+2}^f are not included.) Here f_i and $f_i^\dagger$ are fermionic annihilation and creation operators for site i and $n_i^f = f_i^\dagger f_i$ is the local density operator. The nearest-neighbor (NN) and next-nearest-neighbor (NNN) hopping terms are respectively t and t' and the interaction strengths are V and V'. The schematic depiction of such fermionic chain is illustrated in Fig. 1.1. Later we will also require "local" forms of the Hamiltonian using smaller ranges $(k-l)$. We compute the eigenvalues and eigenvectors of relevant Hamiltonians using exact diagonalization where the software library Linear Algebra Package (LAPACK) in C [90] has been utilized.

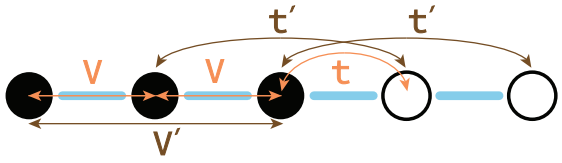

Figure 1.1: A one-dimensional lattice of size $L = 5$ sites and $n = 3$ particles is shown. The right hand side of the figure illustrates the hopping terms t or t' i.e., particles move to the nearest-neighbor (NN) and next-nearest-neighbor (NNN) sites respectively. The left hand side of the figure shows the interactions of strengths V and V' between NN and NNN respectively.

This model is an archetypal example of both non-integrable (generic) and integrable quantum systems. The case in which only nearest-neighbor interaction and hopping exist ($t', V' = 0$), is an example of an integrable system. Whereas the case with both nearest-neighbor and next-nearest-neighbor interaction and hopping ($t', V' \neq 0$) is an example of a non-integrable system. More intuitively, in the latter case, the interaction among particles is sufficient to result in full thermalization. This is however not the case in integrable systems, i.e., the interactions do not sufficiently mix particles; this leads to a large number of constants of motion that prevent

full thermalization [275, 274].

1.2.2 Entropies

The second law of thermodynamics originated the notion of entropy [65]. It then was developed further and extended to other fields such as statistical mechanics and information theory. In the context of quantum mechanics however, there is disagreement as to how to define entropy such that the second law is respected. We briefly cover a few definitions of entropy in thermodynamic, statistical mechanical, and information theory, in both quantum and classical context. We delve into more detail of the two entropies that we take as our case studies in this thesis, observational and entanglement entropy.

Thermodynamic (Clausius) entropy was conceive as a result of Clausius principle 'spontaneous processes are not thermodynamically reversible'. He states that 'the entropy of an isolated system never decreases over time.' and defined a change in system's entropy for a reversible process receiving an infinitesimal amount of heat δQ at absolute temperature T as,

$$\Delta S^{sys} := \int_a^b \frac{\delta Q_{rev}}{T}. \tag{1.10}$$

The integral on the right-hand side depends on the initial and final states, a and b. In other words, entropy is a state function and does not depend on the path taken between the two states [11, 255].

Clausius statement of the second law of thermodynamics and the invention of entropy as the ratio of two macroscopic components, heat and absolute

temperature, was truly a stepping stone in understanding the limits of cyclic processes as well as the relation between the *arrow of time* and the concept of entropy. But the relation to disorder and underlying microscopic structure of systems were investigated later when physicists understood the nature of individual atoms and molecules the microscopic world.

Gibbs entropy is a statistical extension of Clausius entropy and requires macroscopic states to be given by a distribution on the microstates [130]. For a system with a discrete set of microstates this entropy is defined as,

$$S_G = -\sum_i p_i \ln p_i \tag{1.11}$$

where p_i is the probability of a microstate; it specifies the sampling probability of observing a particular state when choosing a system from a large number of identical copies. The sum is extendable to an integral over phase space given a phase-space state density. In that case, p_i can be interpreted as the probability to find the system in a particular region of phase-space [32].

This probability allows one to find macroscopic properties of the system without having access to all degrees of freedom. For instance, in the case of internal energy, one only needs to know the energies of each microstate and the probabilities associated with them,

$$U = \sum_i p_i \epsilon_i, \tag{1.12}$$

where in equilibrium, the probability of a microstate i with energy ϵ_i is,

$$p_i = \frac{e^{-\epsilon_i \beta}}{\sum_i e^{-\epsilon_i \beta}}. \tag{1.13}$$

One notices that this definition of probability in general does not require the system to be in equilibrium and therefore (1.11) is also applicable to states out of equilibrium.

Boltzmann entropy also known as Boltzmann-Planck equation is defined as,

$$S_B = \ln \Omega \tag{1.14}$$

where Ω is the number of available microstates in the macrostate of interest [47]. All microstates are still equally likely (according to the fundamental postulate of Statistical Mechanics for isolated systems), but since some macrostates contain more microstates than others, they are more likely to occur. This definition of entropy enables us to understand this notion from the statistical point of view and is well-defined for non-equilibrium states.

With this view on entropy, Boltzmann made use of the probability theory in the case of interacting gas molecules in a box. As particles interact and evolve over time, the system will explore all accessible phase space; it will spend more time in the larger macrostates (in other words, larger macrostates are more likely to occur). The equilibrium – the state that the system spends the most time in, is the lasrgest macrostate and thus corresponds to maximum entropy. Boltzmann argues that the increase in entropy (the second law of thermodynamics) is simply

a statistical truth and given a colliding set of particles, the states with higher disorder are the most probable ones [47, 255].

The notion of entropy developed from its original statement in thermodynamics, to that of Boltzmann and Gibbs in statistical mechanics. The extension of this concept to other fields was carried on by Claude Shannon (1948) in the field of classical information theory. He saw entropy as a measure of uncertainty in a random variable; in other words, the expected value of information content within a message.

Shannon entropy has been an essential tool in developing a theoretical framework for the processing of electrical signal which revolves around two central issues: 1. The maximum amount of compression of a message while retaining the fidelity of the original information. 2. The rate of reliable transmission of a message over a noisy channel [285, 286, 118].

For a given random variable X (the message) with N elements (total number of characters) consists of n unique characters, the Shannon entropy is given by:

$$H(X) = -\sum_{i=1}^{n} p(x_i) \log_2 p(x_i). \tag{1.15}$$

Intuitively, (1.15) gives us a tool to quantify the number of bits needed to code the transmitting data. The use of base-2 in the logarithm is therefore fitting for this purpose.

Consider a message, for example a string of numbers. The elements of this message are chosen from a reference set of single-digit numbers {0, 1, 2, 3, 4, 5, 6, 7, 8, 9} with corresponding probabilities $p(x_i) = \frac{count}{N}$ where $N = 10$ and *count* is the count of character n_i. The Shannon entropy of message $X =$ "1223334444" for instance then is 1.84644 bits/symbol.

The quantum adaptation of this entropy was introduced by von Neumann (1932), almost 20 years before Shannon entropy was (1948). Quantum versions of many classical entropic notions gradually became of interest and were developed especially due to the advance of research in the field of quantum information theory. Processing, transmission and storage of quantum information, being some of the main tasks in this field, require the use of entropic measures for characterization of quantum states. Some of these quantum entropies are the focal point of the theory of entanglement (e.g. [282]) and quantum communication (e.g. [331, 240]). Here we will focus on a few of these notions and their properties relevant to the study of rare fluctuations in isolated quantum systems.

von Neumann entropy is an extension of Shannon entropy for a discrete probability distribution $\{p_1, p_2, ..., p_n\}$ to density matrices in quantum statistics [315, 160, 326]. Given density matrix $\hat{\rho}$, von Neumann entropy is defined as,

$$S(\hat{\rho})_{VN} = -\mathrm{tr}(\hat{\rho} \ln \hat{\rho}). \tag{1.16}$$

Note the use of natural logarithm instead of log base 2 in (1.16). The latter is commonly used in information theory in order to quantify information in binary

digits as in (1.15). von Neumann entropy quantifies the amount of information present in a quantum system, and in the case of a pure state $S(\hat{\rho})_{VN} = 0$. This can easily be seen by writing (1.16) in terms of eigenvalues of the density matrix, $\{\lambda_i\}$,

$$S(\hat{\rho})_{VN} = -\sum_i \lambda_i \ln \lambda_i \tag{1.17}$$

and realizing that for a pure state all eigenvalues are zero except one. More intuitively, given that the density matrix can be written as $\hat{\rho} = |\psi\rangle\langle\psi|$, one would be completely aware of the state of the quantum system and as a result there would be no surprise in finding out which pure state the system belongs to as long as the measurement is done in that basis.

Another important note is that $S(\hat{\rho})_{VN}$ is manifestly invariant under a unitary transformation,

$$\hat{\rho} \to U\hat{\rho}U^\dagger. \tag{1.18}$$

As a result, the entropy of a pure quantum state stays at zero at all times during a unitary evolution.

von Neumann entropy has many other properties and we will touch on some of them here:

- $S(\hat{\rho})_{VN} \geq 0$ (*Non-negativity*). This can be realized by referring to the definition of this entropy in terms of its eigenvalues (1.17) and using $0 \leq \lambda \leq 1$.

- $0 \leq S(\hat{\rho})_{VN} \leq \dim(\mathcal{H})$. von Neumann entropy is minimal when the state is pure and maximal when the state is maximally mixed.

- $S(\hat{\rho}_A \otimes \hat{\rho}_B)_{VN} = S(\hat{\rho}_A)_{VN} + S(\hat{\rho}_B)_{VN}$ (*Additivity*).

- Given a bipartite state $\hat{\rho}_{AB}$, $S(\hat{\rho}_{AB})_{VN} \leq S(\hat{\rho}_A)_{VN} + S(\hat{\rho}_B)_{VN}$ (*Subadditivity*). The *Additivity* recovers when the bipartite state is a product state, i.e., $\hat{\rho}_{AB} = \hat{\rho}_A \otimes \hat{\rho}_B$.

Rényi entropy is another commonly used measure in quantum information theory. Given a density matrix $\hat{\rho}$, Rényi entropy is given by,

$$S_\alpha = \frac{1}{1-\alpha} \log \mathrm{tr}(\hat{\rho}^\alpha), \quad \alpha \in (0, \infty). \tag{1.19}$$

The Rényi entanglement entropy approaches the Von Neumann in the limit of $\alpha \to 1$. This entropy has the same lower and upper limits as that of von Neumann entropy. It is also *additive* and *non-negative* but not *subadditive* in general [204, 196].

Entanglement entropy is the von Neumann entropy when defined on a subsystem A, described by a reduced density matrix $\mathrm{tr}_B \hat{\rho}_{AB} = \hat{\rho}_A$. This entropy is a measure of mixedness of this state which is linked to the amount of quantum correlations, i.e., entanglement A has with B. To quantify this more precisely, we shall focus on the bipartite case for the moment and introduce Schmidt decomposition (SD) [140, 283]:

Consider a pure state $\psi \in \mathcal{H}_{AB}$ consisting of two subsystems A and B.

Assuming $\dim(\mathcal{H}_A) = m \leq \dim(\mathcal{H}_B) = n$, one can always find a set of orthonormal basis $\{u_1, ..., u_m\} \subset \mathcal{H}_A$ and $\{v_1, ..., v_m\} \subset \mathcal{H}_B$ such that,

$$\psi = \sum_{j=1}^{m} d_j |u_j, v_j\rangle, \tag{1.20}$$

where the real and non-negative scalars $\{d_j\}$ are called *Schmidt coefficients*.

There are a few immediate and useful conclusions one can make from SD. First is the fact that, although dimension of the two Hilbert spaces $\mathcal{H}_A$ and $\mathcal{H}_B$ may be different, $\hat{\rho}_A$ has the same non-zero eigenvalues as that of $\hat{\rho}_B$. In other words, by taking the partial trace of the pure state over system B for instance,

$$\begin{aligned}\hat{\rho}_A = \mathrm{tr}_B(|\psi\rangle\langle\psi|) = \mathrm{tr}_B \sum_{j,j'}^{m} d_j d'_j \left(|u_j\rangle\langle u'_j|\right) \otimes \left(|v_j\rangle\langle v'_j|\right) = \sum_{j,j'}^{m} d_j d'_j \left(|u_j\rangle\langle u'_j|\right) \mathrm{tr}_B \left(|v_j\rangle\langle v'_j|\right) \\ = \sum_{j,j'}^{m} d_j d'_j \left(|u_j\rangle\langle u'_j|\right) \sum_{k} \langle v_k|v_j\rangle\langle v'_j|v_k\rangle = \sum_{j,j'}^{m} d_j d'_j \langle v'_j|v_j\rangle \\ = \sum_{j,j'}^{m} d_j d'_j \left(|u_j\rangle\langle u'_j|\right) \delta jj' = \sum_{j}^{m} d_j^2 |u_j\rangle\langle u_j|,\end{aligned} \tag{1.21}$$

one would get $\{d_j^2\}$ as the eigenvalues of $\hat{\rho}_A$. Similarly, (1.21) can be done for $\hat{\rho}_B$ from which we find that the reduced state of $\hat{\rho}$ on either subsystem would have the same spectrum, i.e., the square of the Schmidt coefficients are the non-zero eigenvalues of both A and B.

Another conclusion is about the so called *Schmidt number*, which is the number of non-zero eigenvalues of the reduced state A (or B). The state is pure if and only if this number is equal to 1. In this case, $\hat{\rho}_{AB} = \hat{\rho}_A \otimes \hat{\rho}_B$ and the state

is known to be a product state (or a separable state.) Otherwise, the state can not be written as a tensor product of the two composite states; the reduced states are mixed and said to be entangled with each other.

The latter conclusion is an indication of the link between mixed-ness and entanglement of the two subsystems. In order to measure entanglement then, we could measure the amount of mixed-ness in a given subsystem, using von Neumann entropy (1.16) of the reduced density matrix, also known as entanglement entropy,

$$S_{ent}(\hat{\rho}) = -\mathrm{tr}(\hat{\rho}_A) \ln \hat{\rho}_A. \tag{1.22}$$

Using (1.20) we immediately find that,

$$S_{ent}(\hat{\rho}_A) = S_{ent}(\hat{\rho}_B) = -\sum_j d_j^2 \ln d_j^2. \tag{1.23}$$

For a product state $d_j = 1$ and entanglement entropy equals 0. On the other hand, if all coefficients d_j^2 are the same ($d_j^2 = 1/m$), entanglement entropy is maximal and the state is said to be maximally entangled. On a more intuitive level, given q qubits in subsystem A and q qubits in subsystem B, then $e^{S_{ent}} = 2^q$ counts the number of entangled states for a maximally entangled state.

As expected, following the properties of von Neumann entropy, entanglement entropy is *additive*, *subadditive* and *non-negative*.

Entanglement entropy can be defined whenever Hilbert space is partitioned into two (or more) factors for a given pure state. For instance, considering an n-body wave function in first quantized form, the partition could be done in

terms of identical particle labels. As discussed in Ref. [19, 309] such a bipartition of indistinguishable particles is solely specified by the number of particles in the subsystem, n_A and entanglement entropy measures the amount of quantum correlations between a the two subsets with n and $n - n_A$ particles.

Another example is when Hilbert space is split into two factors such that the subsystem A is a subregion of space. Two important and well-known geometric properties arise in this case:

Consider a system AB with N particles, the subsystem A with q qubits and the rest, i.e., the bath B with $N - q$ qubits. With the dimension of corresponding Hilbert spaces $1 \ll \dim(\mathcal{H}_A) = m \ll \dim(\mathcal{H}_B) = n$, the Lubkin-Lloyd-Pagels-Page (LLPP) theorem [208, 207, 243, 329] shows that the smaller subsystem A is typically almost maximally mixed with the bath, given that the total system is in a randomly chosen pure state. This maximally mixed state (and with maximum entanglement entropy) leads to the canonical density matrix given in (1.7) [301, 134, 139]. This can be shown using Schurs lemma [337] and by taking advantage of Lagrange multiplier technique [140]. The *volume law* states that the entanglement entropy scales with the volume of the subsystem [243, 228]. In other words,

$$S_{ent} \propto \text{Volume}(A), \quad \text{(random state)}. \tag{1.24}$$

In the case of groundstate however, and for gapped Hamiltonians with local interactions, the entanglement entropy follows the *area law* [140]:

$$S_{ent} \propto \text{Area}(A), \quad \text{(groundstate, gapped Hamiltonian)}. \tag{1.25}$$

Intuitively, the area law suggests that the lower energy states occupy only a small part of the full Hilbert space, and be described by a small number of parameters, unlike the typical states following the volume law. For one-dimensional systems, $S_{ent} \propto$ const and is independent of the system size. This is an important feature used in quantum condensed matter, knwon as the density matrix renormalization group (DMRG) technique [279, 302].

It is worth noting that one can also consider an extension of this entropy to the multipartite case where the entanglement of a subregion with all other partitions in the system is the quantity of interest. This is a more complicated case than in bipartite one [93, 327, 250, 62, 124, 276].

In the following section of this thesis, we will take bipartite entanglement entropy as one of our case studies in order to explore rare entropy fluctuations of a region inside an evolving isolated system.

Observational entropy is an adaptation of Boltzmann entropy to quantum systems. It was mentioned but not developed by von Neumann in 1929 [316, 315] then more recently rediscovered, developed, generalized to include multiple (even non-commuting) coarse-graining, and connected to thermodynamics in [168, 269], using the following construction:

Let us assume that the Hilbert space can be decomposed into a direct sum of orthogonal subspaces $\mathcal{H} = \bigoplus_i \mathcal{H}_i$, where each subspace corresponds to a macrostate specifying a single macroscopic property of the system (such as

energy or number of particles). Defining projector $\hat{P}_i$ as the projector onto a subspace $\mathcal{H}_i$, the set $\mathcal{C} = \{\hat{P}_i\}$ forms a trace-preserving set of orthogonal projectors, denoted a coarse-graining. The probability that a quantum state $\hat{\rho}$ is in a given macrostate can be calculated as $p_i = \mathrm{tr}[\hat{P}_i\hat{\rho}]$. Equivalently, we can say that this is the probability that a system described by a quantum state $\hat{\rho}$ will be found having a value i of a macroscopic property defined by the coarse-graining, when performing a coarse-grained measurement on it in the basis given by the coarse-graining.

Assuming that an observer cannot distinguish between different microstates k within the same macrostate i with their macroscopic measurement, they associate the same probability $p_i^{(k)} = p_i/\dim(\mathcal{H}_i) = p_i/\mathrm{tr}[\hat{P}_i]$ to every microstate (given by a pure quantum state) in the macrostate. Given this inability to distinguish between different microstates within the same macrostate, we consider the Shannon entropy of the probabilities $p_i^{(k)}$,

$$S_{O(\mathcal{C})} \equiv -\sum_{i,k} p_i^{(k)} \ln p_i^{(k)} = -\sum_i p_i \ln \frac{p_i}{\mathrm{tr}[\hat{P}_i]} \tag{1.26}$$

This defines observational entropy with a single coarse-graining.

A generalization of this quantity for multiple coarse-grainings that allows many of its properties to be retained is

$$S_{O(\mathcal{C}_1,\ldots,\mathcal{C}_n)} \equiv -\sum_{\boldsymbol{i}} p_{\boldsymbol{i}} \ln \frac{p_{\boldsymbol{i}}}{V_{\boldsymbol{i}}}, \tag{1.27}$$

where multi-index $\boldsymbol{i} = (i_1, \ldots, i_n)$ denotes a set of macroscopic properties, $p_{\boldsymbol{i}}$ is

the probability of these properties being measured (in the given order), and $V_{\boldsymbol{i}} = \mathrm{tr}[\hat{P}_{i_n} \cdots \hat{P}_{i_1} \cdots \hat{P}_{i_n}]$ denotes a joint Hilbert space volume of all systems that have properties $\boldsymbol{i} = (i_1, \ldots, i_n)$ measured in this order. Equivalently, we can call $V_{\boldsymbol{i}}$ the volume of multi-macrostate $\boldsymbol{i}$.

An important property of S_O is that it depends on the order of coarse-grainings, and that for any ordered set of coarse-grainings $(\mathcal{C}_1, \ldots, \mathcal{C}_n)$ and any density matrix $\hat{\rho}$,

$$S_{VN}(\hat{\rho}) \leq S_{O(\mathcal{C}_1,\ldots,\mathcal{C}_n)}(\hat{\rho}) \leq \ln \dim \mathcal{H}, \tag{1.28}$$

$$S_{O(\mathcal{C}_1,\ldots,\mathcal{C}_n)}(\hat{\rho}) \leq S_{O(\mathcal{C}_1,\ldots,\mathcal{C}_{n-1})}(\hat{\rho}). \tag{1.29}$$

In words, this means that observational entropy is lower bounded by the von Neumann entropy, which can be interpreted as an inherent uncertainty in a quantum system, upper bounded by the maximal uncertainty in the system, and that with each added coarse-graining, the observational entropy does not increase. These properties show that observational entropy can be interpreted as an observers' uncertainty about the system, given that all that the observer can do is to perform a set of macroscopic measurements on this system.

Despite the intuitive interpretation of this general quantity, its physical meaning depends upon the coarse-graining. Several pertinent examples we have identified are as follows:

Observational entropy with energy coarse-graining, S_E, is achieved by choosing coarse-graining $\mathcal{C}_E = \{\hat{P}_E\}_E$, where $\hat{P}_E$ is a projector onto a subspace

associated with eigenvalue E of the Hamiltonian $\hat{H}$ (for non-degenerate Hamiltonians, $\hat{P}_E = |E\rangle\langle E|$ is a projector onto a single energy eigenstate). Observational entropy $S_E \equiv S_{O(\mathcal{C}_E)}$ then gives the equilibrium value of the thermodynamic entropy. For example, for a microcanonical state $\hat{\rho}_{\text{micro}} = \frac{1}{N(E)} \sum_{E \leq \tilde{E} < E+\Delta E} |\tilde{E}\rangle\langle\tilde{E}|$ it gives the microcanonical entropy,

$$S_E(\hat{\rho}_{\text{micro}}) = \ln(N(E)) = \ln(\hat{\rho}(E)\Delta E) = S_{\text{micro}}(E), \tag{1.30}$$

where $\hat{\rho}(E)$ denotes the energy density of states, while for the canonical state $\hat{\rho}_{th} = \frac{1}{Z}\exp(-\beta\hat{H})$ it gives the canonical entropy,

$$S_E(\hat{\rho}_{th}) = \ln Z + \beta\langle E\rangle = S_{VN}(\hat{\rho}_{th}) = S_{th}. \tag{1.31}$$

Observational entropy with coarse-graining in local Hamiltonians, S_F, leads to time-dependence while still pertaining to thermodynamics. the coarse-graining $\mathcal{C}_{\hat{H}_1 \otimes \cdots \otimes \hat{H}_m}$ is such that $\hat{P}_{E_1,\ldots,E_m} = \hat{P}_{E_1} \otimes \cdots \otimes \hat{P}_{E_m}$, $\hat{H}_j\hat{P}_{E_j} = E_j\hat{P}_{E_j}$, are projectors onto local energy eigenstates. The resulting entropy $S_F \equiv S_{O(\mathcal{C}_{\hat{H}_1 \otimes \cdots \otimes \hat{H}_m})}$ is named factorized observational entropy with energy coarse-graining (FOE) which measures how close to equilibrium these local regions are.

As an example, consider the Hilbert space divided into two parts $\mathcal{H}^{(1)}$ and $\mathcal{H}^{(2)}$, with the joint system being $\mathcal{H} = \mathcal{H}^{(1)} \otimes \mathcal{H}^{(2)}$. The Hamiltonian $\hat{H}$ can then be separated into three terms

$$\hat{H} = \hat{H}^{(1)} \otimes \hat{I} + \hat{I} \otimes \hat{H}^{(2)} + \epsilon\hat{H}^{(\text{int})}, \tag{1.32}$$

where $\hat{H}^{(1)}$ and $\hat{H}^{(2)}$ are the Hamiltonians that describe internal interactions in the first and second systems respectively. $\hat{H}^{(\mathrm{int})}$ is an interaction term and ϵ determines the interaction strength. Contribution of this term to the total energy however is expected to be small for large subsystems and local interactions.

FOE is built up from the coarse-graining that projects to the eigenstates of the local Hamiltonians $\hat{H}^{(1)}$ and $\hat{H}^{(2)}$; this corresponds to simultaneous measurements of local energies and can be formally written as,

$$S_F(\hat{\rho}) \equiv S_{O(\mathcal{C}_{\hat{H}^{(1)}} \otimes \mathcal{C}_{\hat{H}^{(2)}})}(\hat{\rho}). \tag{1.33}$$

Explicitly, this factorized coarse-graining is given by $\{\hat{P}_{E_1} \otimes \hat{P}_{E_2}\}_{E_1 E_2}$, and the projectors are given by spectral decompositions of local Hamiltonians, $\hat{H}^{(1)} = \sum_{E_1} E_1 \hat{P}_{E_1}$, $\hat{H}^{(2)} = \sum_{E_1} E_2 \hat{P}_{E_2}$. The generalization of this definition to an arbitrary number of local Hamiltonians is done in [269].

It is shown in Ref. [269] that in the long-time limit, FOE is upper-bounded by the von Neumann entropy of the diagonal density matrix, $\hat{\rho}_d$, defined as the diagonal part of the density matrix written in an energy basis, $\langle E|\hat{\rho}_d|E'\rangle \equiv \frac{p_E(\hat{\rho}_t)}{\mathrm{tr}[\hat{P}_E]}\delta_{EE'}$, equivalent to

$$\hat{\rho}_d = \sum_E \frac{p_E(\hat{\rho}_t)}{\mathrm{tr}[\hat{P}_E]} \hat{P}_E, \tag{1.34}$$

which is a constant density matrix for closed quantum systems, defined fully by the initial density matrix $\hat{\rho}_0$. This density matrix is microcanonical if the diagonal elements are peaked around one set of invariants. Otherwise if they are spread out,

this density matrix is a macroscopic superposition of different thermal states [246]. The latter will be the focus of studies in this thesis. In this case, FOE is bounded by the von Neumann entropy of diagonal density matrix, $S(\hat{\rho}_d)$ up to a correction term of order ϵ representing the interaction strength between the subsystems; this entropy is in turn bounded by the corresponding canonical entropy:

$$S_F(\hat{\rho}) + O(\epsilon) \leq S(\hat{\rho}_d) \leq S(\hat{\rho}_{th}). \tag{1.35}$$

$S_{th} \equiv S(\hat{\rho}_{th})$ is the canonical (thermodynamic) entropy defined as von Neumann entropy of the canonical state, $\hat{\rho}_{th}$ with the mean energy of the system given by $\overline{E} \equiv \mathrm{tr}[\hat{H}\hat{\rho}_t] = \mathrm{tr}[\hat{H}\hat{\rho}_d]$ and thr inverse temperature β given as the solution to equation $\overline{E} = -\frac{\partial \ln Z}{\beta}$. The correction term $O(\epsilon)$ is a finite size correction, and expected to be small for systems with large coarse-grainings. In other words, $O(\epsilon)$ is negligible if the energy of interaction between the subsystems is much smaller than the energies of the subsystems. There are a few exceptions to the bound (1.35) and are discussed in Ref. [269].

Observational entropy with position and energy coarse-graining, S_{xE}**,** is a closely-related example and is the main focus of this thesis. This observational entropy, coarse-grained first in local particle numbers, and then in total energy, can be interpreted as entropy that an observer would associate to a system where m partitions are allowed to exchange energy but not particles, in the long-time limit. S_{xE} is upper bounded by thermodynamic entropy similar to FOE.

Consider an observer who wishes to measure coarse-grained position of

the particles and energy of the system. The two relevant coarse-grainings are

$$\mathcal{C}_{\hat{X}^{(\Delta)}} = \{\hat{P}^{(\Delta)}_{\vec{x}}\}_{\vec{x}}, \quad \hat{P}^{(\Delta)}_{\vec{x}} = \sum_{\vec{\tilde{x}} \in C_{\vec{x}}} |\vec{\tilde{x}}\rangle\langle\vec{\tilde{x}}|, \tag{1.36a}$$

$$\mathcal{C}_{\hat{H}} = \{\hat{P}_E\}_E, \quad \hat{P}_E = |E\rangle\langle E|, \tag{1.36b}$$

where $\mathcal{C}_{\hat{X}^{(\Delta)}}$, which corresponds to coarse-graining in position space with p number of bins of size Δ. For indistinguishable particles, this coarse-graining is equivalent to measuring number of particles in each box, and can be written as $\mathcal{C}_{\hat{X}^{(\Delta)}} = \mathcal{C}_{\hat{N}_1 \otimes \cdots \otimes \hat{N}_p} \equiv \mathcal{C}_{\hat{N}_1} \otimes \cdots \otimes \mathcal{C}_{\hat{N}_p}$. $\mathcal{C}_{\hat{H}}$ consists of projectors from the spectral decomposition of the total Hamiltonian $\hat{H} = \sum_E E\hat{P}_E$.

Observational entropy utilizing the aforementioned coarse-grainings can be written as,

$$S_{xE}(\hat{\rho}) \equiv S_{O(\mathcal{C}_{\hat{X}^{(\delta)}}, \mathcal{C}_{\hat{H}})}(\hat{\rho}). \tag{1.37}$$

which corresponds to first measuring the coarse-grained position and then energy of the system. This entropy increases in a closed system and reaches the correct thermodynamic value given by the microcanonical ensemble, i.e., microcanonical entropy, for initial pure states that are superpositions of energy eigenstates strongly peaked around a given value of energy, and reaches a value that is between the canonical entropy and the mean value of the microcanonical entropies for other initial states.

Denoting by p_{xE} the probability of observing a position macrostate x and then energy state E, and denoting the corresponding Hilbert space volume

$V_{xE} = \mathrm{tr}[\hat{P}_E \hat{P}_x]$, (1.28) implies that S_{xE} is maximized when $p_{xE} \propto V_{xE}$. In general, S_{xE} is large if p_{xE} is high for large volumes V_{xE} while low for small volume; S_{xE} is small if p_{xE} is low for large volumes V_{xE}, and large for small volumes V_{xE}. That is, S_{xE} is low to the extent the state is localized in a small region of space with a well-defined energy, and high otherwise.

The evolution of S_{ent}, FOE, and S_{xE} will be discussed in more detail in section 2.2.

1.3 Methodology

1.3.1 Nelder Mead Simplex algorithm

In this thesis we look for the extreme downward and upward fluctuations of two types of entropies. As a result, optimization is an essential tool for this type of exploration. Numerous optimization algorithms are known and used across field, each suited to solve a particular type of problem. Each algorithm has its own advantages and drawbacks. For instance among the heuristic methods, simulated annealing is guaranteed to find the optimal solution statistically speaking, however the search is normally very slow.

Optimization algorithms also utilize different techniques to converge iteratively to the optimal solution(s). They may use first or second derivatives, or function values, i.e., a direct search method which uses comparison of function

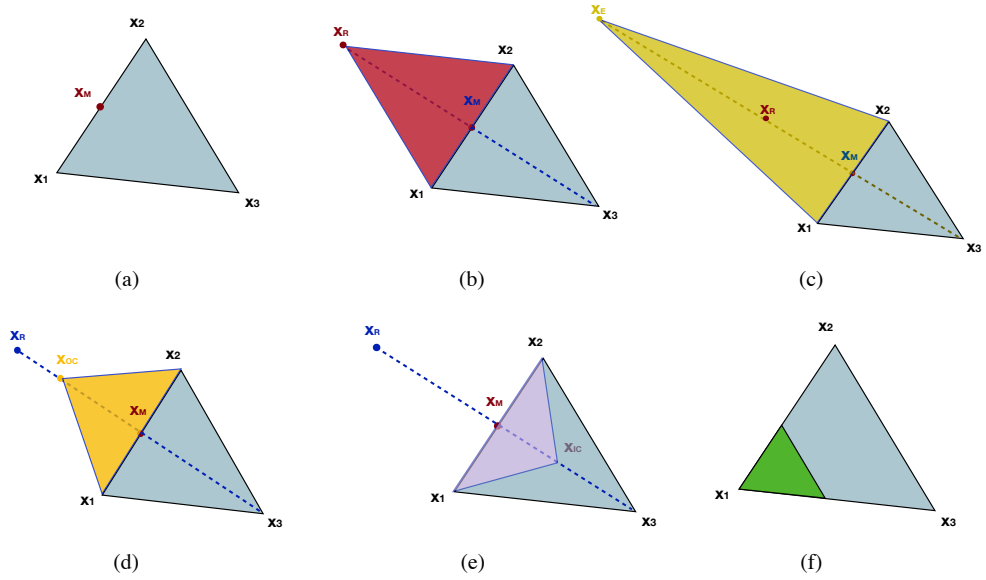

Figure 1.2: Six operations on a simplex with three vertices during the Nelder Meads downhill simplex search [209]. (a) The initial simplex formed by choosing a random set of parameters $\{x_1, x_2, x_3\}$. The centroid, x_M, of all points except the one with highest function value, i.e. x_3 is shown. (b) *Reflection* of the simplex about the reflection point x_R (in red). (c) *Expansion* using the point x_E (in yellow). (d) *Outside contraction* using the point x_{OC} (in orange). (e) *Inside contraction* using the point x_{IC} (in purple). (f) *Shrinkage* on the simplex towards the best point x_1 by replacing all points except x_1 (in green).

values only.

The Nelder Meads simplex method [230, 248, 209] (NMSM) is a popular heuristic method of choice for many practitioners and is also the optimization method of choice in this thesis. It is relatively easy to implement and can optimize a function without calculating its derivatives which is normally more complicated and requires more computational power. In this section, we describe this method in detail and discuss means to overcome the drawbacks of this method.

The Nelder Meads simplex method is a direct downhill search method to search for local minima and is applicable for multidimensional optimization

problems. It uses a special type of polytope, an $n+1$ simplex, to search for its promising directions. A simplex is defined as a geometrical figure which is formed by $n+1$ vertices on $\mathbb{R}^n$ space.

The function values at each vertex is evaluated iteratively. The vertex resulting in the highest function value is replaced with a new vertex. Based on the function value at this new vertex, a new simplex will be formed through operations such as *reflection*, *expansion*, *contraction*, *outside/inside contraction*. Otherwise, i.e., if the function value of the new vertex is worse than all other vertices, the simplex will be shrunk around the best vertex, and this process will be continued until the criterion for convergence are met.

The convergence speed of this algorithm can be controlled by three parameters α, γ, χ, and σ. α is the reflection coefficient, controls the distance from the reflected point to a centroid point and is normally set to $\alpha = 1$; γ is the contraction coefficient, normally set to $\gamma = \frac{1}{2}$ and defines how far a contracted point should be from the worst point; χ is the expansion coefficient and defines how far to expand from the reflected point and has a standard value of $\chi = 2$. And finally, σ is the *shrinkage* parameter with standard value of $\sigma = \frac{1}{2}$

Here are the steps NMSM undertakes for searching for a local minima:

- create a simplex by choosing a random set of parameters $\{x_1, x_2, ..., x_n, x_{n+1}\}$ in the domain of choice 1.2(a).
- compute function values at each vertex, $f_i = f(x_i)$.

- sort the vertices such that the associated function values are in the ascending order, $f_1 \leq f_2 \leq ... \leq f_{n+1}$.
- calculate the centroid of all points except the one with highest function value, i.e., x_{n+1}. This point is shown in 1.2(a), $x_M = \frac{1}{n}\sum_{i=1}^{n} x_i$.
- calculate the reflection point $x_R = x_M + \alpha(x_M - x_{n+1})$.
- calculate f_R at the reflection point x_R,
  - if x_R is better than x_n, but worse than x_1, i.e., $f_1 \leq f_R \leq f_n$, create a new simplex using $\{x_1, x_2, ..., x_n, x_R\}$ vertices: *reflection* 1.2(b).
  - if x_R is better than all other points, i.e., $f_R \leq f_1 \leq f_2 \leq ... \leq f_{n+1}$, compute the expansion point $x_E = x_M + \chi(x_R - x_M)$.
    * if x_E is worse than x_R, accept x_R and perform a *reflection*.
    * otherwise, accept x_E and create a new simplex using $\{x_1, x_2, ..., x_n, x_E\}$ as vertices: *expansion* 1.2(c).
  - if x_R is better than x_{n+1}, but worse than x_n, i.e., $f_n \leq f_R \leq f_{n+1}$, compute the point $x_{OC} = x_M + \gamma(x_R - x_M)$.
    * if x_{OC} is better than x_R, accept x_{OC}, create a new simplex with $\{x_1, x_2, ..., x_n, x_{OC}\}$ vertices: *outside contraction* 1.2(d).
    * Otherwise, perform a *shrinkage* on the simplex 1.2(f).
  - if x_R is worse than all other points, i.e., $f_{n+1} \leq f_R$, compute $x_{IC} = x_M - \gamma(x_M - x_{n+1})$.

* if x_{IC} is better than x_{n+1}, accept x_{IC} and create a simplex using $\{x_1, x_2, ..., x_n, x_{IC}\}$: *inside contraction* 1.2(e).

* Otherwise, perform a *shrinkage* on the simplex 1.2(f).

- if all the the above cases fails, perform a *shrinkage* on the simplex towards the best point x_1 by replacing all points except x_1 with $x_i \to x_1 + \sigma(x_i - x_1)$ 1.2(f).

The search would stop when the values of f on the vertices are close enough to each other, i.e., $\frac{1}{n+1}\sum_{i=1}^{n+1}(f_i - \bar{f})^2 < \epsilon$ where $\bar{f} = \frac{1}{n+1}\sum_{i=1}^{n+1} f_i$. The search would also stop if sufficient number of iterations, *iter* has been completed (both *iter* and ϵ can be controlled by the user).

We apply this method to search for the near global minima and maxima values that the entropies under study can achieve during their time evolution. This optimization is performed with respect to the phases $0 \leq \phi_E = E\tau \leq 2\pi$ that appear in the time evolution of the wave function, $\hat{U}_\tau = e^{-i\hat{H}\tau}$. The number of phases to optimize over is equal to the $\dim H$. As long as the differences of E's are irrational (or close to being to), this method must give the same result as maximizing over all times τ.

As mentioned before, NMSM is a heuristic method and does not guarantee to find the optimal solution. However, there are several possibilities for overcoming this issue. In this study,we do so by repeating the optimization process with many different random initial simplexes.

1.3.2 Monte Carlo sampling method

Getting access to the distribution of entropy far from equilibrium and collecting statistics of super-rare events require evolving the system for extremely long time. A more efficient way to sample the low values of entropy is by using the Metropolis-Hastings (MH) algorithm which provides us with successive iterations in a Markov chain Monte Carlo (MCMC) simulation [154, 177, 212]. The repeated random sampling is performed on the phases $\phi_E = E\tau \leq 2\pi$ that appear in the time evolution of the wave function, $\hat{U}_\tau = e^{-i\hat{H}\tau}$.

We choose deterministic, pseudo-random numbers which make it easy to test and re-run simulations. There are four hyper-parameters in this method: the effective (inverse) temperature, β_{MC}; the number of moves in each iteration, i.e., the number of phases to be changed in one step, m; the step size which determines the size of the jumps from the sampled value, s; the number of iterations to be completed in one round of MC sampling, $iter$. This procedure has the following steps:

- Initialize all phases using pseudo-random numbers between 0 and 2π. Initialize the wave function, ψ_{init} and entropy of interest S_{init} accordingly. Also, initialize an integer called $accept = 0$. This is to keep track of the number of accepted changes on phases.

- Compute the following during each iteration:

- Randomly choose m phases and save them as ϕ_{init}.
- Compute the change in m phases as, $\Delta\phi = 2\pi s(2r - 1)$, where r is a pseudo-random number between 0 and 1.
- Using $\Delta\phi$, compute the new phases as, $\phi_{new} = mod(\phi_{init} + \Delta(\phi), (2\pi))$; where the *mod* function computes the remainder of the two input arguments. This is done in order to prevent the the value of phase from becoming too large. Accordingly, compute ψ_{new} and entropy of interest, $S_{attempt}$. This value of entropy is considered a "candidate" since it not automatically accepted and is supposed to go through the following acceptance procedure.
- Compute the change in entropy, $\Delta S = S_{attempt} - S_{init}$.
- Reject this update if condition for rejection, i.e., $e^{-\beta_{MC}\Delta S} < r$ is satisfied. Otherwise, accept this update, set $S_{init} = S_{attempt}$, save its value, and increment *accept* by one.

During an MH run, the acceptance rate must be monitored to make sure the updates are being accepted at a reasonable rate. If an algorithm rejects too many of the candidates, it would not be able to sample enough from the desired distribution and will not mix well. On the other hand, an algorithm that accepts too many or all candidates, the mixing will occur too slow and many iterations is required to achieve the desired distribution. According to Ref. [177, 212], the ideal acceptance rate is around 50%.

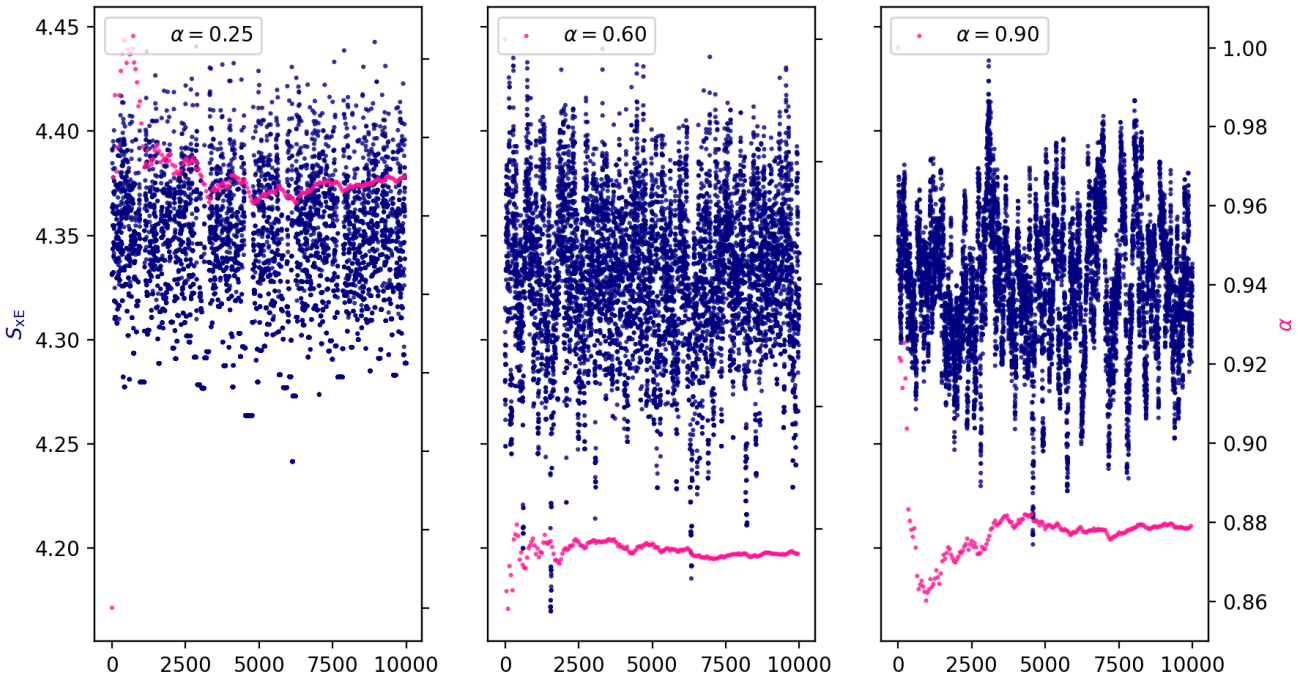

Figure 1.3: Shows three examples of the sampled entropies S_{xE} (blue dots) as well as the evolution of the acceptance rate (pink dots) throughout an MH simulation with fixed $\beta_{MC} = 50$ and step size $s = 5$ for all three cases. The different acceptance rates are due to the difference in the number of moves: 100, 10, and 1 from left to right. This illustrates the insufficient mixing of the cases on the left and right compared to the middle one. It also compares the speed of convergence throughout 10000 iterations.

Fig. 1.3 shows three examples of the sampled entropies S_{xE} (blue dots) as well as the evolution of the acceptance rate (pink dots) throughout an MH simulation with fixed $\beta_{MC} = 50$ and step size $s = 5$ for all three cases. The different acceptance rates are due to the difference in the number of moves: 100, 10, and 1 from left to right. The left plot is an example where acceptance rate

is too low ($\alpha \approx 25\%$). As a result, most candidates are rejected and not many entropies from the desired part of the distribution (left tail) are sampled in 10000 iterations. In the middle graph $\alpha \approx 60\%$ and the sampled values of entropy include the region of interest and there is sufficient amount of mixing. Finally, the graph on the right is an example where acceptance rate is too high ($\alpha \approx 90\%$). In this case, most cases are accepted, the sampled values of entropies are more focused around the mode value, with some entropies sampled from the less likely regions of the distribution. Overall, there is less mixing compared to the middle case.

Chapter 2

Entropy fluctuations in isolated quantum systems

2.1 Overview

In this chapter, we discuss time evolutions of the two aforementioned entropies relevant for describing the dynamics of isolated quantum systems: bipartite entanglement entropy and observational entropy. We illustrate numerically what values these entropies approximately converge to and discuss the intuition behind their evolution – what each entropy mean and is useful for. We first discuss the fluctuations of these entropies over time evolution, not including the rare fluctuations that would only occur if the system has access to long time-scales. We then characterize the rare fluctuations, and find the maximal, minimal, and typical entropy of each type that the system can eventually attain through its evolution. We

find that while both entropies are low for some "special" configurations and high for more "generic" ones, there are several fundamental differences in their behavior. Observational entropy behaves in accord with classical Boltzmann entropy (e.g. equilibrium is a condition of near-maximal entropy and uniformly distributed particles, and minimal entropy is a very compact configuration). Entanglement entropy is rather different: minimal entropy "empties out" one partition while maximal entropy apportions the particles between the partitions, and neither is typical. Beyond these qualitative results, we characterize both entropies and their fluctuations in some detail as they depend on temperature, particle number, and coarse-graining size.

2.2 Time evolution of entropy

Before focusing our attention to the three entropies of interest (S_{xE}, S_F, and S_{ent}), we will consider a simpler example of observational entropy namely the entropy with only a position coarse-graining and discuss its behavior under unitary time evolution.

2.2.1 Time evolution of entropy, S_x

Given a one-dimensional system with n indistinguishable particles, we choose a coarse-graining into p bins, each of size Δ. Such an observation results in the bin number that every particle belongs to. For this purpose, we denote the

binned particle positions by $\vec{x} = (x^{(1)}, \ldots, x^{(n)})$, where each element can take one of the equally spaced values $x_1, \ldots, x_p$.

As an example, the second particle contained in the first bin, is denoted as $x^{(2)} = x_1$. For indistinguishable particles, any permutation π of elements of $\vec{x}$ constitutes the same vector, $\vec{x} \equiv \pi(x^{(1)}, \ldots, x^{(n)})$. We define a set of coarse-grained projectors indexed by $\vec{x}$,

$$\mathcal{C}_{\hat{X}^{(\Delta)}} = \{\hat{P}^{(\Delta)}_{\vec{x}}\}_{\vec{x}}, \text{ where } \hat{P}^{(\Delta)}_{\vec{x}} = \sum_{\vec{\tilde{x}} \in C_{\vec{x}}} |\vec{\tilde{x}}\rangle\langle\vec{\tilde{x}}| \tag{2.1}$$

and $C_{\vec{x}}$ represents a hypercube of dimension n and width $\Delta = x_{j+1} - x_j$. Vector $|\vec{\tilde{x}}\rangle$ contains the exact position of each particle, and corresponds to a basis vector in the Hilbert space. Each hypercube defines one macrostate, which by the above definition is formed by vectors of position $|\vec{\tilde{x}}\rangle$ that correspond to the same vector of positional bins $\vec{x}$. The coarse-graining $\mathcal{C}_{\hat{X}^{(\Delta)}}$ then represents measurements of positional macrostate given a resolution of size Δ.

For indistinguishable particles, this coarse-graining represents the number of particles in a given box of size Δ instead. For example, on a one-dimensional lattice of length $L = 9$ of with $n = 4$ indistinguishable particles coarse-grained into $p = 3$ boxes of size $\Delta = 3$, the first particle could be in the box $\{1-3\}$, the next two could be in box $\{4-6\}$, and the final one could be in the box $\{7-9\}$. This represents one projector of this coarse-graining by the "signature" $[1, 2, 1]$, which represents the number of particles in each box. As a result, in the case of indistinguishable particles, we can write $\mathcal{C}_{\hat{X}^{(\Delta)}} = \mathcal{C}_{\hat{N}_1 \otimes \cdots \otimes \hat{N}_p} \equiv \mathcal{C}_{\hat{N}_1} \otimes \cdots \otimes \mathcal{C}_{\hat{N}_p}$. When

a projector $\hat{P}_{\vec{x}} \in \mathcal{C}_{\hat{X}(\Delta)}$ acts on a wave function, it is projecting out the components of the wave function with $\hat{P}_{\vec{x}}$'s signature.

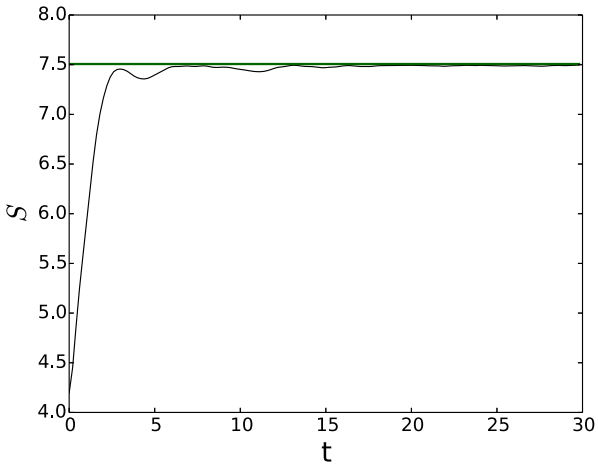

Figure 2.1: Evolution of the observational entropy with positional coarse-graining of the non-integrable system of size $L = 16$, coarse-grained into $p = 4$ parts of size $\delta = 4$, starting at $t = 0$ in a state of $N = 4$ particles contained in the left side of the box (sites $\{1 - 8\}$). As time passes, particles expand through the entire box and the Observational entropy quickly increases, reaching value not far from the maximal value $S_{\max} = \ln \dim \mathcal{H}$, where $\dim \mathcal{H} = \binom{L}{N} = 1820$, depicted by the straight green line [270].

The evolution of this observational entropy is illustrated in Fig. 2.1. We choose an initial condition such that all $n = 4$ particles are confined to the first 8 sites of the lattice at $t = 0$, subject to the Hamiltonian describing a non-integrable system (1.9) with $t = t' = 1.9$, $V = V' = 0.96$. The full lattice has a size of $L = 16$ sites, coarse-grained into $p = 4$ parts of size $\Delta = 4$. Once the right wall is moved to the end of the lattice at $t = 0$, particles expand through the entire lattice and the Observational entropy quickly increases, reaching a value not far from the maximal value $S_{\max} = \ln \dim \mathcal{H}$, where $\dim \mathcal{H} = \binom{L}{N} = 1820$, depicted by the straight green

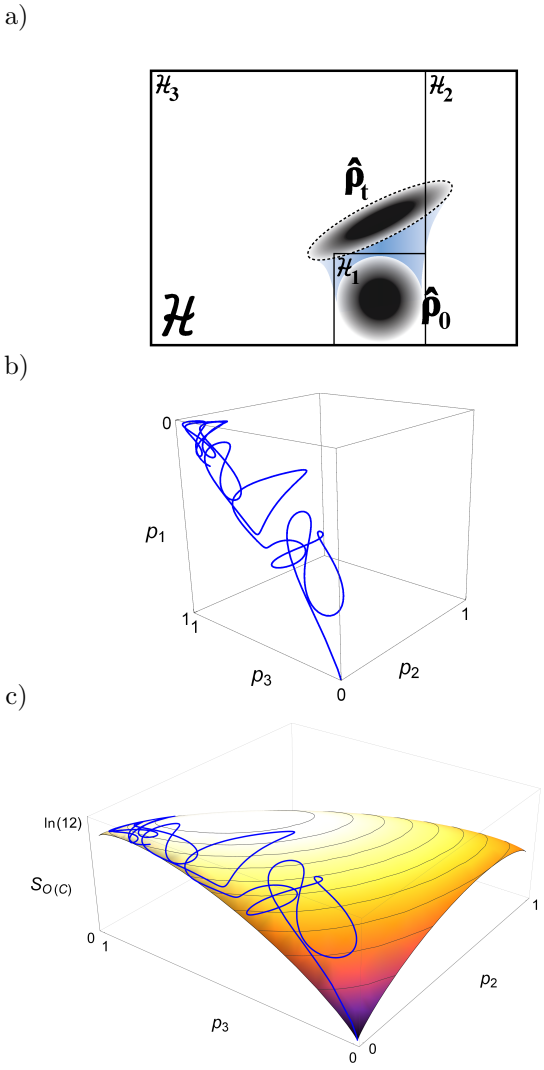

Figure 2.2: a) Sketch of Hilbert space, b) evolution of probabilities, and c) graph of Observational entropy, in 12-dimensional Hilbert space with subspaces of dimensions 1, 3, and 8 respectively. Blobs in a) represent the amount of probability projected into each Hilbert subspace, but it should be kept in mind that the right picture is projecting a density matrix that lives in 12-d space into these lower-d subspaces; this cannot be depicted here. The blue curve in b) represents a possible evolution of probabilities $p_i(t) = \mathrm{tr}[\hat{P}_i\hat{\rho}_t]$, with density matrix starting in the 1-d subspace Hilbert subspace $\mathcal{H}_1$. Panel c) depicts Observational entropy as function of probabilities p_2 and p_3 (where $p_1 = 1 - p_2 - p_3$), and the blue curve is the corresponding entropy $S_{O(C)}(\hat{\rho}_t)$ from evolution b). Observational entropy is a strictly concave function; since each corner of its graph represents one of the subspaces, the entropy must increase at least for a short time when starting in one of them [270].

line.[1] Intuitively, observational entropy measures how uniformly the distribution of particles are over the macrostates. The fact that it almost reaches the maximal value means that in the long-time limit, probability of each particle being in a given macrostate is linearly proportional to the macrostate's volume (1.28).

We refer the reader to Fig. 2.2 for a more intuitive description and depiction of why an observational entropy with an appropriate coarse-graining may increase over time. In Fig. 2.2 (b) a possible evolution of probabilities $p_i(t) = \mathrm{tr}[\hat{P}_i\hat{\rho}_t]$, with density matrix starting in the 1-d subspace Hilbert subspace $\mathcal{H}_1$ probabilities is shown and in Fig. 2.2 (c), the general shape of the evolution of Observational entropy as a function of probabilities is illustrated in blue.

Although the question of to what value observational entropy converges to, for general coarse-graining is difficult to analyze for the case of isolated systems (since the density matrix does not approach the generalized canonical density matrix $\hat{\rho}_{th}$, unlike what happens with an open system[2]), the fact that the amplitudes of the wave-function written in an eigenbasis of the Hamiltonian are fixed and only the respective phases change in isolated systems, hints at a relevant figure of merit, namely the micro-canonical ensemble. What we can say in general however, is that in isolated systems observational entropy increases to a value that depends on the initial state, although entropy for many initial states increases

[1] However, it is important to note that closed quantum systems are not in general ergodic in classical sense, and the Observational entropy does not usually reach the maximal value $S_{\max} = \ln \dim \mathcal{H}$. As an example, if the system starts from an energy eigenstate, this state never evolves and therefore the Observational entropy remains constant for any choice of coarse-graining.

[2] We only consider observational entropy in the context of isolated systems in this thesis. More detailed discussion on what value observational entropy increases to in an open system can be found in Ref. [269].

and converge to a similar value.

The increase of observational entropy (for most initial conditions and appropriate coarse-grainings) then resembles the second law of thermodynamics, but in the context of quantum systems, as it has a tendency to increase or stays the same in an isolated system. Just like the Boltzmann entropy, downward fluctuations exists and one can find states where the entropy decreases, but such states are rare. We will discuss such rare fluctuations in later sections of this thesis.

Now, let's discuss the meaning of the increase in this entropy from the observer's point of view. Consider an observer who chooses a coarse-graining $\mathcal{C} = \{\hat{P}_i\}_i$ that defines macrostates of interest to be measured. The time-dependent Observational entropy,

$$S_{O(\mathcal{C})}(\hat{\rho}_t) = -\sum_i p_i(t) \ln \frac{p_i(t)}{\mathrm{tr}\hat{P}_i} \tag{2.2}$$

describes the increasing amount of disorder in the system with respect to these chosen macrostates. Low Observational entropy means that the state of the system is localized in a few small macrostates. From the subjective point of view of the observer, this is perceived as a highly ordered state. High entropy on the other hand means that the state of the system is contained within a large macrostate, or spans across many small macrostates.Note that this has nothing to do with the system being in pure or mixed state. The Observational entropy does not distinguish between pure and mixed states, but only between different

probability distribution of measurement outcomes. Therefore, even though the system may be pure, an observer (depending on their choice of coarse-graining $\mathcal{C}$) may "see" this state as highly disordered if this pure state cannot be localized in a few small macrostates. It is worth emphasizing again that this entropy is not necessarily linked to any particular *thermodynamic* quantity; such possible connection depends entirely on the choice of coarse-graining.

When the Observational entropy achieves (approximately) its maximum, we say that the system has thermalized with respect to coarse-graining $\mathcal{C}$. Growth of this entropy describes the loss of perceived order due to the time evolution. Given a coarse-graining that leads to an overall increase in observational entropy, as time passes, the state of the system spreads into more and larger macrostates, and the observer loses the ability to say much about the system. With those coarse-graining that correspond to observables that are constant in time, i.e., $[\mathcal{C}, \hat{H}] = 0$, observational entropy remains constant.

2.2.2 Time evolution of entropy, S_{xE}, S_F, and S_{ent}

For the rest of this thesis, we will focus on two types of observational entropies, S_{xE} and FOE, as well as entanglement entropy S_{ent} introduced in section 1.2. Here, we consider the time evolution of these entropies. We discuss to what value they seem to converge and what the effects of different coarse-grainings and initial conditions are on their evolution

We take $n = 3$ particles in a lattice of size $L = 16$ sites and evolve this system using a non-integrable full Hamiltonian $\hat{H}^{(1-L)}$ with parameters $t = V = 1$, $t' = V' = 0.96$ (1.9). We take the inverse temperature $\beta = 0.1$. Taking advantage of the hard wall boundary conditions, we set the system initially to be confined by the hard walls to $L = 8$ sites, evolving through the local Hamiltonian $\hat{H}^{(1-8)}$. At time $t = 0$ the position of the right wall is changed to $L = 16$. The fermions then expand through the evolution of the full Hamiltonian $\hat{H}^{(1-16)}$.

In our first simulation illustrated in Fig. 2.3, we consider S_{xE} (blue lines) and S_F (red lines) for two different initial conditions: Complex RTPS, which models the canonical ensemble in an isolated system 1.2 shown as solid lines, and the second energy eigenstate shown as dashed lines. We compare the two observational entropies using the same partition for positional coarse-graining of S_{xE} and coarse-graining of FOE, i.e., $m = p = 2$ partitions each of size $\Delta = 8$ sites. More specifically, the coarse-graining is given by local Hamiltonian, $\mathcal{C} = \mathcal{C}_{\hat{H}^{(1-8)}} \otimes \mathcal{C}_{\hat{H}^{(8-16)}}$, for FOE, and local position operators for S_{xE}.

Both entropies initially have higher values if their state at $t = 0$ was in a superposition of eigenstates as supposed to one eigenstate. In the latter case, the system initially is in an energy eigenstate of the reduced Hamiltonian – which corresponds to the coarse-graining in FOE. As a result, this entropy has only one non-zero probability which is why it is initially zero.

Once the wall is moved at $t = 0$, due to the interaction term in the full

Hamiltonian between the first and last 8 sites, the local energy representation quickly populates over many other basis vectors and as a result, the entropies increases rapidly. Both entropies evolve to an approximately constant value – with the entropies starting in an eigenstate reaching a value smaller than those initially in RTPS. In both cases however, they are bounded by thermodynamic entropy $S_{\hat{\rho}_{th}}$ (illustrated as dotted horizontal line in Fig. 2.3), as discussed in 1.2.

As one can see from Fig. 2.3, overall, the two observational entropies behave very similarly. As shown analytically in [269], S_{xE} and S_F give the same result as long as a) the coarse-grained position projectors match the partitions of the Hilbert space for the FOE, which is the case in Fig. 2.3 with $p = m = 2$ and b) the interaction energy between partitions is zero, or small such that the difference between energy eigenvalues of the Hamiltonian without the interaction term and the full Hamiltonian is much smaller than the typical energy difference between the eigenvalues of the full Hamiltonian. For large subsystems and local interactions, contributions of this interaction term to the total energy is expected to be small.

In what follows, we will consider different coarse-grainings for only S_{xE} (as we expect S_F to behave similarly, we will not include it in the next simulation). As a comparison, we also plot the evolution of entanglement entropy.

Using the same Hamiltonian parameters, number of particles and initial and final system sizes as before, we compare the evaluations of S_{xE} (dashed lines)

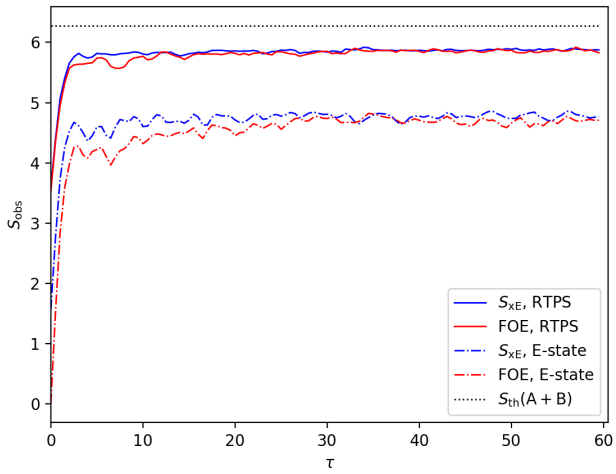

Figure 2.3: The evolution of factorized observational entropy S_F (red lines) and observational entropy with position and energy coarse-graining S_{xE} (blue lines) according to a non-integrable Hamiltonian is shown. The coarse-graining is given by local Hamiltonian, $\mathcal{C} = \mathcal{C}_{\hat{H}^{(1-8)}} \otimes \mathcal{C}_{\hat{H}^{(8-16)}}$, for FOE, and local position operators for S_{xE}. The system of size $L = 8$ sites is initially in either complex RTPS (solid lines) or the 2nd energy eigenstate (dashed lines). The hard wall on the right is then moved to $L = 16$. As a result, the particles expand and both entropies increase. In the case of the system initially in an energy eigenstate of the reduced Hamiltonian – which corresponds to the coarse-graining in FOE, this entropy has only one non-zero probability. As a result, FOE is initially zero given this initial condition. Both entropies increase to a constant bounded by canonical entropy, $S_{\hat{\rho}_{th}}$ (dotted straight line).

and S_{ent} (solid lines), when both start from the same complex RTPS state in the left 8 sites of the lattice. We take entanglement entropy with bath size of $|B| = 12$ sites and therefore subsystem of size $\Delta = 16 - 12 = 4$ (notice that we use the same notation Δ for for the subsystem size and position coarse-graining. This is because, we take these two values to be always the same when comparing the entanglement entropy and S_{xE}) and $|B| = 8$ sites with subsystem of size $\Delta = 16 - 8 = 8$ sites, illustrated as red and blue solid lines respectively.

As depicted in Fig. 2.4 (a), in the latter case of $|B| = 8$, because the

system starts out with all particles confined to the left 8 sites and no particles are in the bath, entanglement entropy is zero initially (see the illustration in 2.4 (b)). Once the right wall is moved to $L = 16$, particles are quickly distributed throughout the lattice according to the non-zero NN and NNN parameters of the Hamiltonian; it then reaches a steady state (which, for all parasitical purposes we may call equilibrium) which is described by the volume law [228] and equals the thermodynamic entropy of the subsystem, $S_{th}(A)$, computed according to (blue straight dashed line),

$$S_{th}(A) = \frac{\Delta}{L} S_{th}. \tag{2.3}$$

S_{th} is computed as the von Neumann entropy of a thermal state of the full system, i.e. $S_{th}(A+B) = -\mathrm{tr}[\hat{\rho}_{th} \ln \hat{\rho}_{th}]$, while $S_{th}(A) = -\mathrm{tr}[\hat{\rho}_{th}^{(A)} \ln \hat{\rho}_{th}^{(A)}]$ where $\hat{\rho}_{th}^{(A)} = \frac{e^{-\beta \hat{H}_A}}{Z}$ for the reduced system.

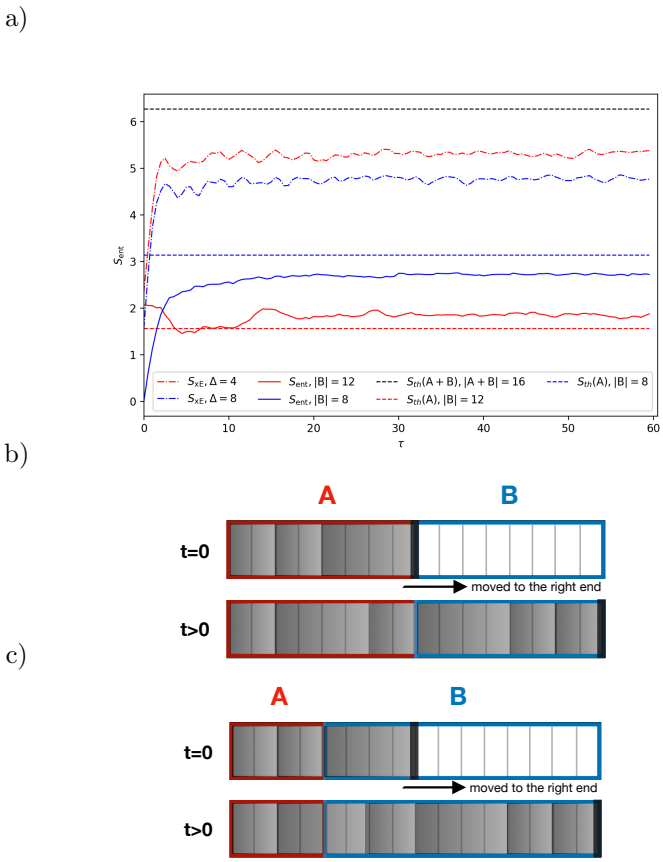

Figure 2.4: (a) Evolution of entanglement entropy S_{ent} and observational entropy S_{xE}. In the former case, we take two bath sizes of $|B| = 12$ and $|B| = 8$ (red and blue solid line respectively). In the latter case, we take two different position coarse-graining sizes of $\Delta = 4$ and 8 sites (red and blue dashes lines respectively). In all cases, the system has an initial size of $L = 8$. The right wall is moved to $L = 16$ at $t = 0$. $S_{\text{ent}} = 0$ initially because the system starts out with all particles confined to the left 8 sites and no particles are in the bath. Once the wall is moved, entanglement entropy evolves to the value close to the thermodynamic entropy of the corresponding subsystem. On the other hand, S_{xE} is initially non-zero in both cases and evolves to an approximately constant value, upper bounded by thermodynamic entropy of the full system of size $L = 16$. With both coarse-grainings, the thermalization (according to the chosen coarse-grainings) occurs very rapidly once the wall is moved at $t = 0$. (b) A sketch of a lattice of total size $L = 16$. The right hard wall depicted as a thick black line. The system initially confined to 8 sites at $t = 0$ and all particles confined to sites $1 - 8$ (the gray scale represents the density of particles in a given region). The subsystem (A) and bath (B), both of size 8 sites are shown as red and blue rectangles respectively. (c) Same as (b) but with subsystem (A) and bath (B) of sizes 4 and 12 sites respectively.

In the former case of $|B| = 12$ on the other hand, the system initially has

non-zero entanglement entropy. As can be seen from Fig. 2.4 (c), at $t = 0$ the left 4 sites belong to the subsystem and the next 4 sites belong to the bath. Since we chose the initial condition to be in RTPS, according to typicality – stating that there exist large subspaces in which all pure states are close to being maximally entangled [157], we expect particles in the initial system to be almost maximally entangled. As a result, we expect the system to have an initial entanglement entropy equivalent to the thermodynamic of the 4-site subsystem inside the system of size $L = 8$. Based on (2.3), this means, $S_{th}(A)(t = 0) \approx \frac{4}{8} \times 3.98 \approx 1.99$, where the initial system of size $L = 8$ with 3 particles has thermodynamic entropy of 3.98. This is in fact the maximum entanglement entropy a system of this size can have (i.e. when $\dim(A) = L/2$) [228].

Once the wall is moved to $L = 16$, entanglement entropy decreases to the value close to the thermodynamic entropy of the subsystem (of size 4 sites), $S_{th}(A)(t > 0) \approx \frac{4}{16} \times 6.28 \approx 1.57$ (red straight dashed line), where 6.28 is the thermodynamic entropy of the full system of size $L = 16$.

We now turn to the evolution of observational entropy S_{xE} with two different position coarse-grainings, $\Delta = 4$ and 8 sites (red and blue dashes lines respectively), depicted in Fig. 2.4 (a). Initially, this entropy is non-zero and evolves to an approximately constant value, upper bounded by thermodynamic entropy of the full system of size $L = 16$. With both coarse-grainings, the thermalization occurs very rapidly once the wall is moved at $t = 0$.

One notices that S_{xE} with finer positional coarse-graining (red line) is higher than that with larger coarse-grainig (blue line). This may seem counter intuitive at first, especially given the theorem on the monotonicity of observational entropy given in Ref. [269],

If $\mathcal{C}_1 \hookrightarrow \mathcal{C}_2$ then

$$S_{O(\mathcal{C}_1)}(\hat{\rho}) \geq S_{O(\mathcal{C}_2)}(\hat{\rho}). \tag{2.4}$$

In other words, observational entropy is a monotonic function of the coarse-graining. However, in the cases where the coarse-grainings do not commute, the aforementioned theorem does not apply and whether the entropy will increase or not depends on the complex relation between the non-commuting coarse-grainings.

Another note to make here in comparing these two types of entropies is that while bipartite entanglement entropy is a useful tool for measuring thermalization of a subsystem connected to a thermal bath, observational entropy S_{xE} can measure thermalization of not only open systems but also of isolated systems. In the latter case however, one should be careful in defining the notion of thermalization since the density matrix does not evolve exactly to the canonical one, as it would in an open system. Here, when the Observational entropy achieves (approximately) its maximum, we say that the system has thermalized with respect to coarse-graining C. This leads to the notion of *subjective thermalization*. An observational entropy such as S_{xE} has the capacity to describe the dynamics based on the observer's knowledge of the isolated system. Its growth then describes the

loss of perceived order due to the time evolution as the state of the system spreads into more and larger macrostates, and the observer loses the ability to say much about the system as time passes.

Given this notion of *subjective thermalization*, we ask how different coarse-grainings may effect thermalization time of the system, from the point of the view of the observer. The time it takes for observational entropy to reach its maximum may be different depending on the choice of the coarse-graining (given the same initial conditions). Although this is yet to be explored in detail in future studies, we expect that given an observational entropy with only one coarse-graining, the thermalization time would be longer with a finer coarse-graining. In other words, with more knowledge of the system, the observer would have to wait longer to observe thermalization. On the other hand, in the case where there are multiple non-commuting coarse-grainings, the problem is more subtle and no decisive statement can be made.

2.3 Typical and rare fluctuations in entropy

In this section we explore the distribution of entropy fluctuations with and without the extreme values. We take entanglement and observational entropy as our case studies and explore the global minima and maxima that they can achieve over long-time evolution. We will discuss the qualitative differences between corresponding states.

2.3.1 Distribution of typical and rare fluctuations

First, we plot histogram of entanglement (Fig. 2.5) and observational entropy (Fig. 2.6), in a system of size $L = 16$ with $n = 2$ particles. We take $t = t' = 1.9$, $V = V' = 0.5$, and $\beta = 1/T = 0.01$. The size of position coarse-graining $\Delta = 4$ sites and the subsystem, when considering entanglement entropy, is also 4 sites. Starting from a complex RPTS, the system is evolved and at each small fixed time step we read out the value of entropy. Evolving for a long time, we therefore achieve sufficient statistics that tells us how likely it is to find any given value of entropy.

We can also ask what the minimum and maximum values of entropy are, given infinite time. Due to the exponential suppression of these extreme values, histogram cannot provide this minimum; we therefore use a minimization algorithm, introduced in section 1.3 and explained in more detail below. We then add these results to the histogram (orange and blue vertical lines in Figs. 2.5 and 2.6).

The search for (near) global minima of entropy goes as follows: For a given L and β, we initialize the state in the same complex RPTS as the one we used to create the histograms in 2.5 and 2.6. We then find the maxima and minima for this initial state by maximizing over phases $\phi_E = E\tau$. For each histogram, we provide three heat maps, displaying the particle density ($\langle n_i \rangle$, $i = 1, ...L$) on the lattice sites for states of maximal, average, and minimal entropy.

Entanglement entropy achieves a minimal value that is very close to zero. We plot the heat map (below the histogram in Fig. 2.5) of the particle density of

the state that corresponds to this minimum. We can see that in this situation, the particles moved almost entirely into the bath, thus naturally producing a separable state $|\psi_{\min}\rangle \approx |0\rangle_A \otimes |\psi\rangle_B$, where $|0\rangle_A$ denotes vacuum in the subsystem. One might think that an alternative state $|\psi_{\min}\rangle \approx |\psi\rangle_A \otimes |0\rangle_B$, could also lead to zero entanglement entropy. However, as it is explained in chapter 3, one can not cluster all particles in a small region when starting in a RPTS.

On the other hand, the state with maximum value of entanglement entropy is the one where the subsystem and the bath contain the same average number of particles.[3] The smaller region therefore has a higher density of particles, as illustrated on the heat map. Intuitively, there have to be some particles in the subsystem and some in the bath, for any correlations to exist; and to create the maximum correlation, there should be the same amount of particles on either side. As can be seen from comparing the heat maps in Fig. 2.5, the state that has the maximum entanglement entropy is quite different from the thermal equilibrium state, where particles are distributed uniformly.

[3] In general, particles distribute themselves throughout the lattice such that the average number of particles in the subsystem follows the necessary but not sufficient condition for the state to be maximally entangled, stated in Ref. [114]. In the numerical studies shown here, the average number of particles in the subsystem is equal to that of the bath but this is not in geenral the case.

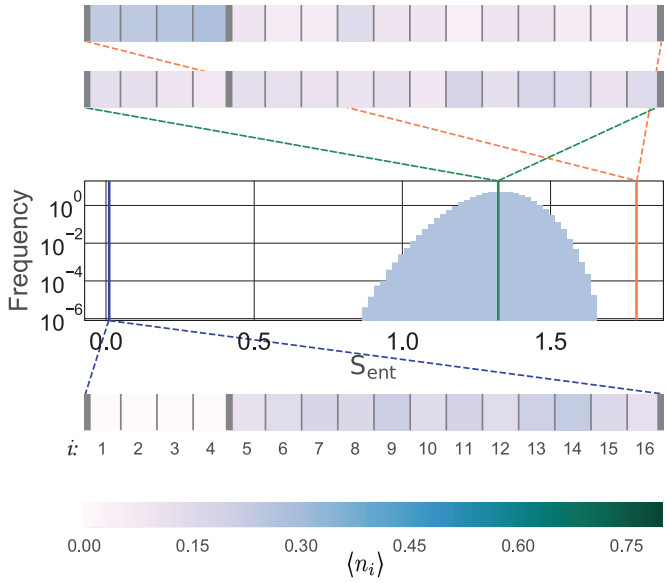

Figure 2.5: Semi-log probability histogram of entanglement entropy, S_{ent}. The y-axis represents the probability of finding the state at any given value of the entropy represented on the x-axis. The heat maps display the particle density ($\langle n_i \rangle$, $i = 1, ...L$) on the lattice sites. The left tail of the histogram, representing the downward fluctuations in entropy, can be fitted with a linear function: this shows that fluctuating to small values is exponentially suppressed in this data set. The blue vertical line on the left is the minimum value the entanglement entropy can achieve, and is found using a minimization algorithm. This value is very close to zero. The heat map below shows the particle density on the lattice of the state that corresponds to this minimum. We can see that in this situation, the particles moved almost entirely into the bath, thus naturally producing a separable state. The orange vertical line on the right is the maximum value of the entanglement entropy, and is also obtained by the minimization algorithm. The heat map above shows the particle density on the lattice of the state that corresponds to this maximum. In this situation, both the subsystem and the bath have the same number of particles, hence we see a higher density of particles in the subsystem. The state that gives the maximal entanglement entropy, is very far from the thermal equilibrium state.

The minimum in S_{xE} is achieved by simply localizing the particles in one of the regions to the extent possible (it does not matter significantly which one, as they all give almost equal entropy; however, if one of the regions was smaller than the others, it would localize into this smallest region). The minimal value of S_{xE} never goes below about half of the maximal entropy; this, again, has to do with

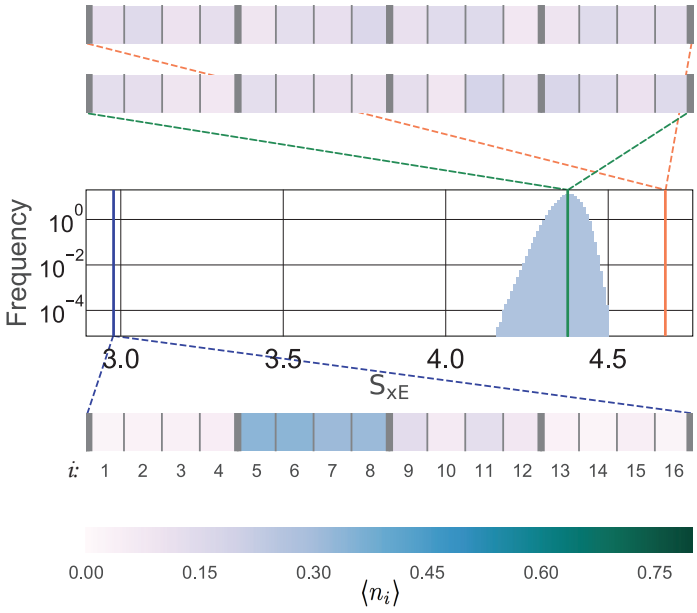

Figure 2.6: Similar to entanglement entropy, downward fluctuations of S_{xE} to small values is exponentially suppressed in this data set. However, in contrast to entanglement entropy, the minimum of S_{xE} represented by the blue vertical line on the left does not go to zero; it is at about 63% of the maximum value. This is because it is impossible to localize the particles entirely into the small region, and the remaining regions still contribute significantly to the total entropy. As one can see from the heat map of the state corresponding to the minimum, a significant number of particles moved into one of the partitions of size 4 sites, resulting in partitions being far from thermal equilibrium from each other. The vertical lines represent the minimum, the average, and the maximum of S_{xE} from left to right. The heat map above shows the uniform distribution of particles for such state. In contrast with entanglement entropy, the states that give the average and maximal values of S_{xE} are very similar to each other, as one would expect from the behavior of Boltzmann entropy.

the inability to cluster all particles in a small region, when starting in an RPTS (see 3.0.2 for more discussion on the relation between spatial localization and minimization of entropy). The maximum of S_{xE} is given by a state where particles are uniformly distribution across all regions. S_{xE} is therefore in accordance with the Boltzmann entropy, in contrast to entanglement entropy.

The distribution of both entropies illustrated in the semi-log histograms 2.5

a)

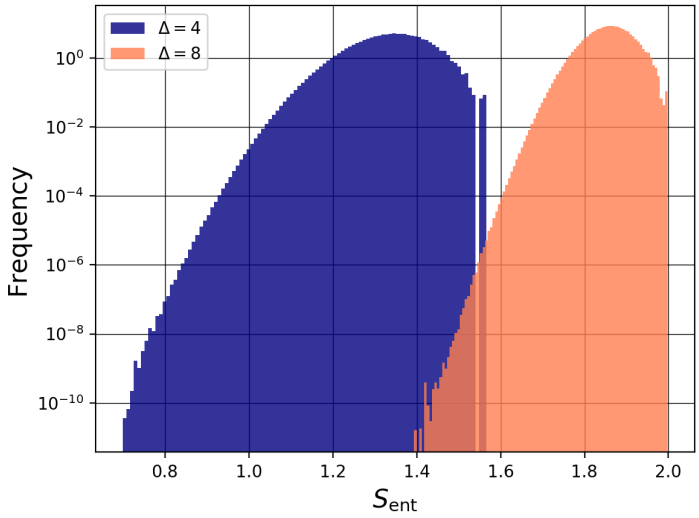

b)

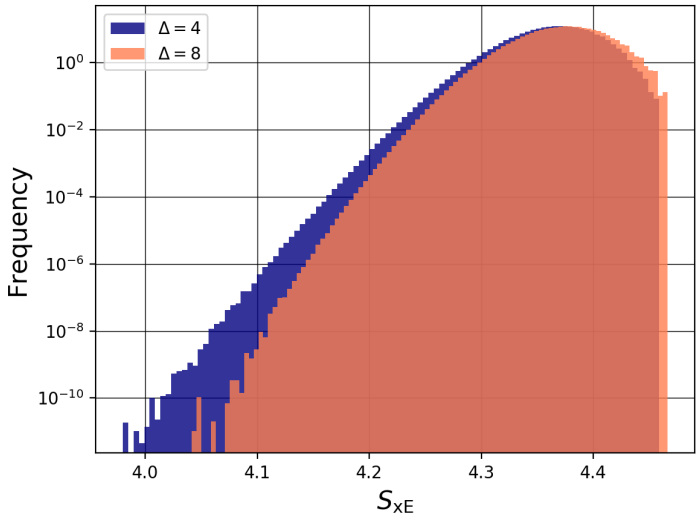

Figure 2.7: Sampled distributions for (a) entanglement and (b) observational entropy using MH algorithm. We take a $L = 16$ site lattice with 2 particles. (a) Entanglement entropy with subsystem of two different sizes $\Delta = 4$ and 8 sites, sampled using $\beta_{MC} = 26$ and 40 shown in blue and orange respectively. (b) Observational entropy with two different position coarse-grainings $\Delta = 4$ and 8 sites, sampled using $\beta_{MC} = 50$ and 57 is illustrated in blue and orange respectively. In all cases, an approximately linear left tail is an indication of the fact that the decreasing of entropy far from equilibrium is exponentially unlikely.

and 2.6, in particular the approximately linear shape of the left tail, suggests that in regions far from equilibrium decreasing entropy is exponentially suppressed. This is similar to the statement given by a group of Fluctuation theorems (FTs) which are fundamental in nonequilibrium statistical mechanics [111, 173, 68, 284, 211] and is given by $p(-\Delta S)/p(+\Delta S) = \exp(-\Delta S)$.

This relation sets a constraint on the probability distributions of entropy fluctuating far from equilibrium. This group of FTs, extensively studied for closed [298, 108, 260] and open systems [109, 50, 215] pertain when an external force drives the system out of equilibrium.

These studies do not however explore the aforementioned relation when the system is completely isolated, i.e., there is no exchange of energy or particles between the system and the surrounding, and the system evolves unitarily in the absence of any external drive. In exploring whether a relation similar to that of FT for driven systems still hold true in the context of observational and entanglement entropy in isolated systems, we take advantage of the MH algorithm introduced in section 1.3 for sampling the entropy distributions. This method allows us to get access to rare fluctuations far from equilibrium more efficiently (compared to evolving the system for extremely long time.)

Fig. 2.7 shows the sampled distributions for entanglement (a) observational (b) entropy. We take the same system and Hamiltonian parameters as those in Figs. 2.5 and 2.6. For both entropies we take two cases for the position

coarse-graining and subsystem size. In Fig. 2.7 (a), entanglement entropy with subsystem of two different sizes $\Delta = 4$ and 8 sites, sampled using $\beta_{MC} = 26$ and 40 shown in blue and orange respectively. In Fig. 2.7 (b), observational entropy with two different position coarse-grainings $\Delta = 4$ and 8 sites, sampled using $\beta_{MC} = 50$ and 57 is shown in blue and orange respectively. The non-zero value of β_{MC} in all cases led to having an acceptance rate $\alpha \simeq 50\%$ and resulted in a biased sampling such that the lower values of entropies are more likely to be sampled. As a result, in obtaining the final distribution one must compensate for this bias, according to the β_{MC} values used in sampling.

In all cases, an approximately linear left tail is an indication of the fact that the decreasing of (observational or entanglement) entropy is exponentially unlikely. This is a qualitative result that hints at the existence of a fluctuation theorem, similar to the aforementioned FT, that holds for truly isolated systems"driven" out of equilibrium by their unitary evolution.

2.3.2 Typical fluctuations

Before discussing the dependencies of extreme fluctuations on system size and temperature, let us take the rare cases aside for the moment and understand the behavior of typical fluctuations in entanglement and observational entropy throughout the unitary evolution of an isolated system. We take two cases of fixed particle density $n/L = 1/3, 1/2$. We vary n from 2 to 7 particles in system of

varying size L between 6 and 15 sites. The rest of the parameters are the same as the ones described in the beginning of section 2.3.

Fig. 2.8 illustrates the dependence of relative standard deviation of entropies $\delta(S)$ on system size L in a semi-log plot. $\delta(S) \equiv \sigma(S)/\bar{S}$ where $\bar{S}$ is the average value of entropy values (which is approximately the value of entropy at equilibrium) and $\sigma(S)$ is the standard deviation of entropy. For a given particle density, fluctuations of entanglement entropy seem to be larger than than of observational entropy (entanglement entropy shown as gray and red marks and observational entropy as light and dark blue for $n/L = 1/3$ and $1/2$ respectively). The dashed lines are the linear fit which indicate an exponential dependence of relative fluctuations of entropy on system size, in other words $\delta(S) \propto e^{-cL}$ with c being a constant corresponding to the slope of the linear fit. This is in contrast with fluctuations of quantities such as particle density and internal energy in classical systems which are proportional to $1/\sqrt{L}$ [300, 213].

For comparison, Fig. 2.8 also illustrates the relative standard deviation of an observable, in this case, the particle density of site number 2, $< n_2 >$. For two cases of fixed $n/L = 1/3, 1/2$ (represented as pink and purple marks). It is indicated again by Fig. 2.8 that $\delta(< n_2 >) \propto e^{-c'L}$ [70] (with c' representing the slope of the linear fit) and hence both (observational and entanglement) entropy and particle density decay exponentially with system size, altough at different rates. As Ref. [70] explains, these fluctuations should not be confused with the

fluctuations of observables that one observes from measurements in which case the fluctuations are larger and decay as $1/\sqrt{L}$.

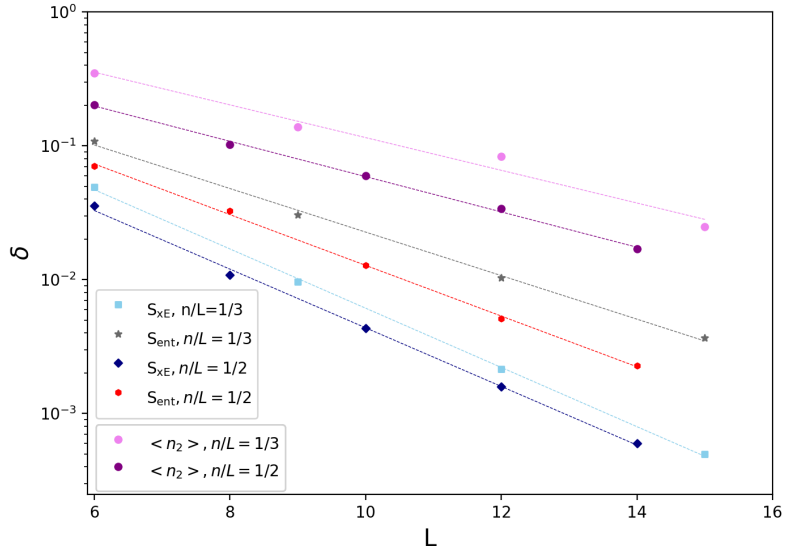

Figure 2.8: Relative fluctuations (δ) of observational and entanglement entropy as well as particle density $< n_2 >$ are shown as a function of system size L. Two cases of fixed $n/L = 1/2, 1/3$ are considered. The relative fluctuations in entropy $\delta(S) \equiv \sigma(S)/\bar{S}$ decay exponentially with L similar to that of the chosen observable, $< n_2 >$. The fluctuations in entanglement entropy seemed to be larger than that of observational entropy given the same n/L.

2.3.3 Dependence of extreme fluctuations on the system size

Next, we study the dependence of the minimum, maximum, and mean values of entropy on the system size. The minimum and maximum values are found using the minimization algorithm as in figures 2.5 and 2.6, and the average value is found by evolving the system for a long time.

These values are shown for entanglement entropy in Fig. 2.9. The size of the subsystem is kept fixed at $\Delta = 4$ while the system size (and hence the bath size)

is varied such that $8 \leq L \leq 28$. The number of particles and inverse temperature are kept fixed at $n = 2$ and $\beta = 0.01$ respectively. For each L, we initialize the state in 6 different complex RPTS, then find the minima, maxima, and average values of entropy for each one of them. The plotted mean value is taken over these six minima, maxima, and average. The standard deviation (denoted as error bars) for a given system size L is also shown.

The first observation is the decrease of the minimum entanglement entropy with system size L. As we discussed in the previous section in relation with Fig. 2.5, the entanglement between the subsystem and the bath is reduced mostly by moving all the particles into the bath. It is clear that as the bath (of size $L - \Delta$ where Δ is fixed) gets larger, it becomes easier to cluster all the particles in the larger bath, which makes the subsystem emptier, thus creating a state that resembles very closely a product state, and thus has a very small entanglement entropy.

It is important to emphasize that reduction in entanglement entropy is not achieved through disentangling the particles, but by disentangling the regions through the means of particles hopping and emptying the smaller region. Therefore the following question is raised: how much entropy would be reduced if particles' hopping between the regions was forbidden? A simulation of this case – where the hopping terms between the two regions are zero – revealed that the reduction of entanglement entropy is much smaller: about a 20% reduction.

On the other hand, maximum entanglement entropy stays constant and independent of system size. The upper bound on entanglement entropy is derived in later chapter 4.3 for closed, fermionic and bosonic systems [114]. Specifically, in Fig. 2.9, where a (one-dimensional) fermionic lattice is considered, we have

$$S_{\text{ent}}(\max) \leq \ln \sum_{n_A=0}^{n} \min \left\{ \binom{\Delta}{n_A}, \binom{L-\Delta}{n-n_A} \right\}. \tag{2.5}$$

In the case of $n = 2$ and $\Delta = 4$ explored in Fig. 2.9, $S_{\text{ent}}(\max)$ achieves exactly this upper bound at $\ln 6 = 1.79$. The upper bound (2.5) is independent of the size of the bath in the limit of large L, which explains the constant maximum value in Fig. 2.9 (the large L in this case is already $L \geq 12$, and $L = 8$ gives coincidentally the same value).

We should also note that relation (2.5) only depends on a few parameters, namely the size of the total system, size of the subsystem, the total number of particles (which is assumed to be fixed), and the assumption that the system is pure. Hence, it does not matter where the subsystem or bath is placed inside the system (for example in the middle or at the edge of the lattice).

The average entanglement entropy in the high temperature limit should be approximately equal to the thermodynamic entropy of the subsystem [253, 81, 330], which is a fraction of the total thermodynamic entropy (2.3).

This has been confirmed in various numerical simulations [291, 334, 181]. We see that this prediction, plotted as a red dashed line in Fig. 2.9, fits quite well with the data. (The relation (2.3) is only approximately true in the high

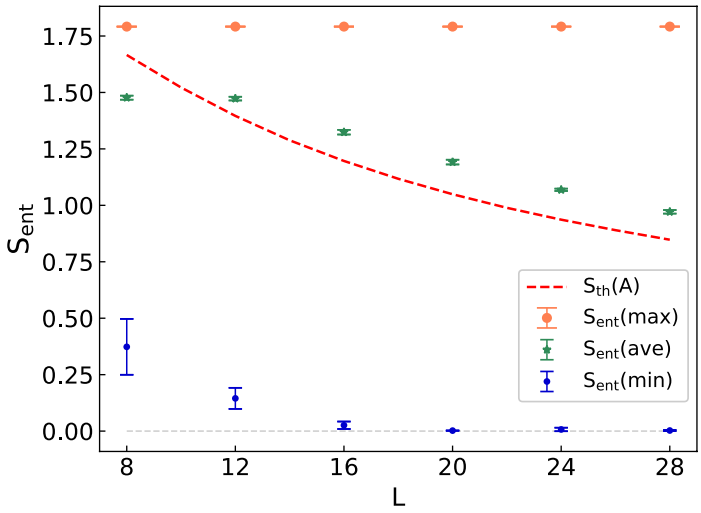

Figure 2.9: The minimum (blue dots), maximum (orange circles), and average (green stars) values of entanglement entropy is computed for 6 different initial random states (complex RPTSs); the mean and standard deviation of these 6 values are illustrated in this figure for various system sizes. $S_{\text{ent}}(\text{min})$ approaches zero in the limit of large L: disentanglement of the two regions is mostly done by moving the particles into the bath and emptying the subsystem and in this limit: almost all particles are in the bath and none in the subsystem. Hence $S_{\text{ent}}(\text{min})$ reaches zero. In contrast $S_{\text{ent}}(\text{max})$ is independent of L (and hence the size of the bath): maximum entanglement is achieved when particles are equally distributed in each region, and enlarging the bath, given this distribution of particles, does not affect the entanglement entropy of the system. $S_{\text{ent}}(\text{ave})$ decreases with L, and is expected to approach zero for large system sizes as almost all particles on average would be in the bath when the system is large and the subsystem is small. We also plot the thermodynamic entropy (2.3) of the subsystem during equilibrium (red dashed line), which is expected to equal $S_{\text{ent}}(\text{ave})$ in the limit of large system sizes and high temperatures (see Eq. (2.3)). Noticeably lower value of $S_{\text{ent}}(\text{ave})$ (by about $\ln 2$) for $L = 8 = 2\Delta$ is due to Page curve [228]. We stress that maximal entanglement entropy does not equal the average.

temperature limit and not the low temperature limit, as is discussed in [147, 164].)

Comparing the maximum value of entanglement entropy with the average, we note that $S_{\text{ent}}(\text{max})$ is constant while $S_{\text{ent}}(\text{ave})$ decreases with L. This is expected, since the average state spreads the particles uniformly over the entire system (creating less entanglement between the subsystem and the bath), while maximizing entanglement entropy maximizes correlations among particles in the

two regions, A and B, such that the probability of measuring n_A particles in sublattice A (which must be the same as the probability of measuring $n - n_A$ particles in sublattice B) follows the relation (4.15). This is discussed in more detail in section 4.3.

Using the same procedure, we find the mean values of minima, maxima, and averages of S_{xE}, and their variances, and plot them as a function of the system size in Fig. 2.10. Partitions have equal sizes fixed at $\Delta = 4$ and the system size L (and therefore the number of partitions $m = \frac{L}{\Delta}$) is varied.

The minimum values of observational entropy S_{xE} reduces to about a half of its maximum value independent of the system size, as long as it is large. These values could be indirectly estimated by simply assuming that the spatial localization is key in minimizing the entropy (see Fig. 3.3 and Eqs. (3.1) and (3.2)).

The maximum value of S_{xE} is almost exactly the same as the thermodynamic entropy of the full system, and very close to the average value of S_{xE}. This is expected from the theory [269], that shows $S_{\mathrm{xE}}(\mathrm{ave}) \leq S_{\mathrm{xE}}(\mathrm{max}) \lessapprox S_{th}$, and $S_{\mathrm{xE}}(\mathrm{ave})$ differs from thermodynamic entropy S_{th} by order-1 corrections (that depend on the energy distribution of the initial state), by $\ln N$ corrections (that depend on how close the initial state is to the thermal state), both of which become irrelevant in the thermodynamic limit, and by finite-size corrections (coming from interaction energy between partitions), which become irrelevant when partitions

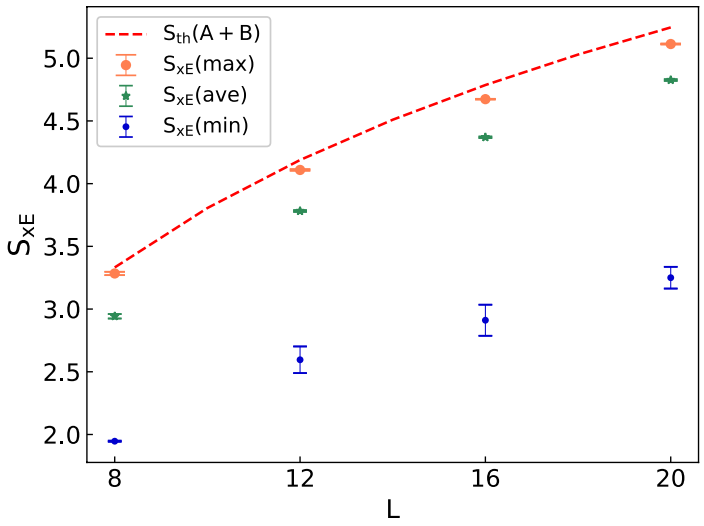

Figure 2.10: The minimum (blue dots), maximum (orange circles), and average (green stars) values of observational entropy S_{xE} is computed for 6 different initial random states(complex RPTSs); the mean and standard deviation of these 6 values are illustrated in this figure for various system sizes. Partitions have equal sizes fixed at $\Delta = 4$. All $S_{\mathrm{xE}}(\mathrm{min})$, $S_{\mathrm{xE}}(\mathrm{ave})$, $S_{\mathrm{xE}}(\mathrm{max})$ increase with L, and $S_{\mathrm{xE}}(\mathrm{ave}) \approx S_{\mathrm{xE}}(\mathrm{max})$ are approximately equal the thermodynamic entropy of the full system $S_{th}(A+B)$, as expected from the theory.

are large enough.

2.3.4 Dependence of extreme fluctuations on temperature

Now, we look at the dependencies of the average and both extremes of S_{ent} and S_{xE} on inverse temperature β. Each data point in Figures 2.11 and 2.12 are computed by taking the mean of the min, max, and average entropies over 6 different complex RPTSs. We also included the thermodynamic entropy of the subsystem, $S_{\mathrm{th}}(A)$, and of the total system, $S_{\mathrm{th}}(A+B)$, in Figures 2.11 and 2.12 respectively.

Fig. 2.11 plots the entanglement entropy versus β. As one would expect,

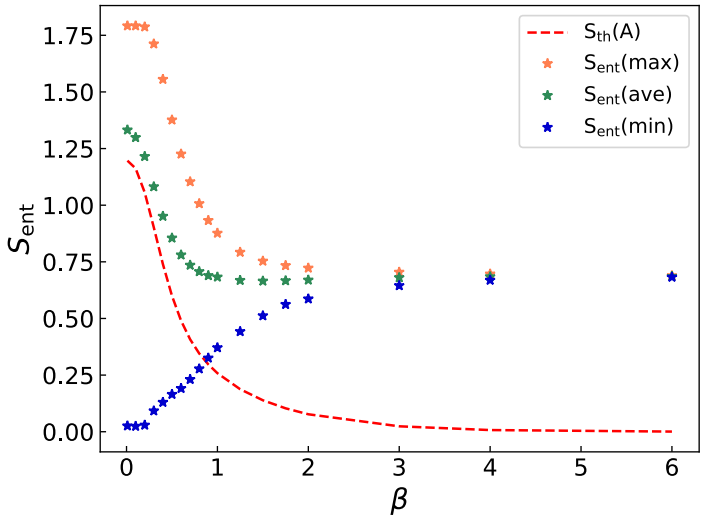

Figure 2.11: The minimum (lower blue stars), maximum (orange upper stars), and average (green middle stars) values of entanglement entropy is computed for 6 different initial random states (complex RPTSs); the means of these 6 values are illustrated in this figure for various inverse temperatures, β. We take $L = 16$, $\Delta = 4$, and $n = 2$. In low β limit, $S_{\text{ent}}(\text{ave})$ follows the volume law, and is approximately equal the thermodynamic entropy of the subsystem $S_{th}(A)$. In high β limit, the initial state is practically the energy ground state, and therefore it does not evolve, so all values coincide, at a value given by the area law.

there are high fluctuations in the low β (high temperature) limit. In this limit, the average entanglement entropy coincides with the thermodynamic entropy of the subsystem, which is known as the Volume law [228]. Both maximal and minimal entanglement entropy diverge from the average at low β, and are almost constant in this limit: $S_{\text{ent}}(\text{max}) \approx 1.79$ (which is the high-temperature limit obtained previously in Fig. 2.9), and $S_{\text{ent}}(\text{min}) \approx 0.05$. There are almost no fluctuations in the opposite high β (low temperature) limit, where the thermal state is almost identical to the ground state, and therefore it does not evolve. The entanglement entropy approaches a constant value given by the Area law [102, 188, 64]. The

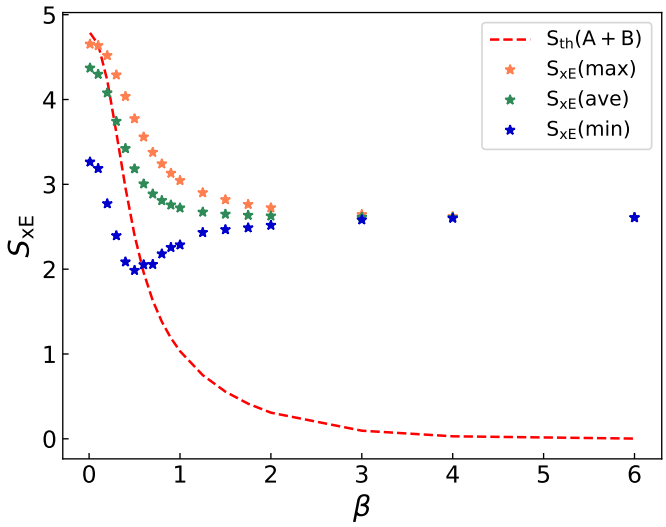

Figure 2.12: The minimum (blue lower stars), maximum (orange upper stars), and average (green middle stars) values of observational entropy $S_{\rm xE}$ is computed for 6 different initial random states (complex RPTSs); the means of these 6 values are illustrated in this figure for various system sizes. We take $L = 16$, $\Delta = 4$, and $n = 2$. In low β limit, $S_{\rm xE}(\text{ave}) \approx S_{\rm xE}(\text{max}) \approx S_{th}(A+B)$, and $S_{\rm xE}(\text{min})$ has the same shape, and about a half of the maximum value, as expected from Eqs. (3.1) and (3.2). All values coincide in the high β limit where the initial state is practically the energy ground state. Its higher value compared to $S_{th}(A+B)$ is expected from the fact that measuring position of this highly non-local state first, creates a large uncertainty in energy, and therefore also large $S_{\rm xE}$. The dip in $S_{\rm xE}(\text{min})$ is the result of two competing factors: higher temperature results in higher entropy on average, but also higher ability of the system to localize, and therefore possibly lower values of $S_{\rm xE}$. $\beta \approx 0.5$ is the lowest possible temperature such that the state can localize in one of the bins of size $\Delta = 4$.

difference between entanglement entropy and thermodynamic entropy is discussed in more detail in [164].

Fig. 2.12 plots the observational entropy $S_{\rm xE}$ versus β, and we took the same settings as with entanglement entropy. One can notice two interesting features in this graph. First, values of $S_{\rm xE}$ at high β (low temperature) limit are quite large, and do not seem to follow the $S_{th}(A+B)$ anymore. The fact that the S_{xE} is not zero in this low temperature limit is because measuring position does

not commute with measuring energy. By measuring the position of the ground state, which is highly non-local, one would add a lot of energy to it, as well as uncertainty in energy. Therefore, since S_{xE} measures the total uncertainty when measuring the position first and then energy, this total uncertainty will be large. S_{xE} can be also interpreted as a thermodynamic entropy of the system, as if the numbers of particles in each bin were fixed, but the energy between the bins was still allowed to exchange [268, 168, 269]. It therefore makes sense that the value of this entropy is relatively large, since by measuring the position we fix the number of particles in each bin, and this state has a relatively large thermodynamic entropy. This effect is smaller (S_{xE} for high β is smaller), when size of the partition Δ becomes large compared to the size of the full system, since position measurement does not affect energy as much in that case. We note that this is a purely quantum effect, however, switching the order of coarse-grainings (while taking some small coarse-graining of width ΔE in energy as well), S_{Ex} leads to an entropy that is bounded above by $S_{th}(A+B)$ even at such low temperatures. This is because measuring energy of a ground state does not affect this state at all, and additional measurement in position does not add any new information (see Theorem 8 in [269]). This effect was not noted in the original paper [269], mainly because defining microcanonical entropy at such low temperatures is problematic, as the energy density of states is not well defined.[4]

The second interesting feature of this graph is the dip in $S_{\mathrm{xE}}(\mathrm{min})$ at

[4]Fig. 7 in [269] does not show S_{xE} nor microcanonical entropy for really low, or really high energies E.

$\beta \approx 0.5$. This dip is a result of two competing factors: first, by increasing the temperature, we increase the ability of the system to localize. Generally, localizing the system in one of the partitions leads to a decrease in S_{xE} (see 3.0.2). Thus, with high enough temperature the system is able to localize in one of the partitions of size $\Delta = 4$ and decrease the entropy. However, further increasing temperature does not help in decreasing $S_{\mathrm{xE}}(\mathrm{min})$ anymore, as the further ability to localize is already below the resolution of the positional coarse-graining in S_{xE}, and its only effect is then an increase in the total thermodynamic entropy, and hence also an increase $S_{\mathrm{xE}}(\mathrm{min})$. That is also why we see the increase in $S_{\mathrm{xE}}(\mathrm{min})$ for really high temperature (low β), in a shape that approximately follows Eqs. (3.1) and (3.2).

2.3.5 Discussion

To complete our analysis of our findings here, we refer to the depction 2.13. In particular, Fig. 2.13 (a) and (b) show entropies for various types of macrostates, described by their particle density, in order of smaller to higher entanglement and observational entropy, respectively. From the Boltzmann point of view, the size of the macrostate is determined by the number of microstates corresponding to the same macroscopic appearance: in this figure, size of the macrostate Ω is the number of orthogonal quantum states that give the same distribution of particle density.

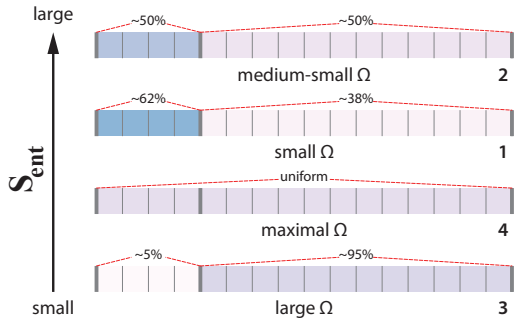

(a)

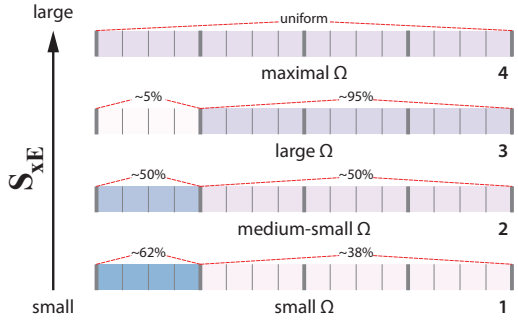

(b)

Figure 2.13: This illustration shows entropies for various types of macrostates described by distributions in their particle density, in order of smaller to higher (a) entanglement entropy and smaller to higher (b) observational entropy. This is done as follows: we compute different types of microstates: state (1) of minimal S_{xE}, state (2) of maximal S_{ent}, state (3) of minimal S_{ent}, and equilibrium state (4) – which is practically identical to the state of maximal S_{xE}. We then plot their particle density and the percentages of the total number of particles in each subsystem. Each distribution of particle density defines a macrostate. The number of microstates that would lead to the same distribution of particle density defines the size of the macrostate, and is denoted Ω. The Boltzmann entropy of a macrostate is then defined as $S_B = \ln \Omega$. In (a), the bottom lattice corresponds to the case of state (3) of minimal S_{ent}: most particles are localized in the bath, and as a result the size of this macrostate is large compared to the other cases. The top lattice corresponds to the case with the state (2) of maximal S_{ent}: in this case the average number of particles in the bath is the same as the average number of particles in the subsystem. This configuration is different than that of the equilibrium state (4), in which case particles are distributed uniformly. In (b), larger macrostates correspond to larger observational entropy, showing correspondence with Boltzmann entropy $S_B = \ln \Omega$.

One notices that higher entanglement entropy does not necessarily mean that the macrostate is larger – the size of the macrostate appears to be rather

unrelated to the amount of entanglement entropy. Specifically, it would be more likely to observe a state with minimal entanglement entropy as compared to the maximal entanglement entropy (as the former has a larger macrostate). The size of the macrostate and the entropy of the state match for the case of observational entropy, showing that (quantum) observational entropy matches well with the classical conception of Boltzmann entropy.

It should be noted that in this thesis we focused on bipartite entanglement entropy, since it is very often used in literature. One could argue that multipartite entanglement entropy, defined as the sum of local von Neumann entropies, could behave similarly to S_{xE} and be more Boltzmann-like, meaning that the larger macrostates have associated higher values of entropy. [5]

Because of its close relation to Boltzmann entropy, observational entropy could accompany the entanglement entropy to better understand the concept of thermalization in isolated quantum systems, and to illuminate the behavior of out-of-equilibrium states which lie at the heart of statistical mechanics. This entropy is also rather new in the field of quantum thermodynamics and hence further work on this particular entropy is of interest

[5] This property would be however dependent upon having equally-sized regions, and the equivalence would break even when the size of a single region is different from others.

Chapter 3

Maximal probability of localization

3.0.1 Overview

In this chapter we show numerically that the result of Deutsch et al. [83] – shown analytically for a toy model with random energy eigenvectors as well as for a non-degenerate weakly interacting gas – holds true for a physical system of a fermionic lattice. We show exolicitely the connection, already hinted in the previous chapter, between the spatial localization and the minimization of entropies.

In particular, Deutsch et al. showed that starting from a RPTS, under certain conditions, the maximum probability $P_{\max} \equiv P_{(N,0)}$ that all particles are localized into the subsystem of interest is 1/2 in the case of initial real RPTS and $\pi^2/16$ in the case of complex RPTS. We show that this localization is key in minimizing S_{xE}.

3.0.2 Role of localization in extreme values of entropies

We are going to require that the same conditions as in [83] to be satisfied: The first condition is that the dimension M of the subspace X (the subspace of Hilbert space associated with "all particles being in the subsystem of interest") is much smaller than the dimension N of the full system, $N \gg M^2$, which can be for example satisfied in the case of dilute gas (small number of particles) when the size of the subsystem of interest Δ into which we localize the particles is much smaller than the size L of the full system, $L \gg \Delta$. At the same time, the second condition is that the size of the subsystem is much larger than a thermal wavelength (specified below), $\Delta \gg \lambda_T$. The third condition is that the size of the subsystem of interest, Δ, is also much greater than the scattering length, i.e., we consider the Hamiltonian with only local interactions, leading to a weakly correlated system. However unlike what is used in [83] – in which the energy eigenstates of the toy model are randomly distributed or are that of a non-degenerate weakly interacting gas – in our case the energy eigenstates are that of a Hamiltonian modeling a fermionic lattice.

First, we investigate the second condition, $\Delta \gg \lambda_T$ in more detail. At any value of β, there exists a spatial scale known as the thermal wavelength such that $\lambda_T \propto \sqrt{\beta}$ (for example, in the case of an ideal gas, $\lambda_T = 2h\sqrt{\frac{\beta}{2m}}$). Qualitatively, λ_T is the minimum size of quantum wavepackets that describe the particles in a given system at a given temperature. Because of this relation between λ_T and

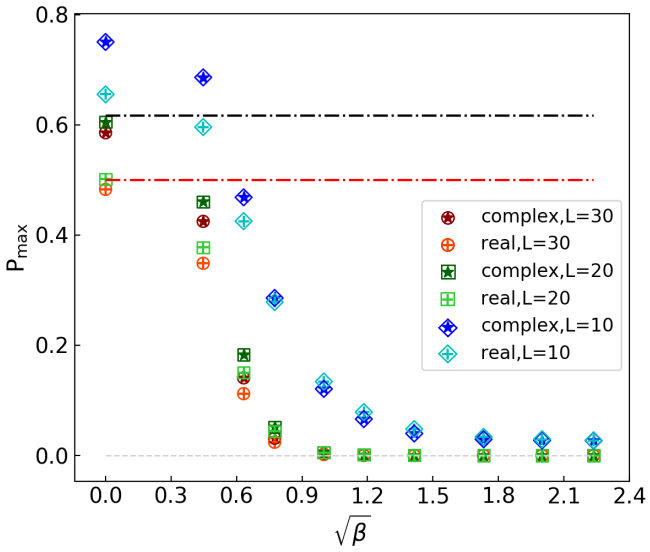

Figure 3.1: Maximum probability $P_{\max}$ of localizing all particles in the middle 5 sites for real (crosses) and complex (stars) initial RPTSs, in a lattice of size L=10 (blue diamonds), 20 (green squares), and 30 (red circles), with 3 particles as a function of $\sqrt{\beta}$. This plot illustrates that at low β, $P_{\max}$ approaches different constant values for real (0.5 red lower line) and complex ($\pi^2/16$ black upper line) RPTSs when the system size is large enough. In the same limit, $P_{\max}$ approaches unity for smaller systems. For higher values of β, $P_{\max}$ approaches zero independent of system size.

$\sqrt{\beta}$, we can focus on the dependence of $P_{\max}$ on $\sqrt{\beta}$.

Therefore, in Fig. 3.1 we study the maximum probability $P_{\max}$ of localization for different values of $\sqrt{\beta}$ while fixing the size of the box Δ. We localize in the region of size $\Delta = 5$, and use the lattice sizes $L = 10$, 20, and 30, with $n = 3$ particles inside. We do this for both real and complex initial RPTSs.

We see that for cold systems (high β), the probability of localization is very small, in fact, $P_{\max}$ approaches zero. This is in accordance with the result of [83] which asserts that, in the limit of large $\sqrt{\beta}$ such that $\Delta \ll \lambda$, $P_{\max} \propto (\frac{\Delta}{\lambda_T})^{N_p d/2}$ where d is the dimension of the lattice (in our case $d = 1$). Intuitively, since λ_T is the minimum size of quantum wavepackets, it makes sense that one can not

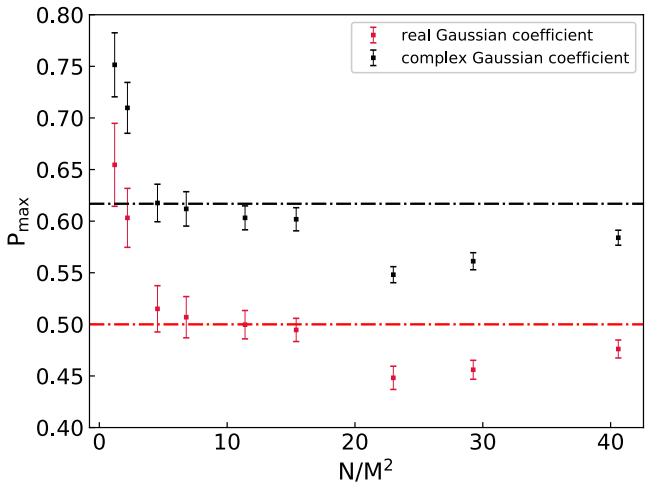

Figure 3.2: The maximal probability $P_{\max}$ is computed for a range of dimensions of Hilbert space N, while M — dimension of the subspace of the Hilbert space associated with "all particles in the localized region" — is kept fixed. Hence the size of the physical region in which particles are localized in is kept fixed as well, at $\Delta = 5$ sites. For each N, we start in 100 different real and complex RPTSs with the same temperature, and plot the mean and standard deviation of $P_{\max}$ (the red lower set of bars as real, and the upper set of black bars as complex). This plot indicates that in the limit of large system sizes, the maximum probability of localization of all particles into a small region approaches ~ 0.5 (red lower line) in the case of real initial states and $\sim \pi^2/16$ (black upper line) in the case of complex initial states.

localize the wavefunction in a subspace smaller than this length scale.

For hot systems (low β), the probability of localization $P_{\max}$ achieves high values. One notices that for small systems for e.g. $L = 10$, the gap between $P_{\max}$ for the real and complex wave functions disappears. This is trivial, since in this case, the size of the subsystem of interest is becoming comparable to that of the full system, and therefore it is very easy to localize all particles in it. For larger system sizes for e.g. $L = 20, 30$ all three conditions stated above are satisfied, and $P_{\max}$ approaches constant values of $\sim 1/2$ in the case of real RPTSs and $\sim \pi^2/16$ in the case of complex RPTSs. The low β regime is further explored in Fig. 3.2.

To generate this graph, we used the same algorithm to maximize probability as the one used in [83], and $\beta = 0.01$. We start in 100 different real and complex RPTSs, and for each one of them we perform the maximization procedure. We use three fermions and choose the small region to be $\Delta 5$ sites. $P_{\max}$ is plotted as a function of N/M^2 for both cases of complex and real RPTSs.

As one can see, when the system is hot enough, it is possible to localize all the particles into the small region, and the probability that we find them there is at most $1/2$ and $\pi^2/16$ for real and complex RPTSs respectively. The presence of some fluctuations is expected since our model is a real system with non-random energy eigenvectors. This numerically confirms that the results of Deutsch et al. [83] also holds for a realistic quantum thermodynamic system such as ours, and we can apply this result in the next section.

In figures 2.5 and 2.6 we showed that minimizing entanglement and observational entropy leads to a substantial probability of localization in the larger and smaller regions respectively. In this section, we investigate what happens to entanglement entropy when one localizes particles into the small region as opposed to the bath, and the extent to which the spatial localization plays a role in minimizing the S_{xE}.

We compute entropies of localized states, for $\Delta = 4$ and varying system sizes L. We consider $n = 2$ particles in the system, and temperature is fixed at $\beta = 0.01$, so that the three conditions from the previous section are satisfied.

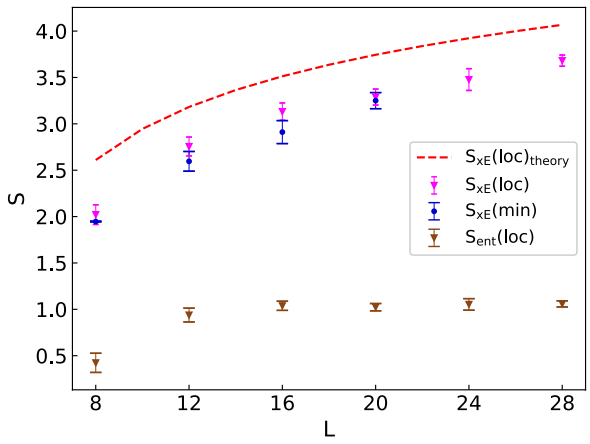

Figure 3.3: $n = 2$ particles are localized in the first 4 sites for varying system sizes L. S_{xE} and S_{ent} of such a state (i.e., when $P_{\max}$ is achieved) are computed and are respectively named $S_{\mathrm{xE}}(\mathrm{loc})$ and $S_{\mathrm{ent}}(\mathrm{loc})$. This is done for 6 different complex RPTSs. What are illustrated here are the mean and standard deviation of these 6 values. For comparison purposes, minimum values of S_{xE} achieved using optimization algorithm, $S_{\mathrm{xE}}(\mathrm{min})$, are also plotted. Comparing these minima with corresponding $S_{\mathrm{xE}}(\mathrm{loc})$ for each system size, one finds that these values are relatively very close to each other. This is an evidence of the key role of spatial localization in minimizing observational entropy. In contrast, entanglement entropy grows to a constant value. This is related to the fact that entanglement entropy depends heavily on the distribution of particles for a given state. When the probability of localization is maximized for large system sizes, this distribution is fixed and independent of system size. We therefore expect entanglement entropy of such localized states to also reach a constant value independent of system size.

For each L, we start in 6 initial complex RPTSs, and localize them into a physical region of fixed size $\Delta = 4$, by maximizing probability $P_{\max}$ for each initial state. We then compute the mean values and standard deviations of S_{ent} and S_{xE} of such localized states, and plot them in Fig. 3.3. The mean values of $P_{\max}$ (averaged over 6 initial RPTSs) for system sizes of $L = [8, 12, 16, 20, 24, 28]$ are $P_{\max} = [0.90, 0.73, 0.67, 0.67, 0.65, 0.63]$.

$S_{\mathrm{xE}}(\mathrm{loc})$ is very close to the minimum $S_{\mathrm{xE}}(\mathrm{min})$ (discussed in detail in Fig. 3.3), showing that spatial localization is key in minimizing S_{xE}. The theory

predicts [83]

$$\begin{aligned} S_{\mathrm{xE}}(\mathrm{loc}) &= S_{\mathrm{th}}(L,n,\beta) \\ &\quad - P_{\max} n \ln \tfrac{L}{\Delta} - (1-P_{\max}) n \ln \tfrac{L}{L-\Delta} \\ &\quad - P_{\max} \ln P_{\max} - (1-P_{\max}) \ln(1-P_{\max}), \end{aligned} \tag{3.1}$$

for large L (where $S_{\mathrm{th}}(L,n,\beta) \equiv S_{\mathrm{th}}(A+B)$), which is bounded below by

$$S_{\mathrm{xE}}(\mathrm{loc}) \geq (1-P_{\max}) S_{\mathrm{th}}(L,n,\beta), \tag{3.2}$$

which shows that $S_{\mathrm{xE}}(\mathrm{loc})$ cannot fall below a certain fraction of the total thermodynamic entropy of the system. Eq. (3.1) is plotted as a dashed line in Fig. 3.3 and as expected from Eq. (3.2), the ratio $R = S_{\mathrm{xE}}(\mathrm{loc})/S_{\mathrm{th}}(A+B)$ remains approximately constant for large L.

The fact that $S_{\mathrm{xE}}(\mathrm{loc})$ and $S_{\mathrm{xE}}(\mathrm{min})$ are almost the same and that $S_{\mathrm{xE}}(\mathrm{min})$ is bounded by a fraction of thermodynamic entropy also explains why the minimum of S_{xE} in Fig. 2.6 does not go to zero, and why $S_{\mathrm{xE}}(\mathrm{min})$ in Fig. 2.12 goes upwards for small β (in the case of low β $P_{\max} = \pi^2/16$).

3.0.3 Discussion

We end this chapter by a discussion on the interpretation of our results accompanied and supported by the original work on the role of localization in entropy fluctuations [83]. We numerically confirmed for the case of a one-dimensional lattice that $S_x E$ can not fluctuate down more than about 50%, given that the initial

state was in equilibrium and not in a low entropy state.[1]

In comparing to the classical case, this demonstrate an importance difference in that a chaotic classical system will eventually explore all accessible phase space whereas in the quantum case, as we have shown by choosing an appropriate measure S_{xE}, the system would like explore subspaces of size $M^2 \ll N$ with at most 50% chance. This result seems to be a unique feature of quantum mechanics (for instance, due to the presence of superposition, particles can be at different positions simultaneously, which leads to increasing the entropy with postion coarse-graining.)

In the context of cosmology, as introduced in section 1.1, the Past Hypothesis states that an extremely low entropy state is required for explaning the evolution of our universe and the existance of the *arrow of time*. One resolution for this fined-tuned initial condition is a rare and extreme localization of matter and energy out of equilibrium. Assuming the universe is an isolated quantum system with well-defined wavefunction[2] and taking S_{xE} as a measure of such localization, our result [83] adds to the implausibility of the aformentioned reslution to the Past Hypothesis.

[1] In the case of low entropy initial state, according to Poincaré recurrence theorem, the system will eventually visit the initial state given long enought time.

[2] How one can assig a wavefunction to the universe including all observers is an open and subtle questions [153, 226].

Chapter 4

Maximum entanglement in closed systems

4.1 Overview

In this chapter, we present a motivation for a precise formulation of a tight upper bound on entanglement entropy for systems constrained to conservation laws. We then provide an analytical proof of such an upper bound and confirm numerically that the entanglement entropy in a subsytem of one-dimensional fermionic lattice can achieve this bound throughout its unitary evolution.

4.2 Motivation

Entanglement is one of the most intriguing characteristics of quantum systems. It evolved from its perception as a mathematical artifact, as a result

of EPR paradox [235], to becoming closely related and applicable to the fields of condensed matter [242, 12, 42, 197, 335, 176], quantum information [104, 33, 233, 321, 231, 63, 190], quantum metrology [131, 89, 132, 79, 305, 296], and quantum gravity [85, 297, 88, 281, 236].

In the field of quantum information, entangled states are the backbone of quantum information protocols as they are considered a resource for tasks such as quantum teleportation [33, 161], cryptography [104], and dense coding [36].

In these quantum information protocols, more entanglement usually leads to a better performance. Therefore, it is important to set precise upper bounds on how much entanglement is in principle available in performing these tasks [336, 202, 175, 14, 290, 314, 313, 26, 24, 123, 167, 166].

As different tasks require different types of entangled states, numerous measures of entanglement have been introduced [324, 35, 251, 133]. As discussed in section 1.2, one of the most prominent measure of entanglement is entanglement entropy [243, 314, 313]. It is defined as the von Neumann entropy of the reduced density matrix $\hat{\rho}_A = \mathrm{tr}_B[|\psi\rangle\langle\psi|]$, where $|\psi\rangle$ denotes the state of the composite system,

$$S_{\mathrm{ent}} \equiv S(\hat{\rho}_A). \tag{4.1}$$

This is a valuable measure as it draws a direct connection between density matrix and the amount of non-local correlations present in a given system. Entanglement entropy also gained significant attention in the past few decades due

to the discovery of its geometric scaling in thermal state as well as ground states (famously known as the volume law [228] and the area law [102, 188, 64] respectively), and its use for characterizing quantum phase transition [242, 145, 195, 20].

Despite its importance, this quantity has proven extremely difficult to probe experimentally, and related Rényi-2 entanglement entropy has been measured instead [170, 181, 52]. However, an experimental proposal for measuring the entanglement entropy has been put forward recently [222], opening new exciting possibilities.

There exists a general bound on entanglement entropy. For a pure state of a bipartite system, it is straight forward to show that $S_{\text{ent}} \equiv S(\hat{\rho}_A) = S(\hat{\rho}_B)$. This leads to [236],

$$S_{\text{ent}} \leq \ln \min \Big\{ \dim \mathcal{H}_A, \dim \mathcal{H}_B \Big\}. \tag{4.2}$$

However, one could wonder whether Eq. (4.2) is stringent enough for systems with additional conservation laws, that effectively restrict some degrees of freedom.

For example, consider a system of 2 fermionic particles contained on a lattice comprising of 6 sites, partitioned into two sublattices of 3 sites. Since there can be any number 0, 1, and 2 particles in each sublattice, the upper bound on entanglement entropy given by Eq. (4.2) is $S_{\text{ent}} \leq \ln \left(\binom{3}{0} + \binom{3}{1} + \binom{3}{2} \right) = \ln 7$, yet because of the conservation law, this could be considerably larger than the actually achievable entropy.

This is important because, among the aforementioned quantum tasks, those that incorporate massive particles — such as the constituents of condensed matter systems — often exhibit constrains such as the conservation of the total number of particles or charge [71, 170, 181, 249, 21, 205, 52, 210]. Such restrictions are described by superselection rules [22, 30]. It has been suggested that these restrictions can in fact be used as a resource and can enhance the security of quantum communication [169, 311, 22, 216, 217] and measurement accuracy [28, 143, 29, 31]. However, among the vast literature on quantum information protocols, specific bounds on entanglement entropy in the presence of superselection rules are not sufficient.

Given the commonality of these conservation laws and recent efforts in probing entanglement entropy experimentally, it is an incentive to provide precise bounds for this quantity. In this Rapid Communication, we derive a general tight upper bound on entanglement entropy for closed systems (in thermodynamic sense), which are defined as those where the total number of particles stays constant. This can be applied to quantum systems evolved with a time-independent or a time-dependent Hamiltonian, as long as this evolution conserves the total number of particles.

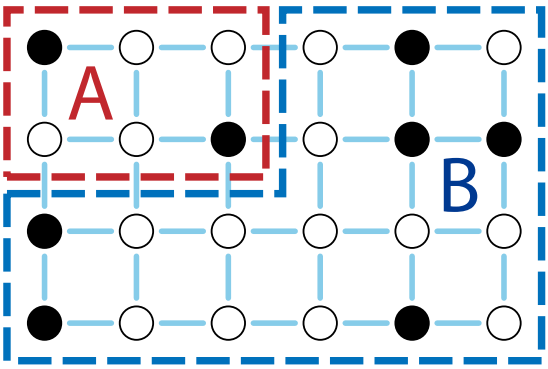

Figure 4.1: A 2-dimensional lattice of size $L = 24$ sites and $n = 8$ particles is shown. The subsystems A and B are also depicted as red and blue regions respectively. The smaller subsystem A has $l = 6$ sites and $n_A = 2$ particles in this example.

For a bipartite system of n spinless particles moving on a system of L number of sites, which is partitioned into two subsystems A and B ($\mathcal{H} = \mathcal{H}_A \otimes \mathcal{H}_B$) with l and $L - l$ number of sites (see Fig. 4.1), assuming that the state of the composite system is pure and that $n \leq l \leq L - l$, the entanglement entropy is bounded by

$$S_{\text{ent}} \leq \ln \sum_{n_A=0}^{n} \min \left\{ \dim \mathcal{H}_A^{(n_A)}, \dim \mathcal{H}_B^{(n-n_A)} \right\}, \tag{4.3}$$

where $\mathcal{H}_A^{(n_A)}$ denotes the Hilbert spaces of exactly n_A particles contained in the subsystem A, and $\mathcal{H}_B^{(n-n_A)}$ denotes the Hilbert space of exactly $n - n_A$ particles contained in subsystem B respectively. This is a tight bound, meaning that it can be saturated with a specific wave function of n particles. An application of this result is shown in Fig. 4.2.

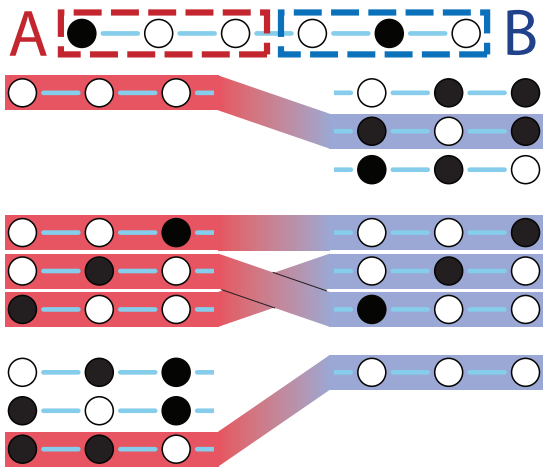

Figure 4.2: A maximally entangled state is such where one has the maximal uncertainty about the state of the full system, but determining the state of subsystem A also determines the state of subsystem B with certainty. This means that when constructing such a state, none of the orthogonal states spanning subsystems A and B can be used twice. But since the conservation law prohibits matching states whose particle numbers do not add up to the total number of particles, the maximal entanglement entropy is lower than initially expected. In this figure, one of the maximally entangled states $|\psi\rangle = \frac{1}{\sqrt{5}}(|000101\rangle + |001001\rangle + |010100\rangle + |100010\rangle + |110000\rangle)$ for the example mentioned in the introduction is shown, leading to $S_{\text{ent}}^{(\max)} = \ln\left(\binom{3}{0} + \binom{3}{1} + \binom{3}{0}\right) = \ln 5$.

The above formula can be generalized to include cases $n > l$, but the fermionic and bosonic cases must be treated separately. For fermionic systems (or systems of hard-core bosons) $\dim \mathcal{H}_A^{(n_A)} = \binom{l}{n_A}$ which leads to

$$S_{\text{ent}} \leq \ln \sum_{n_A=\max\{0,n-L+l\}}^{\min\{n,l\}} \min\left\{\binom{l}{n_A}, \binom{L-l}{n-n_A}\right\}, \tag{4.4}$$

while for bosonic systems $\dim \mathcal{H}_A^{(n_A)} = \binom{l+n_A-1}{n_A}$ which leads to

$$S_{\text{ent}} \leq \ln \sum_{n_A=0}^{n} \min\left\{\binom{l+n_A-1}{n_A}, \binom{L-l+n-n_A-1}{n-n_A}\right\}. \tag{4.5}$$

4.3 Proof

Assuming that $n \leq l$, the Hilbert space of n particles contained on lattice of L sites can be decomposed as

$$\mathcal{H} = \bigoplus_{n_A=0}^{n} \mathcal{H}_A^{(n_A)} \otimes \mathcal{H}_B^{(n-n_A)}. \tag{4.6}$$

This means that any wavefunction $|\psi\rangle \in \mathcal{H}$ can be written as

$$|\psi\rangle = \sum_{n_A=0}^{n} a_{n_A} |\psi_{n_A}\rangle, \tag{4.7}$$

where $|\psi_{n_A}\rangle \in \mathcal{H}_A^{(n_A)} \otimes \mathcal{H}_B^{(n-n_A)}$. Applying the Schmidt decomposition, we can write each of these vectors as

$$|\psi_{n_A}\rangle = \sum_{i=1}^{d_{n_A}} b_i^{(n_A)} |\chi_i^{(n_A)}\rangle \otimes |\phi_i^{(n-n_A)}\rangle \tag{4.8}$$

where $d_{n_A} = \min\left\{ \dim \mathcal{H}_A^{(n_A)}, \dim \mathcal{H}_B^{(n-n_A)} \right\}$, and $\{|\chi_i^{(n_A)}\rangle\}_{i=1}^{d_{n_A}}$ and $\{|\phi_i^{(n-n_A)}\rangle\}_{i=1}^{d_{n_A}}$ form orthogonal sets. , and $\{b_i^{(n_A)}\}_{i=1}^{d_{n_A}}$ are real, non-negative scalars. Also any two vectors $|\chi_i^{(n_A)}\rangle$ and $|\chi_j^{(\tilde{n}_A)}\rangle$, $n_A \neq \tilde{n}_A$, are orthogonal to each other, because they belong into subspaces associated with different eigenvalues n_A of a Hermitian operator $\hat{N}_A$ (measuring the number of particles in sublattice A). The same argument can be made for vectors $|\phi_i^{(n-n_A)}\rangle$ using $\hat{N}_B$. This allows us to compute the reduced density matrix,

$$\hat{\rho}_A = \mathrm{tr}_B[|\psi\rangle\langle\psi|] = \sum_{n_A=0}^{n} \sum_{i=1}^{d_{n_A}} |a_{n_A}|^2 |b_i^{(n_A)}|^2 |\chi_i^{(n_A)}\rangle\langle\chi_i^{(n_A)}|, \tag{4.9}$$

and since vectors $|\chi_i^{(n_A)}\rangle$ are orthogonal to each other, we can also compute the entanglement entropy as

$$S_{\text{ent}} \equiv S(\hat{\rho}_A) = -\sum_{n_A=0}^{n} \sum_{i=1}^{d_{n_A}} |a_{n_A}|^2 |b_i^{(n_A)}|^2 \ln |a_{n_A}|^2 |b_i^{(n_A)}|^2. \tag{4.10}$$

Using Jensen's theorem on the strictly concave function $f(x) = \ln x$, which is a standard procedure for bounding the Shannon entropy, we derive

$$S_{\text{ent}} \leq \ln \sum_{n_A=0}^{n} d_{n_A}, \tag{4.11}$$

which proves the theorem for $n \leq l$. The inequality is saturated if and only if all the probabilities are equal, i.e.,

$$|a_{n_A}|^2 |b_i^{(n_A)}|^2 = \left(\sum_{n_A=0}^{n} d_{n_A} \right)^{-1} \tag{4.12}$$

for all n_A and i. Considering decomposition (4.8), this equation is the sufficient and necessary condition for the state to be maximally entangled in a closed system.

Now let us include cases of $n \geq l$. For a fermionic system, the three cases to consider are: $n \leq l \leq L - l$, $l \leq n \leq L - l$, and $l \leq L - l < n$. Combined, for any $n \leq L$ the Hilbert space can be decomposed as

$$\mathcal{H} = \bigoplus_{n_A=\max\{0,n-L+l\}}^{\min\{n,l\}} \mathcal{H}_A^{(n_A)} \otimes \mathcal{H}_B^{(n-n_A)}. \tag{4.13}$$

The rest of the analysis proceeds analogously and leads to

$$S_{\text{ent}} \leq \ln \sum_{n_A=\max\{0,n-L+l\}}^{\min\{n,l\}} \min \left\{ \dim \mathcal{H}_A^{(n_A)}, \dim \mathcal{H}_B^{(n-n_A)} \right\}, \tag{4.14}$$

with equality if and only if $|a_{n_A}|^2 |b_i^{(n_A)}|^2 = \left(\sum_{n_A=\max\{0,n-L+l\}}^{\min\{n,l\}} d_{n_A} \right)^{-1}$ for all n_A and i. Considering that $\dim \mathcal{H}_A^{(n_A)} = \binom{l}{n_A}$ (combination: the number of ways we can

distribute n_A particles in a sublattice of l sites, where no repetition is possible due to the Pauli exclusion principle or hard-core condition) and $\dim \mathcal{H}_B^{(n-n_A)} = \binom{L-l}{n-n_A}$, we obtain Eq. (4.4).

For a bosonic system, the decomposition of Hilbert space is identical to Eq. (4.6) for any n. The formula therefore remains the same, and considering that for a bosonic system we have $\dim \mathcal{H}_A^{(n_A)} = \binom{l+n_A-1}{n_A}$ (combination with repetition: the number of ways we can distribute n_A particles in a sublattice of l sites, where multiple particles can be in a single site) and $\dim \mathcal{H}_B^{(n-n_A)} = \binom{L-l+n-n_A-1}{n-n_A}$, we obtain Eq. (4.5).

The condition for the maximally entangled state, Eq. (4.12), has an interesting implication. It gives prediction for the number of particles in each of the subsystems: if the state is maximally entangled, then the probability of measuring n_A particles in sublattice A (which must be the same as the probability of measuring $n - n_A$ particles in sublattice B) is equal to

$$p_{n_A} = |a_{n_A}|^2 = \frac{d_{n_A}}{\sum_{n_A=\max\{0,n-L+l\}}^{\min\{n,l\}} d_{n_A}}, \tag{4.15}$$

$d_{n_A} = \min\left\{\binom{l}{n_A}, \binom{L-l}{n-n_A}\right\}$, for the fermionic gas, and

$$p_{n_A} = |a_{n_A}|^2 = \frac{d_{n_A}}{\sum_{n_A=0}^{n} d_{n_A}}, \tag{4.16}$$

$d_{n_A} = \min\left\{\binom{l+n_A-1}{n_A}, \binom{L-l+n-n_A-1}{n-n_A}\right\}$, for the bosonic gas. The mean number of particles in sublattice A is $\overline{n_A} = \sum_{n_A=\max\{0,n-L+l\}}^{\min\{n,l\}} p_{n_A} n_A$ and $\overline{n_A} = \sum_{n_A=0}^{n} p_{n_A} n_A$ (while $\overline{n_B} = n - \overline{n_A}$) for the fermionic and the bosonic gas respectively. Therefore, if a

state of a closed system does not satisfy these properties, it cannot be maximally entangled.[1]

One can also notice that the derived bound stops depending on the total system size L if it is large enough. Specifically, for fermionic systems and

$$L \geq \max\left\{ \max_{n_A \in \{0,\ldots,\min\{n,l\}\}} \left\{ \binom{l}{n_A} \right\}, n \right\} + l, \tag{4.17}$$

the bound becomes

$$S_{\text{ent}} \leq \ln\left(1 + \sum_{n_A=0}^{\min\{n,l\}-1} \binom{l}{n_A}\right), \tag{4.18}$$

which no longer depends on L.

If in addition $n \geq l$, then

$$S_{\text{ent}} \leq \ln \sum_{n_A=0}^{l} \binom{l}{n_A} = \ln 2^l. \tag{4.19}$$

which is equal to the maximal entropy of subsystem $\mathcal{H}_A$. This is the same result that could be recovered from the original bound, Eq. (4.2). Therefore, for fermionic systems with large enough baths (subsystems B), and a large number of particles, these bounds are the same. The same *does not* hold for bosonic systems however, for which $S_{\text{ent}} \leq \ln\left(1 + \sum_{n_A=0}^{n-1} \binom{l+n_A-1}{n_A}\right) < \ln \sum_{n_A=0}^{n} \binom{l+n_A-1}{n_A} = \ln \dim \mathcal{H}_A$, irrespective of n, for large L and $l > 1$. Thus for closed bosonic systems, our bound is always better.

It also turns out that Eq. (4.18) is the value of the bound in the thermodynamic limit, where both the number of particles n and size of the system L

[1] This is necessary, but not a sufficient condition for the state to be maximally entangled. This means that even if the Eqs. (4.15) or (4.16) are satisfied, the state does not have to be maximally entangled. The sufficient and necessary condition is given by Eq. (4.12) for $n \leq l$ and its generalizations for cases $n \geq l$.

grow to infinity, but the particle density $c = n/L$ remains constant, while keeping l constant. This can be shown by dividing condition (4.17) by n and taking the limit, which gives $c \leq 1$, which must be by definition satisfied for any spinless fermionic system.

4.4 Achievability of the bound in 1D fermionic lattice

Here, we illustrate the derived upper bound (4.4) in a simulation. We specifically focus on the case where $n < l \leq L - l$. The other cases turned out to be very similar, and we shall not show them here.

We consider a system of n spin-less fermions in a one-dimensional lattice of size L, with Hamiltonian introduced in section 1.2 and illustrated in Fig. 1.1.

In the simulation depicted in Fig. 4.3, we take $t = t' = 1.9$, $V = V' = 0.5$ [2], and cases with NN hopping only, and with interaction only. The total number of particles is $n = 3$, and we take subsystem A to be the $l = 4$ sites on the left side of the chain, while the full system size L, and inverse temperature $\beta = 1/T$ are both varied.

We take the initial state to be the complex RPTS which is entangled but not maximally entangled. For instance, in the case of $\beta = 0.01$ and a given initial RPTS, the initial entanglement entropies associated with system sizes $L = [8, 9, 10, 11, 12, 13]$ are $S_{\text{ent}} = [2.031, 2.091, 2.118, 2.122, 2.080, 2.020]$. The initial

[2] It does not matter much which particular values we choose, as long as $t, t', V, V' \neq 0$, the evolution is qualitatively the same.

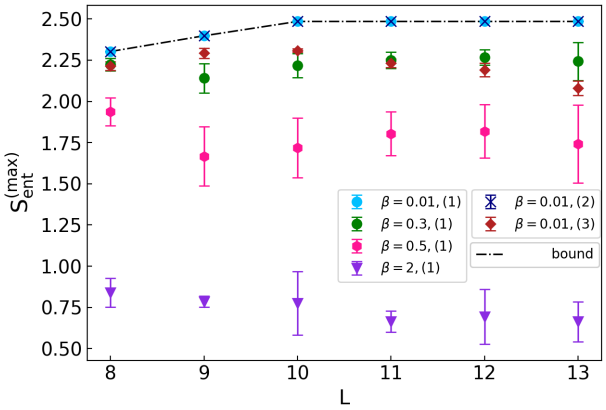

Figure 4.3: $S_{\text{ent}}^{(\max)} = \max_\tau S_{\text{ent}}(|\psi_\tau\rangle)$ for different values of L and β, $n = 3$ particles, for a subsystem A being fixed as the left $l = 4$ sites of the chain. In the low temperature limit, $\beta = 2$, the initial state is close to being a ground state. In the high temperature limit, $\beta = 0.01$, the initial state becomes a *random pure state* [208, 207, 243, 69], in which all the energy coefficients are equal on average. We show cases of (1) non-integrable system ($t = t' = 1.9$, $V = V' = 0.5$) and varying temperatures, and cases of high temperature with (2) NN hopping only ($t = 1.9$, $t' = V = V' = 0$), and with (3) interaction only ($V = V' = 0.5$, $t = t' = 0$). In cases (1) and (2) and high temperature, the maximum value of S_{ent} reaches exactly the theoretical bound (dashed line) for all L, but not in case (3). This shows that the non-zero hopping term is the most important for reaching the maximum.

state is then evolved as $|\psi_\tau\rangle = e^{-i\hat{H}\tau}|\psi\rangle$.

To find the maximum value that S_{ent} can achieve during its time evolution, we use the simplex search algorithm. For a given L and β, we initialize the state in 6 different complex RPTS, and find the maxima for each initial state by maximizing over phases $\phi_E = E\tau$ that appear in the time evolution of the wavefunction, $\hat{U}_\tau = e^{-i\hat{H}\tau}$. As long as the differences of E's are irrational (or close to being to), this method must give the same result as maximizing over all times τ. We do this because maximizing over the time by simply evolving the system would take an extremely long time. We then plot the mean value of these six

maxima as well as the standard deviation (depicted as error bars) in Fig. 4.3. The theoretical bound, Eq. (4.4) for the case where $n < l \leq L - l$, is plotted in the same figure (dashed line) for various values of L.

As Fig. 4.3 illustrates, in the non-integrable case for $\beta = 0.01$ the theoretical bound (4.4) is saturated exactly. For large L the bound flattens, as expected from Eq. (4.18). As the temperature drops, the system can no longer achieve this bound, but the maximum entanglement entropy still stays approximately constant for large L. Interestingly, we found that the upper bound is reached during the unitary evolution also for integrable systems with NN interaction and hopping ($t' = V' = 0$), or even for systems with just the NN hopping term ($t' = V = V' = 0$), but not when there is no hopping, which we can summarize as "As long as there is some hopping, in both cases of integrable or non-integrable systems, the bound is achieved during the unitary evolution, if the temperature is high enough."

Regarding the average number of particles in the subsystem, states for which S_{ent} has reached its maximum in $L = [8, 9, 10, 11, 12, 13]$ were measured to have $\overline{n_A} = [1.50, 1.55, 1.58, 1.58, 1.58, 1.58]$, which corresponds exactly to the prediction of Eq. (4.15).

4.5 Discussion

In this chapter, we derived a tight upper bound on entanglement entropy for bipartite systems with a conserved number of spinless particles. We

showed numerically that at high temperature, the maximum entanglement entropy of a fermionic lattice in fact reaches this upper bound during its time evolution. Furthermore, by studying the maximally entangled states, we found that measuring the particle number in one of the subsystems can serve as a simple test of whether the state can be maximally entangled. In contrast to Ref. [313], which derived bounds for the average entanglement entropy of all eigenstates of quadratic fermionic Hamiltonians, our bound holds for any state in any spinless fermionic and bosonic system with a conserved number of particles, irrespective of the Hamiltonian being used.

Our results can be also directly transferred to lattices of identical spin-1/2 particles with the total spin conserved, where spin-up and spin-down take the place of a particle and a hole respectively, or to lattices of qubits consisting of different energy states (such as cold atoms [42, 170, 181, 49], trapped ions [333, 122, 52], or superconducting qubits [119, 125, 328, 229]), when the total energy, and therefore also the total number of excited states is conserved, while neglecting the interaction energy.

Using that for a pure state $\hat{\rho}_{AB}$, $S(\hat{\rho}_{AB}) = 0$ and $S(\hat{\rho}_A) = S(\hat{\rho}_B)$, a noteworthy consequence of the bound, Eqs. (4.4) and (4.5), is that it sets a lower bound on conditional entropy $S(A|B)_{\hat{\rho}} = S(\hat{\rho}_{AB}) - S(\hat{\rho}_B)$ [61, 257, 323] which gives a sufficient and necessary condition for teleportation [325], and an upper bound on the mutual information $I(A;B) = S(\hat{\rho}_A) + S(\hat{\rho}_B) - S(\hat{\rho}_{AB})$ [307, 257, 78], which

determines the largest possible rate of communication [241, 86, 322], and has applications in quantum machine learning [306, 74, 184].

Another implication of this result is with regards to Rényi entropies of higher order. For a general density matrix, entanglement entropy (Rényi entropy of order $\alpha = 1$) is related to Rényi entropies of higher order, $S_{\alpha>1}$, by inequality $S_{\text{ent}}(\hat{\rho}) \geq S_{\alpha>1}(\hat{\rho})$ [116]. This means that the upper bound on entanglement entropy found in this Rapid Communication could be taken as a loose upper bound on $S_{\alpha>1}(\hat{\rho})$.

This is important due to the existence of experiments involving measurements on Rényi-2 entanglement entropy $S_{\alpha=2}$ [170, 181, 52], which allows us to compare our bound with experimental data. Ref. [170] used a system of ultracold bosonic atoms trapped in an optical lattice, evolving by the Bose-Hubbard Hamiltonian. The maximum Rényi entropy of a ground state for a system of $L = 4$ sites and $n = 4$ particles, and various sizes of subsystems $l = [1, 2, 4]$ was obtained from Fig. 4 in [170] (including an offset of about 0.5) as $S_{\alpha=2} = [0.6, 0.9, 0]$, which is below the bound $S_{\text{ent}}^{(\text{bound})} = [1.6, 2.2, 0]$ calculated from Eq. (4.5). The maximal achieved entropy obtained from Fig. 6 in [170] for $L = n = 2$ and $l = 1$ is $S_{\alpha=2} = 0.8$ which is much closer to the bound $S_{\text{ent}}^{(\text{bound})} = 1.1$. Ref. [181] focused on measuring the Rényi entropy of an evolving system using the same model. The maximum values of the Rényi entropy read out from Fig. 3 in [181] for $L = n = 6$ and $l = [1, 2, 3, 6]$ are $S_{\alpha=2} = [0.8, 1.9, 2.6, 0]$, while the bound gives

$S_{\text{ent}}^{(\text{bound})} = [1.9, 3.0, 3.4, 0]$. Finally, Ref. [52] used a system of trapped ions, each carrying a spin, evolved by an XY Hamiltonian which conserves the total spin. This model is therefore mathematically identical to a lattice of spinless fermions. $L = 10$ atoms were prepared in the Néel state ($n = 5$), and after 5 ms the Rényi entropy was read out for $l = [1, 2, 3, 4, 5, 6, 7, 8, 9]$ (Fig. 2 in [52]) at values scattered around $S_{\alpha=2} \approx [0.6, 1.3, 1.7, 2.1, 2.4, 2.3, 1.9, 1.5, 0.8]$ (recalculated by changing the base of logarithm $\log_2 \to \ln$). These values are comparable but two of them are slightly higher than the bound $S_{\text{ent}}^{(\text{bound})} = [0.7, 1.4, 2.1, 2.8, 3.5, 2.8, 2.1, 1.4, 0.7]$ calculated from Eq. (4.4), due to inadvertently introduced decoherence (the total Rényi entropy was 0.5 at the time of measurement).

Chapter 5

Discussion

Physical systems are commonly in states that are far from equilibrium. This demand for new notions of measures such as entropy that are meaningful out of equilibrium. In this work, we took two definitions of entropy as our case studies that are capable of describing quantum systems in this context. We presented an interpretation of each notion and their differences and discussed to what degree their non-equilibrium behavior carries over from the equilibrium case.

Our numerical work on the extreme fluctuations demonstrated significantly different behavior of extreme values of observational and entanglement entropy. In particular, we found that starting from a typical state, S_{ent} can reach values very close to zero during the course of a unitary evolution, whereas there exists a non-zero lower bound for S_{xE}. We showed how these minimal values of the two entropies are achieved through localization in the larger and smaller region for S_{ent} and S_{xE}, respectively.

We found in the high temperature limit, the maximum entanglement entropy between a smaller subsystem and the rest of the system becomes large in comparison with typical values, and this ratio grows with system size. This is because the typical value is the thermodynamic entropy for the smaller subsystem which will tend to zero as total system size increases, (at fixed particle number and subsystem size) but the maximum S_{ent} goes to a constant independent of total system size. On the other hand, the maximal observational entropy stays close to its typical value. The latter is qualitatively similar to classical Boltzmann entropy: the average – which is close to the most likely state – should be assigned a very high entropy.

The particle distribution given a state with maximum entanglement or observational entropy is also remarkably different: in the former case the particles distribute themselves throughout the lattice such that the average number of particles in the subsystem follows the necessary but not sufficient condition for the state to be maximally entangled, stated in Ref. [114] (in the numerical studies shown here, the average number of particles in the subsystem is equal to that of the bath but this is not in general the case). In the latter case, particles tend to distribute themselves uniformly, similar to what happens at thermal equilibrium.

As discussed in section 2.2, entanglement entropy is a well-known and useful measure of thermalization of systems in contact with a thermal bath. However, in relation to quantum systems that are approximately isolated from their

environment [317], measures such as von Neumann entropy are not capable of describing the evolution as they are strictly constant. Such notions of entropy make the assumption that the observer has full access to the density matrix. However, this is not in practice the case unless the observer has control over the system's preparation or can perform sufficiently many measurements in different bases on an ensemble of identically prepared systems. In fact, von Neumann wrote himself [316]: "The expressions for entropy given by the author [von Neumann] are not applicable here in the way they were intended, as they were computed from the perspective of an observer who can carry out all measurements that are possible in principle, i.e., regardless of whether they are macroscopic (for example, there every pure state has entropy 0, only mixtures have entropies greater than 0!)".

Intuitively, we expect an increase in some measure of disorder even in the absence of external influences. Take an example similar to what we have illustrated in this work through the simulations of one-dimensional lattice of spin-less fermions: a system initially in a "special" state of all (or most) particles localized in a small region of space. When evolved according to the Schrödinger equation (which is time-symmetric), particles tend to distribute themselves throughout the lattice. A quantification of such dynamics according to observational entropy however, would depend not only on the initial conditions of the system, but on the observer's choice of coarse-graining(s) as well.

Observational entropy provides us with a notion of entropy that respects the second law of thermodynamics, regardless of whether the system is pure or mixed. Analogous to classical thermodynamics where the emergence of the arrow of time is commonly known to be due to the tendency of thermodynamic entropy to increase, in an isolated quantum system an arrow of time could emerge due to the increase of observational entropy. One may refer to this arrow as a "subjective arrow of time" since the evolution of observational entropy depends on the choice of coarse-graining.[1] The connection between the quantum arrow of time that is in general (asides from the fluctuations) in accordance with the thermodynamic arrow of time is discussed in more detail in the work of Hartle [151] (although the exact formulation of observational entropy is not used, his work is not completely unrelated to our argument). He explains that the reason for isolated subsystems evolving towards a seemingly equilibrium state in the same direction as the thermodynamic arrow of time is the initial low entropy state of quantum subsystems that was inherited from the low entropy origin of the universe.

On a cosmological level, discussions of entropy and the arrow of time (e.g. [76, 4, 10, 247, 59, 3]) require a definition that applies to non-equilibrium states of a truly isolated system, the Universe, and potentially for indefinitely long timescales over which large entropy fluctuations might occur. These discussions often employ a definition of entropy that in practice mixes different notions. Ob-

[1] A similar concept was discussed by Hartle in Ref. [150] using models of information gathering and utilizing systems.

servational entropy applies in this context as well and therefore may be useful in these discussions, for instance in relation to the Past Hypothesis.

In chapter 3 we confirmed numerically the work of Deutsch et al. [83] stating that the probability of finding a generic state of the system in a small subspace ($M^2 \ll N$) is about 50%. Expressed in terms of an entropy with appropriate coarse-graining such as S_{xE}, this means that even the most extreme fluctuations will not reduce this quantity by more than half. This result has an important implication regarding the Past Hypothesis; one of the resolutions to this hypothesis is the occurrence of extreme localization of matter and energy out of a generic equilibrium state of the universe (i.e., an extreme downward fluctuation of entropy). The argument that S_{xE} can not reduce by more than half of its maximum value, weakens the aforementioned resolution to the Past Hypothesis.

Other resolutions to the emergence of the arrow of time due to increasing entropy have been put forward where no special low-entropy initial state is required. Examples are the cosmological models proposed by Carroll and Chen [59, 57] and Barbour et al. [17] (for more review on these arguments see [138, 194].) Other studies such as [5, 87, 318, 27, 183] provide arguments for and against the collapse of the wave function as the primary link to the existence of the arrow of time.

The work of Rovelli [265, 266] is among the studies that does not require a special initial condition of the universe for entropy to increase. His argument

suggests that the observed low entropy of the past is not because of a special configuration of the microstate. Rather, it is due to the way we, as observers, couple to the universe and the observables (coarse-grainings) we are naturally evolved to use in describing the universe. The entropy of choice in his work is von Neumann entropy of the subsystem (i.e., entanglement entropy) – the region where the observer is interested in measuring. The coarse-graining then is given by restricting the choice of observables to those of the subsystem. He further explains that for any general $\psi(t)$, one can find a split of the system into subsystems such that entanglement entropy is initially zero but grows with time.

The situation where the measurements on the subsystem are imperfect is not however considered in the aforementioned argument. If $\{\hat{P}_i\}_i$ – a trace-preserving set of non-zero projectors acting on the Hilbert space that corresponds to the subsystem, represents our coarse-graining, there is a scenario where the measurement may not be complete. In other words, the projection is not onto a pure state. In this case, observational entropy (of the subsystem) could be a more suitable choice in which case it would be lower bounded by the von Neumann entropy of the subsystem according to theorem 3 in Ref. [269]

The role of coarse-grained observations also appeared in the work of Hartle [152] where a generalization of Copenhagen quantum mechanics with no built in time asymmetry is presented. He makes use of time-neutral decoherent (or consistent) histories formulation of quantum theory [142, 178]. However, this formula-

tion does not account for non-commuting coarse-grainings such as the one used in the definition of general observational entropy with multiple coarse-graining (for example S_{xE}). This may also bring up a question of whether non-commutativity of observables in the measurement process introduces a built-in asymmetry that can be responsible for the arrow of time in quantum systems.

We should emphasize the primary remaining obstacle to such arguments that define and use notions of entropy of the universe in the context of quantum mechanics is a lack of understanding of the state-space of gravity and space-time as well as a well-defined wave function of the universe without observers on the "outside". This also brings up issues about how an observer inside the isolated system can make measurements. Would they make the measurement on the reduced state of the universe (by tracing over part of the universe that describes themselves and anything else that they may not be interested in measuring)?

Questions of this nature have been long-standing in physics and philosophy. A careful extension of the second law of thermodynamics to quantum systems, rigorous studies on the meaning and implications of different notions of entropy and the intuition behind them are a few examples of how we may take a step forward in these discussions. This thesis was an attempt to improve the understanding of two types of entropy relevant to quantum systems. We hope for progress in endeavors to experimentally measure entanglement and observational entropy in the near future.

Bibliography

[1] Obinna Abah, Johannes Rossnagel, Georg Jacob, Sebastian Deffner, Ferdinand Schmidt-Kaler, Kilian Singer, and Eric Lutz. Single-ion heat engine at maximum power. *Phys. Rev. Lett.*, 109(20):203006, 2012.

[2] Johan Aberg. Fully quantum fluctuation theorems. *arXiv preprint arXiv:1601.01302*, 2016.

[3] Anthony Aguirre, Sean M Carroll, and Matthew C Johnson. Out of equilibrium: understanding cosmological evolution to lower-entropy states. *J. Cosmol. Astropart. Phys.*, 2012(02):024, 2012.

[4] Anthony Aguirre and Steven Gratton. Inflation without a beginning: a null boundary proposal. *Phys. Rev. D*, 67(8):083515, 2003.

[5] Yakir Aharonov, Peter G Bergmann, and Joel L Lebowitz. Time symmetry in the quantum process of measurement. *Physical Review*, 134:B1410, 1964.

[6] Mehdi Ahmadi, David Edward Bruschi, Carlos Sabín, Gerardo Adesso, and

Ivette Fuentes. Relativistic quantum metrology: Exploiting relativity to improve quantum measurement technologies. *Scientific reports*, 4:4996, 2014.

[7] Vincenzo Alba. Eigenstate thermalization hypothesis and integrability in quantum spin chains. *Phys. Rev. B*, 91(15):155123, 2015.

[8] David Z Albert. Time and chance harvard university press. *Cambridge, MA*, 2000.

[9] David Z Albert. *Time and chance*. American Association of Physics Teachers, 2001.

[10] Andreas Albrecht and Lorenzo Sorbo. Can the universe afford inflation? *Phys. Rev. D*, 70(6):063528, 2004.

[11] Bernhard Altaner. Foundations of stochastic thermodynamics. *arXiv preprint arXiv:1410.3983*, 2014.

[12] Luigi Amico, Rosario Fazio, Andreas Osterloh, and Vlatko Vedral. Entanglement in many-body systems. *Rev. Mod. Phys.,*, 80(2):517, 2008.

[13] Arvind. Quantum entanglement and quantum computational algorithms. *Pramana*, 56(02-03), 2001.

[14] Steven G Avery and Miguel F Paulos. Universal bounds on the time evolution of entanglement entropy. *Phys. Rev. Lett.*, 113(23):231604, 2014.

[15] Gary Ayton, Denis J Evans, and Debra J Searles. A local fluctuation theorem. *J. Chem. Phys.*, 115(5):2033–2037, 2001.

[16] Francisco Balibrea. On clausius, boltzmann and shannon notions of entropy. *Journal of Modern Physics*, 7(02):219, 2016.

[17] Julian Barbour, Tim Koslowski, and Flavio Mercati. A gravitational origin of the arrows of time. *arXiv preprint arXiv:1310.5167*, 2013.

[18] Rami Barends, Alireza Shabani, Lucas Lamata, Julian Kelly, Antonio Mezzacapo, Urtzi Las Heras, Ryan Babbush, Austin G Fowler, Brooks Campbell, Yu Chen, et al. Digitized adiabatic quantum computing with a superconducting circuit. *Nature*, 534(7606):222, 2016.

[19] Hatem Barghathi, Emanuel Casiano-Diaz, and Adrian Del Maestro. Particle partition entanglement of one dimensional spinless fermions. *Journal of Statistical Mechanics: Theory and Experiment*, 2017(8):083108, 2017.

[20] Hatem Barghathi, Emanuel Casiano-Diaz, and Adrian Del Maestro. Operationally accessible entanglement of one dimensional spinless fermions. *arXiv:1905.03312 [quant-ph]*, 2019.

[21] Hatem Barghathi, C. M. Herdman, and Adrian Del Maestro. Rényi generalization of the accessible entanglement entropy. *Phys. Rev. Lett.*, 121:150501, Oct 2018.

[22] Stephen D Bartlett, Terry Rudolph, and Robert W Spekkens. Reference frames, superselection rules, and quantum information. *Rev. Mod. Phys.*, 79(2):555, 2007.

[23] Michael Baudin. Nelder mead user's manual, 2009.

[24] Stefan Bäuml, Siddhartha Das, and Mark M Wilde. Fundamental limits on the capacities of bipartite quantum interactions. *Phys. Rev. Lett.*, 121(25):250504, 2018.

[25] Vincent Beaud, Julian Sieber, and Simone Warzel. Bounds on the bipartite entanglement entropy for oscillator systems with or without disorder. *Phys. Rev. A*, 2019.

[26] Vincent Beaud and Simone Warzel. Bounds on the entanglement entropy of droplet states in the xxz spin chain. *J. Math. Phys.*, 59(1):012109, 2018.

[27] DJ Bedingham and OJE Maroney. Time symmetry in wave-function collapse. *Physical Review A*, 95(4):042103, 2017.

[28] Fabio Benatti, Roberto Floreanini, and Ugo Marzolino. Sub-shot-noise quantum metrology with entangled identical particles. *Ann. Phys.*, 325(4):924–935, 2010.

[29] Fabio Benatti, Roberto Floreanini, and Ugo Marzolino. Entanglement and squeezing with identical particles: ultracold atom quantum metrology. *J. Phys. B*, 44(9):091001, 2011.

[30] Fabio Benatti, Roberto Floreanini, and Ugo Marzolino. Bipartite entanglement in systems of identical particles: the partial transposition criterion. *Ann. Phys.*, 327(5):1304–1319, 2012.

[31] Fabio Benatti, Roberto Floreanini, and Ugo Marzolino. Entanglement in fermion systems and quantum metrology. *Phys. Rev. A*, 89(3):032326, 2014.

[32] Lucien Benguigui. The different paths to entropy. 34(2):303, 2013.

[33] Charles H Bennett, Gilles Brassard, Claude Crépeau, Richard Jozsa, Asher Peres, and William K Wootters. Teleporting an unknown quantum state via dual classical and einstein-podolsky-rosen channels. *Phys. Rev. Lett.*, 70(13):1895, 1993.

[34] Charles H Bennett, David P DiVincenzo, John A Smolin, and William K Wootters. Mixed-state entanglement and quantum error correction. *Physical Review A*, 54(5):3824, 1996.

[35] Charles H Bennett, Andrzej Grudka, Michał Horodecki, Paweł Horodecki, and Ryszard Horodecki. Postulates for measures of genuine multipartite correlations. *Phys. Rev. A*, 83(1):012312, 2011.

[36] Charles H Bennett and Stephen J Wiesner. Communication via one-and two-particle operators on einstein-podolsky-rosen states. *Phys. Rev. Lett.*, 69(20):2881, 1992.

[37] Bernd A Berg. Introduction to markov chain monte carlo simulations and their statistical analysis. *Markov Chain Monte Carlo Lect Notes Ser Inst Math Sci Natl Univ Singap*, 7:1–52, 2005.

[38] Alice Bernamonti, Federico Galli, Robert C Myers, and Jonathan Oppenheim. Holographic second laws of black hole thermodynamics. *J. High Energy Phys.*, 2018(7):111, 2018.

[39] Wouter Beugeling, Roderich Moessner, and Masudul Haque. Finite-size scaling of eigenstate thermalization. *Phys. Rev. E*, 89(4):042112, 2014.

[40] Robert T Beyer. *Mathematical foundations of quantum mechanics*. 1955.

[41] Amandeep Singh Bhatia and Mandeep Kaur Saggi. Implementing entangled states on a quantum computer. *arXiv:1811.09833 [quant-ph]*, 2018.

[42] Immanuel Bloch, Jean Dalibard, and Wilhelm Zwerger. Many-body physics with ultracold gases. *Rev. Mod. Phys.*, 80(3):885, 2008.

[43] Jaap Boender, Florian Kammüller, and Rajagopal Nagarajan. Formalization of quantum protocols using coq. *arXiv:1511.01568 [cs.LO]*, 2015.

[44] L Boltzmann. Lectures on gas theory, translation by stephen g. brush.

[45] Ludwig Boltzmann. Zu hrn. zermelo's abhandlung ueber die mechanische erklärung irreversibler vorgänge". *Annalen der Physik*, 296(2):392–398.

[46] Ludwig Boltzmann. Further studies on the thermal equilibrium of gas molecules. In *The kinetic theory of gases: an anthology of classic papers with historical commentary*, pages 262–349. World Scientific, 2003.

[47] Ludwig Boltzmann. Lectures on gas theory. 2012.

[48] Edward Stuart Boyden. *Quantum computation: theory and implementation*. PhD thesis, Massachusetts Institute of Technology, Dept. of Physics; and(S. B. and S. M.), Massachusetts Institute of Technology, Dept. of Electrical Engineering and Computer Science, 1999.

[49] Antoine Browaeys, Daniel Barredo, and Thierry Lahaye. Experimental investigations of dipole–dipole interactions between a few rydberg atoms. *J. Phys. B*, 49(15):152001, 2016.

[50] M Brunelli, L Fusco, R Landig, W Wieczorek, J Hoelscher-Obermaier, G Landi, F L Semião, A Ferraro, N Kiesel, T Donner, et al. Experimental determination of irreversible entropy production in out-of-equilibrium mesoscopic quantum systems. *Phys. Rev. Lett.*, 121(16):160604, 2018.

[51] Stephen G Brush. *History of the Kinetic Theory of Gases*, volume 7, chapter 44. Istituto della Enciclopedia Italiana, 2004.

[52] Tiff Brydges, Andreas Elben, Petar Jurcevic, Benoît Vermersch, Christine Maier, Ben P. Lanyon, Peter Zoller, Rainer Blatt, and Christian F. Roos.

Probing rényi entanglement entropy via randomized measurements. *Science*, 364(6437):260–263, 2019.

[53] Pierfrancesco Buonsante, Roberto Franzosi, and Augusto Smerzi. On the dispute between boltzmann and gibbs entropy. *Ann. Physics*, 375:414–434, 2016.

[54] Pasquale Calabrese and John Cardy. Entanglement entropy and quantum field theory. *J. Stat. Mech., Theory. Exp.*, 2004(06):P06002, 2004.

[55] Ilse Callens, Woyciech De Roeck, Tim Jacobs, Christian Maes, and K Netočnỳ. Quantum entropy production as a measure of irreversibility. *Physica D: Nonlinear phenomena*, 187(1-4):383–391, 2004.

[56] Michele Campisi, Jukka Pekola, and Rosario Fazio. Nonequilibrium fluctuations in quantum heat engines: theory, example, and possible solid state experiments. *New Journal of Physics*, 17(3):035012, 2015.

[57] Sean Carroll and Sean M Carroll. *From eternity to here: the quest for the ultimate theory of time*. Penguin, 2010.

[58] Sean M Carroll. Why boltzmann brains are bad. *arXiv:1702.00850 [hep-th]*, 2017.

[59] Sean M Carroll and Jennifer Chen. Spontaneous inflation and the origin of the arrow of time. *arXiv:1905.038 [hep-th]*, 2004.

[60] Sean M Carroll and Jennifer Chen. Does inflation provide natural initial conditions for the universe? *International Journal of Modern Physics D*, 14(12):2335–2339, 2005.

[61] Nicolas J Cerf and Chris Adami. Negative entropy and information in quantum mechanics. *Phys. Rev. Lett.*, 79(26):5194, 1997.

[62] A Yu Chernyavskiy. Entanglement measure for multipartite pure states and its numerical calculation. *arXiv preprint arXiv:0905.0201*, 2009.

[63] Eric Chitambar and Gilad Gour. Quantum resource theories. *Rev. Mod. Phys.*, 91(2):025001, 2019.

[64] Jaeyoon Cho. Realistic area-law bound on entanglement from exponentially decaying correlations. *Phys. Rev. X*, 8(3):031009, 2018.

[65] Rudolf Clausius. I. on the moving force of heat, and the laws regarding the nature of heat itself which are deducible therefrom. *The London, Edinburgh, and Dublin Philosophical Magazine and Journal of Science*, 2(8), 1851.

[66] Valerie Coffman, Joydip Kundu, and William K Wootters. Distributed entanglement. *Phys. Rev. A*, 61(5):052306, 2000.

[67] Luis A Correa, Mohammad Mehboudi, Gerardo Adesso, and Anna Sanpera. Individual quantum probes for optimal thermometry. *Physical review letters*, 114(22):220405, 2015.

[68] Gavin E Crooks. Entropy production fluctuation theorem and the nonequilibrium work relation for free energy differences. *Phys. Rev. E*, 60(3):2721, 1999.

[69] Oscar CO Dahlsten, Cosmo Lupo, Stefano Mancini, and Alessio Serafini. Entanglement typicality. *J. Phys. A: Math. Theor.*, 47(36):363001, 2014.

[70] Luca D'Alessio, Yariv Kafri, Anatoli Polkovnikov, and Marcos Rigol. From quantum chaos and eigenstate thermalization to statistical mechanics and thermodynamics. *Advances in Physics*, 65(3):239–362, 2016.

[71] A J Daley, H Pichler, J Schachenmayer, and P Zoller. Measuring entanglement growth in quench dynamics of bosons in an optical lattice. *Phys. Rev. Lett.*, 109(2):020505, 2012.

[72] Giacomo Mauro D'Ariano, Franco Manessi, Paolo Perinotti, and Alessandro Tosini. Fermionic computation is non-local tomographic and violates monogamy of entanglement. *Europhys. Lett.*, 107(2):20009, 2014.

[73] Saurya Das, S Shankaranarayanan, and Sourav Sur. Black hole entropy from entanglement: a review. *arXiv preprint arXiv:0806.0402 [gr-qc]*, 2008.

[74] Nilanjana Datta, Christoph Hirche, and Andreas Winter. Convexity and operational interpretation of the quantum information bottleneck function. *arXiv:1810.03644 [quant-ph]*, 2018.

[75] Matthew Davenport and Ken D Olum. Are there boltzmann brains in the vacuum. *arXiv:1008.0808 [hep-th]*, 2010.

[76] Paul Charles William Davies. *The physicsvon2010proof*. University of California Press, 1977.

[77] G De Chiara, T Calarco, M Anderlini, S Montangero, PJ Lee, BL Brown, WD Phillips, and JV Porto. Optimal control of atom transport for quantum gates in optical lattices. *Physical Review A*, 77(5):052333, 2008.

[78] Giuseppe De Tomasi, Soumya Bera, Jens H Bardarson, and Frank Pollmann. Quantum mutual information as a probe for many-body localization. *Phys. Rev. Lett.*, 118(1):016804, 2017.

[79] Rafał Demkowicz-Dobrzański, Jan Kołodyński, and Mădălin Guţă. The elusive heisenberg limit in quantum-enhanced metrology. *Nat. Commun.*, 3:1063, 2012.

[80] J M Deutsch. Thermodynamic entropy of a many-body energy eigenstate. *New J. Phys.*, 12(7):075021, 2010.

[81] J M Deutsch, Haibin Li, and Auditya Sharma. Microscopic origin of thermodynamic entropy in isolated systems. *Phys. Rev. E*, 87(4):042135, 2013.

[82] Josh M Deutsch. Quantum statistical mechanics in a closed system. *Phys. Rev. A*, 43(4):2046, 1991.

[83] Joshua M Deutsch, Dominik Šafránek, and Anthony Aguirre. Probabilistic bound on extreme fluctuations in isolated quantum systems. *Physical Review E*, 101(3):032112, 2020.

[84] Igor Devetak, Aram W Harrow, and Andreas Winter. A family of quantum protocols. *Phys. Rev. Lett.*, 93(23):230504, 2004.

[85] Bryce S DeWitt and Giampiero Esposito. An introduction to quantum gravity. *Int. J. Geom. Meth. Mod. Phys.* , 5(01):101–156, 2008.

[86] P Ben Dixon, Gregory A Howland, James Schneeloch, and John C Howell. Quantum mutual information capacity for high-dimensional entangled states. *Phys. Rev. Lett.*, 108(14):143603, 2012.

[87] Shahar Dolev, Avshalom C Elitzur, and Meir Hemmo. Does indeterminism give rise to an intrinsic time arrow? *arXiv preprint quant-ph/0101088*, 2001.

[88] Xi Dong. Holographic entanglement entropy for general higher derivative gravity. *J. High Energy Phys.*, 2014(1):44, 2014.

[89] Jonathan P Dowling. Quantum optical metrology–the lowdown on high-n00n states. *Contemp. Phys.*, 49(2):125–143, 2008.

[90] doxygen.

[91] Jiangfeng Du, Xing Rong, Nan Zhao, Ya Wang, Jiahui Yang, and RB Liu.

Preserving electron spin coherence in solids by optimal dynamical decoupling. *Nature*, 461(7268):1265, 2009.

[92] Jörn Dunkel and Stefan Hilbert. Consistent thermostatistics forbids negative absolute temperatures. *Nat. Phys.*, 10(1):67, 2014.

[93] Wolfgang Dür, Guifre Vidal, and J Ignacio Cirac. Three qubits can be entangled in two inequivalent ways. *Physical Review A*, 62(6):062314, 2000.

[94] Lisa Dyson, Matthew Kleban, and Leonard Susskind. Disturbing implications of a cosmological constant. *J. High Energy Phys.*, 2002(10):011, 2002.

[95] John Earman. The "past hypothesis": Not even false. *Stud. Hist. Philos. Sci. A*, 37(3):399–430, 2006.

[96] Kate Eckerle. A simple system for coleman-de luccia transitions. *arXiv preprint arXiv:2003.04365*, 2020.

[97] Arthur Stanley Eddington. Arrow of time. *On space and time*, page 46.

[98] Sheri Edwards. Elements of information theory, thomas m. cover, joy a. thomas, john wiley & sons, inc.(2006), 2008.

[99] Albert Einstein. Theorie der opaleszenz von homogenen flüssigkeiten und flüssigkeitsgemischen in der nähe des kritischen zustandes. *Annalen der Physik*, 338(16):1275–1298, 1910.

[100] Albert Einstein. *General Relativity; an Einstein Centenary Survey*. CUP Archive, 1979.

[101] Albert Einstein, Boris Podolsky, and Nathan Rosen. Can quantum-mechanical description of physical reality be considered complete? *Physical review*, 47(10):777, 1935.

[102] Jens Eisert, Marcus Cramer, and Martin B Plenio. Area laws for the entanglement entropy-a review. *Rev. Mod. Phys.*, 82:277, 2010.

[103] Jens Eisert, Timo Felbinger, P Papadopoulos, M B Plenio, and Martin Wilkens. Classical information and distillable entanglement. *Phys. Rev. Lett.*, 84(7):1611, 2000.

[104] Artur K Ekert. Quantum cryptography based on bell's theorem. *Phys. Rev. Lett.*, 67(6):661, 1991.

[105] George Francis Rayner Ellis. The arrow of time and the nature of spacetime. *Studies in History and Philosophy of Science Part B: Studies in History and Philosophy of Modern Physics*, 44(3):242–262, 2013.

[106] Roberto Emparan. Black hole entropy as entanglement entropy: a holographic derivation. *J. High Energy Phys.*, 2006(06):012, 2006.

[107] Volkan Erol. Entanglement monotones and measures: an overview. *arXiv:1704.05058 [quant-ph]*, 2017.

[108] Massimiliano Esposito, Upendra Harbola, and Shaul Mukamel. Nonequilibrium fluctuations, fluctuation theorems, and counting statistics in quantum systems. *Rev. Mod. Phys.*, 81(4):1665, 2009.

[109] Massimiliano Esposito and Shaul Mukamel. Fluctuation theorems for quantum master equations. *Phys. Rev. E*, 73(4):046129, 2006.

[110] Massimiliano Esposito and Christian Van den Broeck. Three detailed fluctuation theorems. *Physical review letters*, 104(9):090601, 2010.

[111] Denis J Evans, Ezechiel Godert David Cohen, and Gary P Morriss. Probability of second law violations in shearing steady states. *Phys. Rev. Lett.*, 71(15):2401, 1993.

[112] Denis J Evans and Debra J Searles. The fluctuation theorem. *Advances in Physics*, 51(7):1529–1585, 2002.

[113] Alexandr A Ezhov and Gennady Berman. *Role of interference and entanglement in quantum neural processing*, volume 4591, pages 367–379. 2001.

[114] Dana Faiez and Dominik Šafránek. How much entanglement can be created in a closed system. *Phys. Rev. B*, 101(6):060401, 2020.

[115] Dana Faiez, Dominik Šafránek, JM Deutsch, and Anthony Aguirre. Typical and extreme entropies of long-lived isolated quantum systems.

[116] Mark Fannes and Nicholas Van Ryn. Connecting the von neumann and rényi entropies for fermions. *J. Phys. A: Math. Theor.*, 45(38):385003, 2012.

[117] J Doyne Farmer. Information dimension and the probabilistic structure of chaos. *Zeitschrift für Naturforschung A*, 37(11):1304–1326, 1982.

[118] William Fedus. Entropy in classical and quantum information theory. 2014.

[119] Mattias Fitzpatrick, Neereja M Sundaresan, Andy C Y Li, Jens Koch, and Andrew A Houck. Observation of a dissipative phase transition in a one-dimensional circuit qed lattice. *Phys. Rev. X*, 7(1):011016, 2017.

[120] G Francica, J Goold, and F Plastina. The role of coherence in the non-equilibrium thermodynamics of quantum systems. *arXiv preprint arXiv:1707.06950*, 2017.

[121] Roman Frigg. In what sense is the kolmogorov-sinai entropy a measure for chaotic behaviour?—bridging the gap between dynamical systems theory and communication theory. *The British journal for the philosophy of science*, 55(3):411–434, 2004.

[122] Nicolai Friis, Oliver Marty, Christine Maier, Cornelius Hempel, Milan Holzäpfel, Petar Jurcevic, Martin B Plenio, Marcus Huber, Christian Roos, Rainer Blatt, et al. Observation of entangled states of a fully controlled 20-qubit system. *Phys. Rev. X*, 8(2):021012, 2018.

[123] Hiroyuki Fujita, Yuya O Nakagawa, Sho Sugiura, and Masataka Watanabe. Page curves for general interacting systems. *J. High Energy Phys.*, 2018(12):112, 2018.

[124] Andreas Gabriel. Detection and characterisation of multipartite quantum entanglement. *arXiv preprint arXiv:1305.7401*, 2013.

[125] Jay M Gambetta, Jerry M Chow, and Matthias Steffen. Building logical qubits in a superconducting quantum computing system. *npj Quantum Inf.*, 3(1):2, 2017.

[126] Bartłomiej Gardas and Sebastian Deffner. Thermodynamic universality of quantum carnot engines. *Physical Review E*, 92(4):042126, 2015.

[127] Murray Gell-Mann and James B Hartle. Time symmetry and asymmetry in quantum mechanics and quantum cosmology. *Physical origins of time asymmetry*, 1:311–345, 1994.

[128] Jochen Gemmer and Robin Steinigeweg. Entropy increase in k-step markovian and consistent dynamics of closed quantum systems. *Phys. Rev. E*, 89(4):042113, 2014.

[129] Stefano Gherardini, Matthias M Muller, Andrea Trombettoni, Stefano Ruffo, and Filippo Caruso. Reconstructing quantum entropy production to probe irreversibility and correlations. *Quantum Science and Technology*, 2018.

[130] Josiah Willard Gibbs. On the equilibrium of heterogeneous substances. 1879.

[131] Vittorio Giovannetti, Seth Lloyd, and Lorenzo Maccone. Quantum metrology. *Phys. Rev. Lett.*, 96(1):010401, 2006.

[132] Vittorio Giovannetti, Seth Lloyd, and Lorenzo Maccone. Advances in quantum metrology. *Nat. Photonics*, 5(4):222, 2011.

[133] Davide Girolami, Tommaso Tufarelli, and Cristian E Susa. Quantifying genuine multipartite correlations and their pattern complexity. *Phys. Rev. Lett.*, 119(14):140505, 2017.

[134] Christian Gogolin and Jens Eisert. Equilibration, thermalisation, and the emergence of statistical mechanics in closed quantum systems. *Reports on Progress in Physics*, 79(5):056001, 2016.

[135] Christian Gogolin and Jens Eisert. Equilibration, thermalisation, and the emergence of statistical mechanics in closed quantum systems. *Reports on Progress in Physics*, 79(5):056001, 2016.

[136] Sheldon Goldstein and Joel L Lebowitz. On the (boltzmann) entropy of non-equilibrium systems. *Physica D*, 193(1-4):53–66, 2004.

[137] Sheldon Goldstein, Joel L Lebowitz, Roderich Tumulka, and Nino Zanghi. Gibbs and boltzmann entropy in classical and quantum mechanics. *arXiv:1903.11870 [cond-mat.stat-mech]*, 2019.

[138] Sheldon Goldstein, Roderich Tumulka, and Nino Zanghi. Is the hypothesis about a low entropy initial state of the universe necessary for explaining the arrow of time? *Physical Review D*, 94(2):023520, 2016.

[139] John Goold, Marcus Huber, Arnau Riera, Lídia del Rio, and Paul Skrzypczyk. The role of quantum information in thermodynamics—a topical review. *Journal of Physics A: Mathematical and Theoretical*, 49(14):143001, 2016.

[140] Federico Grasselli and Gianluca Grignani. Entanglement Entropy, master's thesis. Master's thesis, Grasselli, Federico and Grignani, Gianluca, 2014.

[141] Hilary Greaves. Towards a geometrical understanding of the cpt theorem. *The British journal for the philosophy of science*, 61(1):27–50, 2010.

[142] Robert B Griffiths. Consistent histories and the interpretation of quantum mechanics. *Journal of Statistical Physics*, 36(1-2):219–272, 1984.

[143] Christian Gross, Tilman Zibold, Eike Nicklas, Jerome Esteve, and Markus K Oberthaler. Nonlinear atom interferometer surpasses classical precision limit. *Nature*, 464(7292):1165, 2010.

[144] Tarun Grover and Matthew PA Fisher. Quantum disentangled liquids. *J. Stat. Mech., Theory. Exp.*, 2014(10):P10010, 2014.

[145] Shi-Jian Gu, Shu-Sa Deng, You-Quan Li, and Hai-Qing Lin. Entanglement

and quantum phase transition in the extended hubbard model. *Phys. Rev. Lett.*, 93(8):086402, 2004.

[146] Jonathan Halliwell. Quantum cosmology and time asymmetry. *Physical Origins of Time Asymmetry*, pages 369–389, 1994.

[147] Peter Hänggi, Gert-Ludwig Ingold, and Peter Talkner. Finite quantum dissipation: the challenge of obtaining specific heat. *New J. Phys.*, 10(11):115008, 2008.

[148] Daniel Harlow and Hirosi Ooguri. Symmetries in quantum field theory and quantum gravity. *arXiv preprint arXiv:1810.05338*, 2018.

[149] James Hartle and Thomas Hertog. Arrows of time in the bouncing universes of the no-boundary quantum state. *Physical Review D*, 85(10):103524, 2012.

[150] James B Hartle. The physics of now. *Am. J. Phys.*, 73(2):101–109, 2005.

[151] James B Hartle. The quantum mechanical arrows of time. In *Quantum Theory: A Two-Time Success Story*, pages 113–128. Springer, 2014.

[152] James B Hartle. Arrows of time and initial and final conditions in the quantum mechanics of closed systems like the universe. *arXiv preprint arXiv:2002.07093*, 2020.

[153] James B Hartle and Stephen W Hawking. Wave function of the universe. *Physical Review D*, 28(12):2960, 1983.

[154] W Keith Hastings. Monte carlo sampling methods using markov chains and their applications. *Oxford University Press*, 1970.

[155] Stephen W Hawking. The direction of time. *New Sci.*, 115(Print-87-0849 (DAMTP)):46, 1987.

[156] Stephen W Hawking and Don N Page. Thermodynamics of black holes in anti-de sitter space. *Communications in Mathematical Physics*, 87(4):577–588, 1983.

[157] Patrick Hayden, Debbie W Leung, and Andreas Winter. Aspects of generic entanglement. *Communications in mathematical physics*, 265(1):95–117, 2006.

[158] Libby Heaney. Teleportation of a quantum state of a spatial mode with a single massive particle. In *Conference on Quantum Computation, Communication, and Cryptography*, pages 175–186. Springer, 2010.

[159] Torsten Heinrich, Benjamin Knopp, and Heinrich Päs. Entropy, biological evolution and the psychological arrow of time. *arXiv preprint arXiv:1401.3734*, 2014.

[160] Johannes Helmes. *An entanglement perspective on phase transitions, conventional and topological order*. PhD thesis, Universität zu Köln, 2017.

[161] Wolfram Helwig, Wei Cui, José Ignacio Latorre, Arnau Riera, and Hoi-

Kwong Lo. Absolute maximal entanglement and quantum secret sharing. *Phys. Rev. A*, 86(5):052335, 2012.

[162] Fedor Herbut. On schmidt decomposition: Approach based on correlation operator as bipartite entanglement entity. *Quanta*, 7(1):19–39, 2018.

[163] Stefan Hilbert, Peter Hänggi, and Jörn Dunkel. Thermodynamic laws in isolated systems. *Phys. Rev. E*, 90(6):062116, 2014.

[164] Christian Hörhammer and Helmut Büttner. Information and entropy in quantum brownian motion. *J. Stat. Phys.*, 133(6):1161–1174, 2008.

[165] Michał Horodecki, Jonathan Oppenheim, and Andreas Winter. Quantum state merging and negative information. *Commun. Theor. Phys.*, 269(1):107–136, 2007.

[166] Yichen Huang. Dynamics of renyi entanglement entropy in local quantum circuits with charge conservation. *arXiv:1902.00977 [quant-ph]*, 2019.

[167] Yichen Huang. Universal eigenstate entanglement of chaotic local hamiltonians. *Nucl. Phys. B*, 938:594–604, 2019.

[168] Dominik Šafránek, J. M. Deutsch, and Anthony Aguirre. Quantum coarse-grained entropy and thermodynamics. *Phys. Rev. A*, 99:010101(R), Jan 2019.

[169] Radu Ionicioiu and Paolo Zanardi. Quantum-information processing in bosonic lattices. *Phys. Rev. A*, 66(5):050301(R), 2002.

[170] Rajibul Islam, Ruichao Ma, Philipp M Preiss, M Eric Tai, Alexander Lukin, Matthew Rispoli, and Markus Greiner. Measuring entanglement entropy in a quantum many-body system. *Nature*, 528(7580):77, 2015.

[171] Eiki Iyoda, Kazuya Kaneko, and Takahiro Sagawa. Fluctuation theorem for many-body pure quantum states. *Physical review letters*, 119(10):100601, 2017.

[172] Matthew James. Quantum control theory. *arXiv preprint arXiv:1406.5260*, 2014.

[173] Christopher Jarzynski. Nonequilibrium equality for free energy differences. *Phys. Rev. Lett.*, 78(14):2690, 1997.

[174] Edwin T Jaynes. *Probability theory: The logic of science*. Cambridge university press, 2003.

[175] Sania Jevtic, David Jennings, and Terry Rudolph. Maximally and minimally correlated states attainable within a closed evolving system. *Phys. Rev. Lett.*, 108(11):110403, 2012.

[176] Hong-Chen Jiang, Zhenghan Wang, and Leon Balents. Identifying topological order by entanglement entropy. *Nat. Phys.*, 8(12):902, 2012.

[177] Valen E Johnson and James H Albert. *Ordinal data modeling*. Springer Science & Business Media, 2006.

[178] Eric Joos and H Dieter Zeh. The emergence of classical properties through interaction with the environment. *Zeitschrift für Physik B Condensed Matter*, 59(2):223–243, 1985.

[179] Palle ET Jorgensen. The road to reality: a complete guide to the laws of the universe. *The Mathematical Intelligencer*, 28(3):59–61, 2006.

[180] Jürgen Jost. *Dynamical systems: examples of complex behaviour*. Springer Science & Business Media, 2006.

[181] Adam M Kaufman, M Eric Tai, Alexander Lukin, Matthew Rispoli, Robert Schittko, Philipp M Preiss, and Markus Greiner. Quantum thermalization through entanglement in an isolated many-body system. *Science*, 353(6301):794–800, 2016.

[182] Sang Wook Kim, Takahiro Sagawa, Simone De Liberato, and Masahito Ueda. Quantum szilard engine. *Physical review letters*, 106(7):070401, 2011.

[183] AY Klimenko. The direction of time and boltzmann's time hypothesis. *Physica Scripta*, 94(3):034002, 2019.

[184] Maciej Koch-Janusz and Zohar Ringel. Mutual information, neural networks and the renormalization group. *Nat. Phys.*, 14(6):578, 2018.

[185] Kamil Korzekwa. Structure of the thermodynamic arrow of time in classical and quantum theories. *Physical Review A*, 95(5):052318, 2017.

[186] R John Koshel. Enhancement of the downhill simplex method of optimization. In *International Optical Design Conference*, page ITuC2. Optical Society of America, 2002.

[187] Solomon Kullback and Richard A Leibler. On information and sufficiency. *The annals of mathematical statistics*, 22(1):79–86, 1951.

[188] Nicolas Laflorencie. Quantum entanglement in condensed matter systems. *Phys. Rep.*, 646:1–59, 2016.

[189] Sourabh Lahiri and AM Jayannavar. Total entropy production fluctuation theorems in a nonequilibrium time-periodic steady state. *The European Physical Journal B*, 69(1):87–92, 2009.

[190] Joseph M Landsberg. *A very brief introduction to quantum computing and quantum information theory for mathematicians*, pages 5–41. Springer, 2019.

[191] Peter T Landsberg. Irreversibility and time's arrow. *Dialectica*, 50(4):247–258, 1996.

[192] Vito Latora and Michel Baranger. Kolmogorov-sinai entropy rate versus physical entropy. *Physical Review Letters*, 82(3):520, 1999.

[193] José Ignacio Latorre, Enrique Rico, and Guifré Vidal. Ground state entanglement in quantum spin chains. *Quant. Inf. Comput.*, 4:48–92, 2003.

[194] Dustin Lazarovici and Paula Reichert. Arrow (s) of time without a past hypothesis. *arXiv preprint arXiv:1809.04646*, 2018.

[195] Karyn Le Hur. Entanglement entropy, decoherence, and quantum phase transitions of a dissipative two-level system. *Annals of Physics*, 323(9):2208–2240, 2008.

[196] Felix Leditzky. Relative entropies and their use in quantum information theory. *arXiv preprint arXiv:1611.08802*, 2016.

[197] Dean Lee. Lattice simulations for few-and many-body systems. *Prog. Part. Nucl. Phys.*, 63(1):117–154, 2009.

[198] Dietrich Leibfried, Rainer Blatt, Christopher Monroe, and David Wineland. Quantum dynamics of single trapped ions. *Reviews of Modern Physics*, 75(1):281, 2003.

[199] Craig S Lent. Quantum operator entropies under unitary evolution. *Phys. Rev. E*, 100(1):012101, 2019.

[200] Yoav Levine, Or Sharir, Nadav Cohen, and Amnon Shashua. Quantum entanglement in deep learning architectures. *Phys. Rev. Lett.*, 122(6):065301, 2019.

[201] Maciej Lewenstein. Quantum perceptrons. *J. Mod. Opt.*, 41(12):2491–2501, 1994.

[202] Ming Li and Shao-Ming Fei. Measurable bounds for entanglement of formation. *Phys. Rev. A*, 82(4):044303, 2010.

[203] Youning Li, Muxin Han, Markus Grassl, and Bei Zeng. Invariant perfect tensors. *New Journal of Physics*, 19(6):063029, 2017.

[204] Noah Linden, Milán Mosonyi, and Andreas Winter. The structure of rényi entropic inequalities. *Proceedings of the Royal Society A: Mathematical, Physical and Engineering Sciences*, 469(2158):20120737, 2013.

[205] Norbert M Linke, Sonika Johri, Caroline Figgatt, Kevin A Landsman, Anne Y Matsuura, and Christopher Monroe. Measuring the renyi entropy of a two-site fermi-hubbard model on a trapped ion quantum computer. *Phys. Rev. A*, 98(5):052334, 2018.

[206] Yuhan Liu, Xiao Zhang, Maciej Lewenstein, and Shi-Ju Ran. Entanglement-guided architectures of machine learning by quantum tensor network. *arXiv preprint arXiv:1803.09111*, 2018.

[207] Seth Lloyd and Heinz Pagels. Complexity as thermodynamic depth. *Ann. Phys.*, 188(1):186–213, 1988.

[208] Elihu Lubkin. Entropy of an n-system from its correlation with ak-reservoir. *J. Math. Phys.*, 19(5):1028–1031, 1978.

[209] Patrick Ludl. Linking models with data-the nelder-mead method. *University of Vienna*, 2012.

[210] Alexander Lukin, Matthew Rispoli, Robert Schittko, M. Eric Tai, Adam M. Kaufman, Soonwon Choi, Vedika Khemani, Julian Léonard, and Markus Greiner. Probing entanglement in a many-body–localized system. *Science*, 364(6437):256–260, 2019.

[211] David Luposchainsky, Andre Cardoso Barato, and Haye Hinrichsen. Strong fluctuation theorem for nonstationary nonequilibrium systems. *Phys. Rev. E*, 87(4):042108, 2013.

[212] Scott M Lynch. *Introduction to applied Bayesian statistics and estimation for social scientists*. Springer Science & Business Media, 2007.

[213] Yu V Lysogorskiy, QA Wang, and DA Tayurskii. Study of energy fluctuation effect on the statistical mechanics of equilibrium systems. In *Journal of Physics: Conference Series*, volume 394, page 012006. IOP Publishing, 2012.

[214] Sreenath K Manikandan, Cyril Elouard, and Andrew N Jordan. Fluctuation theorems for continuous quantum measurement and absolute irreversibility. *arXiv preprint arXiv:1807.05575*, 2018.

[215] Gonzalo Manzano, Jordan M Horowitz, and Juan M R Parrondo. Quantum fluctuation theorems for arbitrary environments: adiabatic and nonadiabatic entropy production. *Phys. Rev. X*, 8(3):031037, 2018.

[216] Ugo Marzolino and Andreas Buchleitner. Quantum teleportation with identical particles. *Phys. Rev. A*, 91(3):032316, 2015.

[217] Ugo Marzolino and Andreas Buchleitner. Performances and robustness of quantum teleportation with identical particles. *Proc. R. Soc. A* , 472(2185):20150621, 2016.

[218] Mohammad Mehboudi, Maria Moreno-Cardoner, Gabriele De Chiara, and Anna Sanpera. Thermometry precision in strongly correlated ultracold lattice gases. *New Journal of Physics*, 17(5):055020, 2015.

[219] Mohammad Mehboudi, Anna Sanpera, and Luis A Correa. Thermometry in the quantum regime: Recent theoretical progress. *arXiv preprint arXiv:1811.03988*, 2018.

[220] Karsten Meier and Stephan Kabelac. Pressure derivatives in the classical molecular-dynamics ensemble. *J. Chem. Phys.*, 124(6):064104, 2006.

[221] RG Melko, CM Herdman, Dmitri Iouchtchenko, P-N Roy, and Adrian Del Maestro. Entangling qubit registers via many-body states of ultracold atoms. *Phys. Rev. A*, 93(4):042336, 2016.

[222] T Mendes-Santos, G Giudici, R Fazio, and M Dalmonte. Measuring von neumann entanglement entropies without wave functions. *arXiv:1904.07782 [cond-mat.str-el]*, 2019.

[223] A Mielke. Exact ground states for the hubbard model on the kagome lattice. *Journal of Physics A: Mathematical and General*, 25(16):4335, 1992.

[224] Andreas Mielke. The hubbard model and its properties. *Many Body Physics: From Kondo to Hubbard. Modeling and Simulation*, 5, 2015.

[225] Leonard Mlodinow and Todd A Brun. Relation between the psychological and thermodynamic arrows of time. *Physical Review E*, 89(5):052102, 2014.

[226] Ali Mostafazadeh. Wave function of the universe and its meaning. *zechoslovak journal of physics*, 54(1):93–99, 2004.

[227] Shinji Mukohyama. Comments on entanglement entropy. *Phys. Rev. D*, 58(10):104023, 1998.

[228] Yuya O Nakagawa, Masataka Watanabe, Hiroyuki Fujita, and Sho Sugiura. Universality in volume-law entanglement of scrambled pure quantum states. *Nat. Comm.*, 9(1):1635, 2018.

[229] Charles Neill, Pedran Roushan, K Kechedzhi, Sergio Boixo, Sergei V Isakov, V Smelyanskiy, A Megrant, B Chiaro, A Dunsworth, K Arya, et al. A blueprint for demonstrating quantum supremacy with superconducting qubits. *Science*, 360(6385):195–199, 2018.

[230] John A Nelder and Roger Mead. A simplex method for function minimization. *Comput. J.*, 7(4):308–313, 1965.

[231] Nelly Ng and Mischa P Woods. *Resource theory of quantum thermodynamics: Thermal operations and Second Laws*, pages 625–650. Springer, 2018.

[232] Rosanna Nichols, Thomas R Bromley, Luis A Correa, and Gerardo Adesso. Practical quantum metrology in noisy environments. *Physical Review A*, 94(4):042101, 2016.

[233] Michael A Nielsen and Isaac Chuang. Quantum computation and quantum information, 2002.

[234] Th M Nieuwenhuizen and AE Allahverdyan. Statistical thermodynamics of quantum brownian motion: Birth of perpetuum mobile of the second kind. *[cond-mat.stat-mech]*, 2000.

[235] Hrvoje Nikolić. Epr before epr: a 1930 einstein–bohr thought experiment revisited. *Eur. J. Phys.*, 33(5):1089, 2012.

[236] Tatsuma Nishioka. Entanglement entropy: holography and renormalization group. *Rev. Mod. Phys.*, 90(3):035007, 2018.

[237] Tatsuma Nishioka, Shinsei Ryu, and Tadashi Takayanagi. Holographic entanglement entropy: an overview. *Journal of Physics A: Mathematical and Theoretical*, 42(50):504008, 2009.

[238] Yasunori Nomura. A note on boltzmann brains. *Phys. Lett. B*, 749:514–518, 2015.

[239] Masanori Ohya. *Fundamentals of quantum mutual entropy and capacity*. World Scientific, 2008.

[240] Masanori Ohya and Igor V Volovich. On quantum capacity and its bound. *Infinite Dimensional Analysis, Quantum Probability and Related Topics*, 6(02):301–310, 2003.

[241] Masanori Ohya and Noboru Watanabe. Quantum entropy and its applications to quantum communication and statistical physics. *Entropy*, 12(5):1194–1245, 2010.

[242] Tobias J Osborne and Michael A Nielsen. Entanglement in a simple quantum phase transition. *Phys. Rev. A*, 66(3):032110, 2002.

[243] Don N Page. Average entropy of a subsystem. *Phys. Rev. Lett.*, 71(9):1291, 1993.

[244] Don N Page. Return of the boltzmann brains. *Phys. Rev. D*, 78:063536, 2008.

[245] Fernando Pastawski, Beni Yoshida, Daniel Harlow, and John Preskill. Holographic quantum error-correcting codes: Toy models for the bulk/boundary correspondence. *Journal of High Energy Physics*, 2015(6):149, 2015.

[246] O Penrose. Foundations of statistical mechanics. *Rep. Prog. Phys*, 42(12):1937, 1979.

[247] R Penrose. *The Road to Reality. A Complete Guide to the Laws of the Universe, Joanthan Cape*. Random House, London, 2004.

[248] Nam Pham and Bogdan M Wilamowski. Improved nelder mead's simplex method and applications. *Journal of Computing*, 2012.

[249] Hannes Pichler, Guanyu Zhu, Alireza Seif, Peter Zoller, and Mohammad Hafezi. Measurement protocol for the entanglement spectrum of cold atoms. *Phys. Rev. X*, 6(4):041033, 2016.

[250] Martin B Plenio. Logarithmic negativity: a full entanglement monotone that is not convex. *Physical review letters*, 95(9):090503, 2005.

[251] Martin B Plenio and Shashank S Virmani. *An introduction to entanglement theory*, pages 173–209, 2011.

[252] Anatoli Polkovnikov. Microscopic diagonal entropy and its connection to basic thermodynamic relations. *Annals of Physics*, 326(2):486–499, 2011.

[253] Sandu Popescu, Anthony J Short, and Andreas Winter. Entanglement and the foundations of statistical mechanics. *Nat. Phys.*, 2(11):754, 2006.

[254] Sandu Popescu, Anthony J Short, and Andreas Winter. Entanglement and the foundations of statistical mechanics. *Nat. Phys.*, 2(11):754, 2006.

[255] Marko Popovic. Researchers in an entropy wonderland: A review of the entropy concept. *arXiv preprint arXiv:1711.07326*, 2017.

[256] John Preskill. Lecture notes for physics-quantum information and computation. *California Institute of Technology*, 2014.

[257] John Preskill. Quantum shannon theory. *arXiv:1604.07450 [quant-ph]*, 2016.

[258] MA Rajabpour. Multipartite entanglement and quantum fisher information in conformal field theories. *Phys. Rev. D*, 96(12):126007, 2017.

[259] Giovanni Ramírez, Javier Rodríguez-Laguna, and Germán Sierra. From conformal to volume law for the entanglement entropy in exponentially deformed critical spin 1/2 chains. *J. Stat. Mech., Theory. Exp.*, 2014(10):P10004, 2014.

[260] Shubhashis Rana, Sourabh Lahiri, and AM Jayannavar. Generalized entropy production fluctuation theorems for quantum systems. *Pramana J. Phys.*, 80(2):207–222, 2013.

[261] Bernhard Rauer, Sebastian Erne, Thomas Schweigler, Federica Cataldini, Mohammadamin Tajik, and Jörg Schmiedmayer. Recurrences in an isolated quantum many-body system. *Science*, page eaan7938, 2018.

[262] Hans Reichenbach. *The direction of time*, volume 65. Univ of California Press, 1991.

[263] Marcos Rigol, Vanja Dunjko, and Maxim Olshanii. Thermalization and its mechanism for generic isolated quantum systems. *Nature*, 452(7189):854–858, 2008.

[264] Gustavo Rigolin, Thiago R de Oliveira, and Marcos C de Oliveira. Operational classification and quantification of multipartite entangled states. *Phys. Rev. A*, 74(2):022314, 2006.

[265] Carlo Rovelli. Why do we remember the past and not the future? the'time oriented coarse graining'hypothesis. *arXiv preprint arXiv:1407.3384*, 2014.

[266] Carlo Rovelli. Is time's arrow perspectival. *The Philosophy of Cosmology, Chamcham, K., Silk, J., Barrow, JD, Saunders, S.(eds.)*, pages 285–296, 2017.

[267] Mark Saffman. Quantum computing with atomic qubits and rydberg interactions: progress and challenges. *J. Phys. B*, 49(20):202001, 2016.

[268] Dominik Šafránek, Anthony Aguirre, and J M Deutsch. Classical dynamical coarse-grained entropy and comparison with the quantum version. *arXiv:1905.03841 [cond-mat.stat-mech]*, 2019.

[269] Dominik Šafránek, JM Deutsch, and Anthony Aguirre. Quantum coarse-grained entropy and thermalization in closed systems. *Phys. Rev. A*, 99:012103, Jan 2019.

[270] Dominik Šafránek, JM Deutsch, and Anthony Aguirre. Quantum coarse-grained entropy and thermalization in closed systems. 99:012103, 2019. "Copyright (2019) by the American Physical Society.".

[271] Takahiro Sagawa and Masahito Ueda. Second law of thermodynamics with discrete quantum feedback control. *Physical review letters*, 100(8):080403, 2008.

[272] Varun Sahni, Yuri Shtanov, and Aleksey Toporensky. Arrow of time in dissipationless cosmology. *Classical and Quantum Gravity*, 32(18):182001, 2015.

[273] Manfred Salmhofer. Renormalization in condensed matter: Fermionic systems–from mathematics to materials. *Nucl. Phys. B*, 941:868–899, 2019.

[274] Lea F Santos, Anatoli Polkovnikov, and Marcos Rigol. Weak and strong typicality in quantum systems. *Phys. Rev. E*, 86(1):010102(R), 2012.

[275] Lea F Santos and Marcos Rigol. Onset of quantum chaos in one-dimensional bosonic and fermionic systems and its relation to thermalization. *Phys. Rev. E*, 81(3):036206, 2010.

[276] Joseph Schindler, Dominik Šafránek, and Anthony Aguirre. Entanglement entropy from coarse-graining in pure and mixed multipartite systems. *arXiv:2005.05408 [quant-ph]*, 2020.

[277] Ulrich Schneider, Stephan Mandt, Akos Rapp, Simon Braun, Hendrik Weimer, Immanuel Bloch, and Achim Rosch. Comment on" consistent thermostatistics forbids negative absolute temperatures". *arXiv:1407.4127 [cond-mat.quant-gas]*, 2014.

[278] JF Schneiderman, MD Shaw, B Palmer, P Delsing, and PM Echternach. Quasiparticle poisoning and quantum coherence in a differential charge qubit. *arXiv preprint arXiv:0705.0695*, 2007.

[279] Ulrich Schollwöck. The density-matrix renormalization group: a short introduction. *Philosophical Transactions of the Royal Society A: Mathematical, Physical and Engineering Sciences*, 369(1946):2643–2661, 2011.

[280] Klaus R Schubert. T violation and cpt tests in neutral-meson systems. *Progress in Particle and Nuclear Physics*, 81:1–38, 2015.

[281] Benjamin Schulz. Review on the quantization of gravity. *arXiv:1409.7977 [gr-qc]*, 2014.

[282] Benjamin Schumacher. Sending entanglement through noisy quantum channels. *Physical Review A*, 54(4), 1996.

[283] Stefania Sciara, Rosario Lo Franco, and Giuseppe Compagno. Universality of schmidt decomposition and particle identity. *Scientific reports*, 7:44675, 2017.

[284] Udo Seifert. Stochastic thermodynamics, fluctuation theorems and molecular machines. *Rep. Prog. Phys.*, 75(12):126001, 2012.

[285] Claude E Shannon. A mathematical theory of communication. *Bell system technical journal*, 27(3):379–423, 1948.

[286] Claude E Shannon. Communication theory of secrecy systems. *Bell system technical journal*, 28(4):656–715, 1949.

[287] Akshata Shenoy-Hejamadi, Anirban Pathak, and Srikanth Radhakrishna. Quantum cryptography: key distribution and beyond. *Quanta*, 6(1):1–47, 2017.

[288] Sergey N Solodukhin. Entanglement entropy of black holes. *Living Rev. Relativ.*, 14(1):8, 2011.

[289] Jie Song, Yan Xia, He-Shan Song, Jin-Liang Guo, and Jing Nie. Quantum computation and entangled-state generation through adiabatic evolution in two distant cavities. *Europhys. Lett.*, 80(6):60001, 2007.

[290] Wei Song, Lin Chen, and Zhuo-Liang Cao. Lower and upper bounds for entanglement of rényi-α entropy. *Sci. Rep.*, 6(1):23, 2016.

[291] Erik S Sørensen, Ming-Shyang Chang, Nicolas Laflorencie, and Ian Affleck. Quantum impurity entanglement. *J. Stat. Mech.*, 2007(08):P08003, 2007.

[292] Mark Srednicki. Chaos and quantum thermalization. *Phys. Rev. E*, 50(2):888, 1994.

[293] Philipp Strasberg. Entropy production as change in observational entropy. *arXiv:1906.09933 [cond-mat.stat-mech]*, 2019.

[294] Sho Sugiura and Akira Shimizu. Thermal pure quantum states at finite temperature. *Phys. Rev. Lett.*, 108(24):240401, 2012.

[295] Sho Sugiura and Akira Shimizu. Canonical thermal pure quantum state. *Phys. Rev. Lett.*, 111(1):010401, 2013.

[296] Magdalena Szczykulska, Tillmann Baumgratz, and Animesh Datta. Multi-parameter quantum metrology. *Adv. Phys. X*, 1(4):621–639, 2016.

[297] Tadashi Takayanagi. Entanglement entropy from a holographic viewpoint. *Class. Quantum Gravity*, 29(15):153001, 2012.

[298] Peter Talkner, Peter Hänggi, and Manuel Morillo. Microcanonical quantum fluctuation theorems. *Phys. Rev. E*, 77(5):051131, 2008.

[299] D Ter Haar. Theory and applications of the density matrix. *Reports on progress in Physics*, 24(1):304, 1961.

[300] Yakov P Terletskii and Howard Falk. Statistical physics. *PhT*, 25(12):50, 1972.

[301] Walter Thirring. *Quantum mathematical physics: atoms, molecules and large systems*. Springer Science & Business Media, 2013.

[302] Emanuele Tirrito, Shi-Ju Ran, Andrew J Ferris, Ian P McCulloch, and Maciej Lewenstein. Efficient perturbation theory to improve the density matrix renormalization group. *Physical Review B*, 95(6):064110, 2017.

[303] Yury S Tokpanov, James S Fakonas, Benjamin Vest, and Harry A Atwater. Quantum coherence is preserved in extremely dispersive plasmonic media. *arXiv preprint arXiv:1810.00114*, 2018.

[304] Richard Chace Tolman. *The principles of statistical mechanics*. Courier Corporation, 1979.

[305] Géza Tóth and Iagoba Apellaniz. Quantum metrology from a quantum information science perspective. *J. Phys. A: Math. Theor.*, 47(42):424006, 2014.

[306] Deniz Türkpençe, Tahir Çetin Akıncı, and Serhat Şeker. Quantum neural networks driven by information reservoir. *arXiv:1709.03276 [quant-ph]*, 2017.

[307] Jaegon Um, Hyunggyu Park, and Haye Hinrichsen. Entanglement versus mutual information in quantum spin chains. *J. Stat. Mech., Theory. Exp.*, 2012(10):P10026, 2012.

[308] R G Unanyan and M Fleischhauer. Entanglement and criticality in translationally invariant harmonic lattice systems with finite-range interactions. *Phys. Rev. Lett.*, 95(26):260604, 2005.

[309] Ion V Vancea. Entanglement entropy in the σ-model with the de sitter target space. *Nuclear Physics B*, 924:453–476, 2017.

[310] Lorenzo Campos Venuti. The recurrence time in quantum mechanics. *arXiv preprint arXiv:1509.04352*, 2015.

[311] Frank Verstraete and J Ignacio Cirac. Quantum nonlocality in the presence of superselection rules and data hiding protocols. *Phys. Rev. Lett.*, 91(1):010404, 2003.

[312] Guifre Vidal, José Ignacio Latorre, Enrique Rico, and Alexei Kitaev. Entanglement in quantum critical phenomena. *Phys. Rev. Lett.*, 90(22):227902, 2003.

[313] Lev Vidmar, Lucas Hackl, Eugenio Bianchi, and Marcos Rigol. Entanglement entropy of eigenstates of quadratic fermionic hamiltonians. *Phys. Rev. Lett.*, 119(2):020601, 2017.

[314] Lev Vidmar and Marcos Rigol. Entanglement entropy of eigenstates of quantum chaotic hamiltonians. *Phys. Rev. Lett.*, 119(22):220603, 2017.

[315] John von Neumann. *Mathematical foundations of quantum mechanics*, pages 410–416. Princeton university press, 1955.

[316] John von Neumann. Proof of the ergodic theorem and the h-theorem in quantum mechanics. *Eur. Phys. J. H*, 35(2):201–237, 2010.

[317] John Von Neumann. *Mathematische grundlagen der quantenmechanik*, volume 38. Springer-Verlag, 2013.

[318] David Wallace. The arrow of time in physics. *A Companion to the Philosophy of Time*, pages 262–281, 2013.

[319] GM Wang, Edith M Sevick, Emil Mittag, Debra J Searles, and Denis J Evans. Experimental demonstration of violations of the second law of thermodynamics for small systems and short time scales. *Phys. Rev. Lett.*, 89:050601, 2002.

[320] Alfred Wehrl. General properties of entropy. *Rev. Mod. Phys*, 50(2):221, 1978.

[321] G Wendin. Quantum information processing with superconducting circuits: a review. *Rep. Prog. Phys.*, 80(10):106001, 2017.

[322] Mark M. Wilde. *From Classical to Quantum Shannon Theory*, pages xi–xii. Cambridge University Press, 2 edition, 2017.

[323] Andreas Winter. Tight uniform continuity bounds for quantum entropies: conditional entropy, relative entropy distance and energy constraints. *Commun. Math. Phys.*, 347(1):291–313, 2016.

[324] H M Wiseman and John A Vaccaro. Entanglement of indistinguishable particles shared between two parties. *Phys. Rev. Lett.*, 91(9):097902, 2003.

[325] Edward Witten. A mini-introduction to information theory. *arXiv:1805.11965 [hep-th]*, 2018.

[326] Edward Witten. A mini-introduction to information theory. *La Rivista del Nuovo Cimento*, pages 1–41, 2020.

[327] Alexander Wong and Nelson Christensen. Potential multiparticle entanglement measure. *Physical Review A*, 63(4):044301, 2001.

[328] Kai Xu, Jin-Jun Chen, Yu Zeng, Yu-Ran Zhang, Chao Song, Wuxin Liu, Qiujiang Guo, Pengfei Zhang, Da Xu, Hui Deng, et al. Emulating many-body localization with a superconducting quantum processor. *Phys. Rev. Lett.*, 120(5):050507, 2018.

[329] Koji Yamaguchi. Theorems on entanglement typicality in non-equilibrium dynamics. *Journal of the Physical Society of Japan*, 88(6):064002, 2019.

[330] Koji Yamaguchi. Theorems on entanglement typicality in non-equilibrium dynamics. *J. Phys. Soc. Jpn.*, 88(6):064002, 2019.

[331] Horace P Yuen and Masanao Ozawa. Ultimate information carrying limit of quantum systems. *Physical review letters*, 70(4):363, 1991.

[332] Pablo R Zangara, Axel D Dente, EJ Torres-Herrera, Horacio M Pastawski, Aníbal Iucci, and Lea F Santos. Time fluctuations in isolated quantum systems of interacting particles. *Physical Review E*, 88(3):032913, 2013.

[333] Jiehang Zhang, Guido Pagano, Paul W Hess, Antonis Kyprianidis, Patrick Becker, Harvey Kaplan, Alexey V Gorshkov, Z-X Gong, and Christopher

Monroe. Observation of a many-body dynamical phase transition with a 53-qubit quantum simulator. *Nature*, 551(7682):601, 2017.

[334] Liangsheng Zhang, Hyungwon Kim, and David A Huse. Thermalization of entanglement. *Phys. Rev. E*, 91(6):062128, 2015.

[335] Yi Zhang, Tarun Grover, and Ashvin Vishwanath. Entanglement entropy of critical spin liquids. *Phys. Rev. Lett.*, 107(6):067202, 2011.

[336] O S Zozulya, M Haque, K Schoutens, and E H Rezayi. Bipartite entanglement entropy in fractional quantum hall states. *Phys. Rev. B*, 76(12):125310, 2007.

[337] Roman Zwicky. *Symmetries of Quantum Mechanics*. PhD thesis, University of Edinburgh, 2015.